UNIVERSITY OF CALIFORNIA SANTA CRUZ

THE RESPONSE OF MARINE CARBONATE CHEMISTRY TO RAPID CARBON INJECTION DURING THE PALEOCENE-EOCENE THERMAL MAXIMUM

A dissertation submitted in partial satisfaction
of the requirements for the degree of

DOCTOR OF PHILOSOPHY

in

EARTH SCIENCES

by

Donald E. Penman

March 2015

The Dissertation of Donald Penman is approved:

_____
Professor James C. Zachos, chair

_____
Professor A. Christina Ravelo

_____
Professor Paul L. Koch

_____
Professor Richard E. Zeebe

_____

Tyrus Miller

Vice Provost and Dean of Graduate Studies

Table of Contents **iii**

Abstract: "THE RESPONSE OF MARINE CARBONATE CHEMISTRY TO RAPID CARBON INJECTION DURING THE PALEOCENE-EOCENE THERMAL MAXIMUM" by Donald E. Penman

This dissertation reconstructs the response of marine carbonate chemistry to rapid carbon injection during the Paleocene-Eocene Thermal Maximum (PETM). Chapter 1 uses boron-based proxies to reconstruct ocean acidification during the PETM for the first time, concluding that surface seawater pH declined by ~0.3 units at the onset of the event, and remained acidified for at least 70 thousand years before recovering in step with temperature and the carbon isotopic signature of the PETM. Chapter 2 describes a new sedimentary record of the PETM from the deep North Atlantic which provides the first evidence for a hypothesized "overshoot" of carbonate saturation in the aftermath of the PETM in response to long-term weathering feedbacks on climate. Stable isotope records from that section demonstrate that this overshoot occurred during the recovery of the PETM, ~70 thousand years after its onset, which provides novel constraints on the evolution of the carbonate compensation depth over the event. Finally, Chapter 3 uses these new (and previous) records to constrain carbon cycle model simulations of the PETM. Consistent runs require both a large initial release as well as a protracted release over tens of thousands of years (possibly representing a slow positive feedback to warming) and the removal of isotopically light carbon to accelerate the PETM recovery, likely representing organic carbon burial. No consistent scenarios feature under-saturated conditions in the surface ocean during the PETM, consistent with the

lack of calcifier extinctions during the event. Comparison of the most consistent PETM scenarios with forecasts of anthropogenic carbon emissions demonstrate that carbonate chemistry change during the PETM was less severe and far more gradual than what might be expected in coming centuries.

Acknowledgements

I am indebted first and foremost to my advisor, Jim Zachos, for immersing me in such an interesting topic and also for his guidance and intellectual collaboration throughout my time at UCSC. Richard Zeebe, who cannot be held responsible for my (mis?)use of his model, was extremely generous with his time and interest even when our opinions differed. Importantly, Bärbel Hönisch played a very important role both in sparking my interest in climate and the carbon cycle as well as in the present dissertation itself. Ellen Thomas, Clay Kelly, Tim Bralower, Andy Ridgwell and Alex Dickson contributed various indispensible material, analyses, and advice without which my dissertation would not be nearly as comprehensive.

The bulk of the data presented in my thesis was generated using the mass spectrometers of the Stable Isotope Lab and Marine Analytical Lab at UCSC, which simply would not function if it weren't for the hard work of Rob Franks and Dyke Andreasen. Colin Carney, Linda Anderson, Sarah White, and Rachel Brown also deserve credit for refining the techniques used in this study.

Perhaps the most fortuitous event of my graduate research was the opportunity to sail on IODP's Expedition 342, which in addition to my new favorite PETM section, gave me a gang of new collaborators and friends that I hope to be lucky enough to work with for the rest of my career. I need to thank the entire crew and staff of the JOIDES Resolution, as well as co-chiefs Paul Wilson and Dick Norris, plus the scientific party, especially Pincelli Hull, Howie Scher, Phil Sexton, Pete Lippert, Chris Junium, Sandy Kirtland-Turner.

The National Science Foundation and the IODP provided the funding without which this work would not be possible.

Finally, I need to thank the friends I've been fortunate to spend the last 5 years with and who make Santa Cruz an even more beautiful little corner of the world, and most importantly Norah for her love and support.

Introduction

Since its discovery almost 25 years ago, a great deal of research into the Paleocene-Eocene Thermal Maximum (PETM, ~56 million years ago) has expanded and refined our knowledge of this unique climatic and paleoceanographic event. There currently exists a broad agreement that the global negative carbon isotope excursion, temperature increase, and deep-sea carbonate dissolution that characterize the event resulted from the release of thousands of gigatons of carbon (GtC) into the atmosphere and ocean within a geologic instant (thousands of years). The event has thus often been interpreted as something of a geologic analogue for the current anthropogenic release of thousands of GtC into the atmosphere due to rapidly increasing fossil fuel combustion, deforestation, and cement production. My dissertation utilizes this event as an opportunity to study the response of marine carbonate chemistry to rapid carbon injection on short (thousands of years, Chapter 1) and long (hundreds of thousands of years, Chapter 2) timescales, and offers new estimates of the magnitude and timing of carbon release and sequestration during the event (Chapter 3) using geochemical modeling constrained by these new observations of carbonate chemistry response.

Our current understanding of the exogenic carbon cycle predicts with high certainty that carbon rapidly released into the atmosphere will dissolve into the surface ocean and be subsequently mixed into the deep ocean. This CO_2 invasion

lowers seawater pH and carbonate ion concentration ($[CO_3^{=}]$) in tandem, a process known as ocean acidification. Ocean acidification is currently occurring as a result of anthropogenic carbon emissions and may threaten marine calcifiers, which rely on high $[CO_3^{=}]$ to precipitate their shells. The currently accepted mechanism for the PETM predicts ocean acidification during the event, however this has so far gone undocumented. In my first chapter I utilize boron based proxies (B/Ca ratio and boron isotopic composition) in planktonic foraminifers to reconstruct acidification across the PETM. Results indicate rapid, global acidification of the surface and thermocline, confirming the role of CO_2 as the cause of warming during the PETM. Acidification of the surface ocean during the PETM was ~0.3 pH units (a doubling of acidity) and lasted for tens of thousands of years followed by a recovery to pre-event levels over several more tens of thousands of years.

Carbon cycle theory predicts that on longer timescales (hundreds of thousands of years), increased rates of terrestrial silicate weathering in response to elevated pCO_2 should gradually restore carbonate saturation to the ocean and eventually result in a period of oversaturation (relative to pre-event levels) which results in greater carbonate burial; the long-term fate of carbon released during the PETM. In Chapter 2, I utilize new sedimentary records of the PETM recovered during the Integrated Ocean Drilling Project (IODP)'s Expedition 342 to the North Atlantic (on which I sailed as a shipboard scientist) to constrain the evolution of carbonate sedimentation over this event. In particular, the deep Site U1403 documents this hypothesized period of increased carbonate burial with an interval of high carbonate content during

the recovery of the PETM, at a depth which had been carbonate barren before the event. The presence of this saturation overshoot confirms the key role of silicate weathering as a long-term negative climatic feedback, and its timing and depth provide new constrains on the strength of this feedback during the PETM.

In Chapter 3, I present a series of experiments using a geochemical box model of the carbon cycle (LOSCAR) to evaluate which scenarios of carbon release and sequestration processes are consistent with new and existing constraints on marine carbonate chemistry. Results indicate that ~3,000 or 4,000 GtC of carbon released over several thousand years are most consistent with observations of acidification during the onset of the event. Furthermore, a sustained, slow release of a similar mass over the following ~60 thousand years are required to generate sustained acidification and delayed CCD overshoot documented by Chapters 1 and 2, and the sequestration of several thousand GtC (possibly as burial of organic C) are required to match the rapidity of recovery suggested by boron records. Comparison of the most consistent PETM scenarios to forecasts of anthropogenic acidification reveal that carbonate chemistry during the PETM was less severe and far less rapid than what might be expected for the future, suggesting that the lack of calcifier mass extinctions during the PETM cannot be taken as evidence for the invulnerability of such taxa to ocean acidification in the future.

Chapter 1: Rapid and sustained surface ocean acidification during the Paleocene-Eocene Thermal Maximum

Donald E. Penman

with Bärbel Hönisch, Richard E. Zeebe, Ellen Thomas, James C. Zachos

Abstract

The Paleocene-Eocene Thermal Maximum (PETM) has been associated with the release of several thousands of petagrams of carbon (Pg C) as methane and/or carbon dioxide into the ocean-atmosphere system within ~10 thousand years (ky), on the basis of the co-occurrence of a carbon isotope excursion (CIE), widespread dissolution of deep sea carbonates, and global warming. In theory, this rapid carbon release should have severely acidified the surface ocean, though no geochemical evidence has yet been presented. Using boron-based proxies for surface-ocean carbonate chemistry, we present the first observational evidence for a drop in the pH of surface and thermocline seawater during the PETM. Planktic foraminifers from a drill site in the North Pacific (ODP Site 1209) show a ~0.8‰ decrease in boron isotopic composition ($\delta^{11}B$) at the onset of the event, along with a 30-40% reduction in shell B/Ca. Similar trends in $\delta^{11}B$ are present in two lower resolution records from the South Atlantic and Equatorial Pacific. These observations are consistent with significant, global acidification of the surface ocean lasting at least 70 ky and requiring sustained carbon release. The anomalies in the B records are consistent with an initial surface pH drop of ~0.3 units, at the upper range of model-based estimates of acidification.

1. Introduction

The Paleocene-Eocene Thermal Maximum (~56 million years ago, Ma) is marked by a 3-4‰ decrease in the carbon isotopic composition ($\delta^{13}C$) of both organic and inorganic carbon in marine and terrestrial records (Kennett and Stott, 1991; Koch et al., 1992). Concurrent with this CIE, marine sediments show a rapid decrease in calcium carbonate ($CaCO_3$) content (Colosimo et al., 2005; Thomas and Shackleton, 1996; Zachos et al., 2005) and a transient global warming of 4-8°C as indicated by various paleothermometers (Dunkley-Jones et al., 2013; McInerney and Wing, 2011; Zachos et al., 2003). This combined evidence points to a massive release of ^{13}C-depleted carbon into the ocean-atmosphere system (Dickens et al., 1997; Pagani et al., 2006), thus this interval presents an opportunity to examine the response of ocean chemistry to a geologically rapid increase in the atmospheric concentration of carbon dioxide (CO_2)(Hönisch et al., 2012). Ocean carbon cycle modeling (Panchuk et al., 2008; Zeebe et al., 2009a), using sediment $CaCO_3$ content to constrain the changes in the calcite compensation depth (CCD), estimates the mass of carbon released to between 3,000 and 9,000 Pg C, with marine methane clathrate, terrestrial and/or marine organic carbon, or some combination thereof as the probable source of carbon (Dickens et al., 1997; Pagani et al., 2006). In all cases, a significant decrease in surface seawater pH is predicted, the extent of which scales with the rate and magnitude of carbon release (Hönisch et al., 2012; Ridgwell and Schmidt, 2010).

Current observational constraints on the changes in the carbonate chemistry of the surface ocean across the PETM are largely limited to the abundance and/or

morphology of marine calcifiers preserved in sediments (Bown and Pearson, 2009; Gibbs et al., 2006; Gibbs et al., 2010; Raffi et al., 2005), which should be sensitive to rapid ocean acidification (Bijma et al., 2002). Planktic foraminifers show transient population changes and ecosystem disruption over the PETM, including the temporary disappearance of species abundant before the event, and the evolution of "excursion taxa" (Kelly et al., 1996; Raffi et al., 2009; Raffi and De Bernardi, 2008). In addition, changes in shell morphology may reflect rapid acidification during the CIE followed by elevated saturation during the "overshoot" phase of the recovery (Kelly et al., 1996; Kelly et al., 2010). Calcareous nannoplankton experienced significant yet transient changes in species abundance, though without the major extinction that might be expected during rapid acidification (Bown and Pearson, 2009; Gibbs et al., 2006). Calcareous plankton likely also responded to coeval changes in temperature, salinity, and nutrient concentrations (Bown and Pearson, 2009; Gibbs et al., 2010). Inferring surface ocean saturation from pelagic fossil assemblages is further complicated by preservational biases, such as $CaCO_3$ dissolution at the seafloor (Gibbs et al., 2010). Therefore, biotic records provide ambiguous evidence of acidification, and we turn to geochemical proxies for independent evidence for ocean acidification.

We used boron-based proxies for reconstructing past variations in seawater carbonate chemistry. In culture experiments, both the boron/calcium ratio (B/Ca) and the boron isotopic composition ($\delta^{11}B$) of planktic foraminifer shells have been shown to reflect carbonate chemistry parameters (Allen et al., 2012; Henehan et al., 2013;

Sanyal et al., 2001; Sanyal et al., 1996a). These relationships are based on the inference from boron isotope studies that the borate ion ($B(OH)_4^-$) is the species predominantly incorporated into calcite (Hemming and Hanson, 1992), and both the aqueous abundance of $B(OH)_4^-$ and its isotopic composition increase with seawater pH (Kakihana et al., 1977). $\delta^{11}B$ in planktic foraminifer shells increases with pH (Henehan et al., 2013; Hönisch et al., 2007; Sanyal et al., 2001; Sanyal et al., 1996a) and has previously been used to reconstruct seawater pH on Pleistocene (Henehan et al., 2013; Hönisch and Hemming, 2005) and Cenozoic (Foster et al., 2012; Pearson et al., 2009) timescales. A full understanding of the controls on B/Ca in planktic foraminifera is still emerging, but culturing experiments have demonstrated that B incorporation is well-correlated to the ratio of aqueous $B(OH)_4^-$ to total dissolved inorganic carbon (DIC) or bicarbonate (HCO_3^-) (Allen et al., 2012; Allen et al., 2011b). However, quantification of the carbonate chemistry changes documented by B/Ca remains complicated and cannot be used by itself to quantify pH changes (Allen et al., 2012). In addition, the [B] and $\delta^{11}B$ of ancient seawater are poorly constrained (Lemarchand et al., 2000; Raitzsch and Hönisch, 2013; Simon et al., 2006), but the combination of these proxies can be used to reconstruct the timing, duration, and relative magnitude of ocean acidification during the PETM, which can be calculated independently of $\delta^{11}B_{seawater}$ by assuming pre-PETM pH.

2. Materials and Methods

During ODP Leg 198, 3 holes were drilled at Site 1209 (Shatsky Rise, N. Pacific 32°39.1081N, 158°30.3564E) at a water depth of 2387 m (Bralower et al.,

2002), equivalent to a paleodepth during the PETM of ~ 1900 m (Takeda and Kaiho, 2007). The Paleocene-Eocene boundary interval, recovered at 109 meters composite depth (mcd), is composed primarily of a carbonate-rich nannofossil ooze. Investigations of this interval documented a prominent carbon isotope excursion (CIE), warming, carbonate dissolution and the benthic foraminiferal extinction horizon (Colosimo et al., 2005; Takeda and Kaiho, 2007; Zachos et al., 2005). Site 1209 was chosen for this study because of its location within a sub-tropical gyre, away from regions of upwelling. Moreover, its high $\%CaCO_3$ and foraminiferal abundance facilitated collection of a high resolution B/Ca record and large samples for measuring boron isotopes. Sediment samples, collected at 1-3 cm resolution across a 2-meter interval spanning the CIE, were washed and sieved, and specimens of the mixed-layer-dwelling planktic species *Morozovella velascoensis* and *Acarinina soldadoensis* were picked from the 250-300 and 300-425 μm size fraction. On the basis of shell size - $\delta^{13}C$ relations, these species likely harbored photosynthetic algal symbionts and were thus restricted to the photic zone of the surface ocean (D'Hondt et al., 1994). Additionally, specimens of the smooth-walled, thermocline-dwelling genus *Subbotina* were picked from the 250-300 μm size fraction. Isotopic depth ranking suggests that this taxon was non-symbiotic and occupied the thermocline (Berggren and Norris, 1997). Boron isotope analyses at Site 1209 were restricted to *M. velascoensis*, and complemented by low-resolution $\delta^{11}B$ analyses of the same taxon from Sites 1263 (Walvis Ridge, Southeast Atlantic, 28°31.98S, 02°46.77E, 2717 m depth; paleodepth ~1500 m; (Zachos et al., 2004)) and 865 (Allison Guyot,

Equatorial Pacific, 18°26.41N, 179°22.24W, 1518 m depth; paleodepth ~ 1400 m;(Bralower et al., 1995)) to evaluate whether the Site 1209 record is representative of a global signal, or compromised by local or preservational effects. At each of these sites, previous work has identified the P-E boundary and accompanying CIE (Colosimo et al., 2005; Kelly et al., 1996; Zachos et al., 2005), which is used to correlate between sites.

We measured $\delta^{11}B$ using standard NTIMS methods (Hemming and Hanson, 1994) and complemented the $\delta^{11}B$ data at Site 1209 by higher-resolution records of B/Ca and Mg/Ca measured by ICP-MS, and $\delta^{13}C$ and $\delta^{18}O$ measured by standard dual-inlet techniques (see supplement for detailed description of analytical methods). In addition to *M. velascoensis*, trace elements and stable isotopes were analyzed in shells of *A. soldadoensis,* and *Subbotina*.

Applying simple assumptions about seawater chemistry (described below and in SI), we estimate not the absolute pH values, but the pH excursion (ΔpH), from $\delta^{11}B$ values across the P-E boundary. As a second constraint, we compare measured B/Ca records with model-derived estimates of B/Ca based on the observed sensitivity of modern foraminifera. These two techniques complement each other in that the more complete understanding of the $\delta^{11}B$ proxy allows a more quantitative interpretation, while the smaller sample size requirement of B/Ca analyses allows generation of a much higher resolution record, so that timing and structure can be resolved more precisely.

Age models were constructed by correlating the fine fraction $\delta^{13}C$ record of Sites 1209 and 1263 with the bulk $\delta^{13}C$ record for ODP Site 690, which has an orbitally tuned age model (Röhl et al., 2007) (Figure S3). For Site 865, the benthic foraminiferal $\delta^{13}C$ record was correlated with that at Site 690 (Zachos et al., 2001) to generate an age model. Our age models lead to a slightly shorter duration for the CIE than other estimates (Farley and Eltgroth, 2003; Murphy et al., 2010). The resulting age model for Site 1209, similar to that for other pelagic PETM sites, implies greatly reduced sedimentation rates immediately below and within the 'core' of the CIE, resulting from chemical erosion of uppermost Paleocene $CaCO_3$ sediments and decreased production and/or preservation of $CaCO_3$ during the CIE, followed by enhanced sedimentation rates during and after the recovery interval (Farley and Eltgroth, 2003), representing a carbonate saturation overshoot phase (Kelly et al., 2010; Zachos et al., 2005).

3. Results

The $\delta^{13}C$ and Mg/Ca values of the mixed layer -dwelling foraminifera accurately replicate previously published records for Site 1209 (Zachos et al., 2003), and extend them by 200 ky into the early Eocene (Figure 1). The 50% rise in Mg/Ca (~2 mmol/mol) at the onset of the CIE is consistent with a ~5°C increase in sea surface temperature (SST) (Zachos et al., 2003), whereas the comparably smaller decrease in oxygen isotopes presented in Zachos et al. (2003) is consistent with a rise in local $\delta^{18}O_{sw}$ and 1.5 ppt increase in salinity (S) (Zachos et al., 2003). These excursion SST and S estimates are used to constrain the boric acid dissociation

constant and boron isotopic fractionation factor required for pH calculations from $\delta^{11}B$ across the CIE. Before and after the event, a baseline of 30°C and S=37 are assumed, similar to other estimates of late Paleocene low-latitude SST and S (Kozdon et al., 2011).

Site 1209 $\delta^{11}B$ values decrease from an average of ~15.5‰ below the CIE to an average of ~14.7‰ within the body of the CIE (Figure 1). This decrease is rapid, occurring within 5 cm, and values remain low for at least 15 cm (at least 70 ky) before recovering more gradually to pre-event levels, more or less in parallel with the $\delta^{13}C$ recovery. $\delta^{11}B$ values at Sites 1263 and 865 also show a significant decrease within the CIE (Figure 4), supporting that the Site 1209 record reflects global environmental change. However, the excursion is covered by only one or two data points in each of these complementary records, and we therefore restrict calculation of the magnitude of acidification to Site 1209 data.

B/Ca data generally parallel the Site 1209 boron isotope excursion and recovery. The upper Paleocene baseline *M. velascoensis* and *A. soldadoensis* B/Ca values of ~70 μmol/mol fall towards the low end of those of modern symbiont-

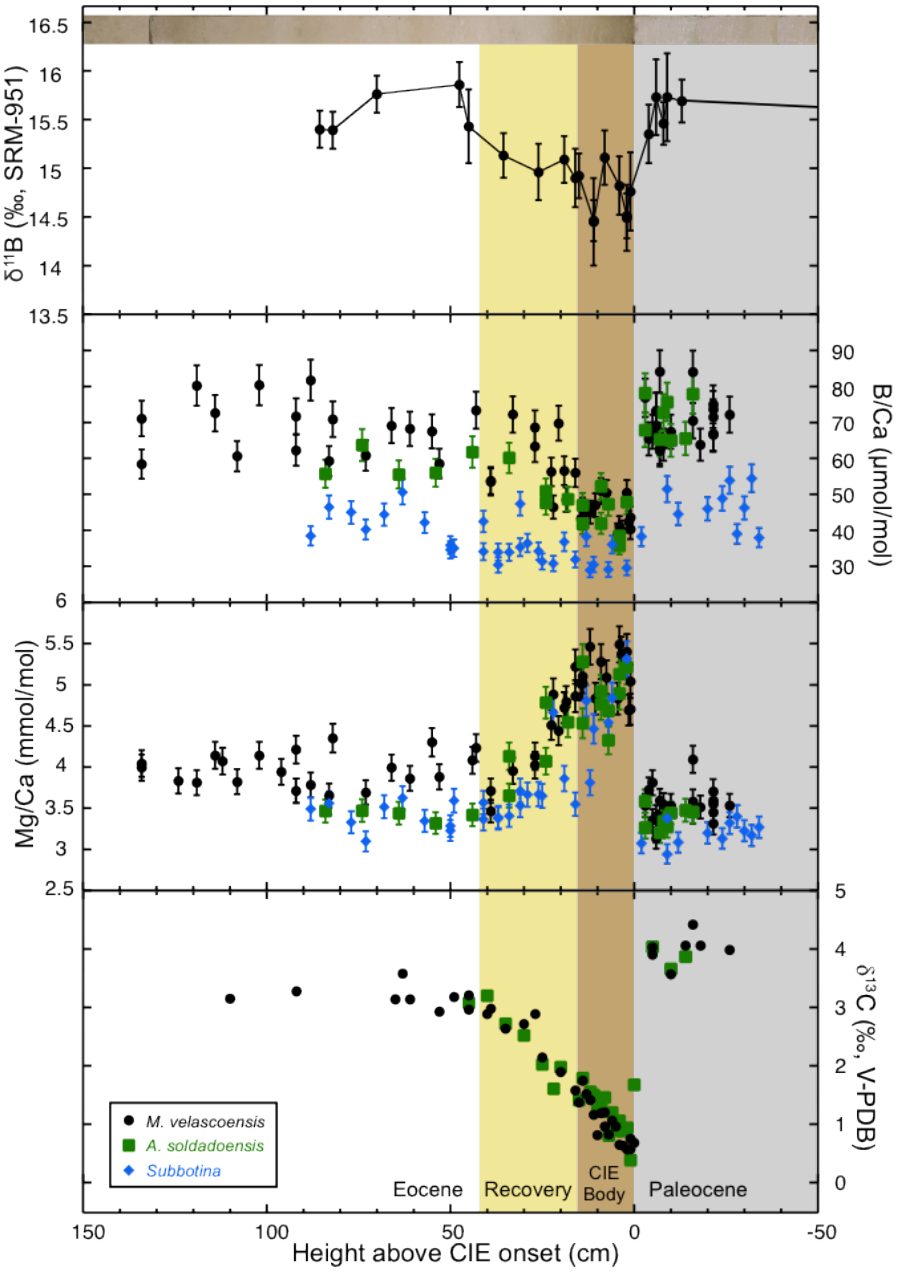
δ11B (‰, SRM-951)
B/Ca (μmol/mol)
Mg/Ca (mmol/mol)
δ13C (‰, V-PDB)
M. velascoensis
A. soldadoensis
Subbotina
Eocene
Recovery
CIE Body
Paleocene
Height above CIE onset (cm)

Figure 1: Data from Core 198-1209B-22H plotted against distance in the core in cm relative to the CIE onset, at 134 cm in Section 1209B-22H-1W. Shown are a core photograph, foraminiferal $\delta^{11}B$, B/Ca, Mg/Ca and $\delta^{13}C$. (Zachos et al., 2003) The grey shaded area indicates the baseline conditions before the onset of the PETM, brown shading indicates the body of the CIE, yellow shading represents the CIE recovery interval, and the unshaded interval is considered post-event. Error bars on Mg/Ca and B/Ca are 2 s.d. of repeat measurements of an in-house carbonate standard: 7% on B/Ca and 4% on Mg/Ca. Error bars on $\delta^{11}B$ are 2 s.e. of repeat sample analyses (n>3), or 2 s.e. of repeat analyses of an in-house vaterite standard given the same n, whichever is larger.

bearing foraminifers (Allen et al., 2012), consistent with lower than modern seawater pH and [B] (Lemarchand et al., 2000). Values in both species show a rapid drop from an average of 70 to 45 μmol/mol across the onset of the CIE (Figure 1), remain low for 15 cm (at least ~70 ky) above the boundary, then recover gradually, in step with $\delta^{11}B$ to pre-CIE levels. B/Ca data for the thermocline-dwelling *Subbotina* follow the same trend as the data for mixed layer-dwelling species, but are offset toward lower values over the entire record, likely reflecting the lower environmental pH of their habitat. *Subbotina* record a smaller B/Ca excursion (from 45 to 30 μmol/mol) than mixed layer-dwellers, consistent with model predictions that the magnitude of acidification decreases with depth in the water column (Ridgwell and Schmidt, 2010).

4. Discussion

4.1 Evidence for Acidification

The similarity and timing of the $\delta^{11}B$ and B/Ca anomalies suggest that both proxies are documenting the surface acidification caused by the geologically rapid (within 1 to 20 ky) release of thousands of PgC . (e.g., Zeebe and Zachos, 2012). However, given the drastic environmental changes documented during the PETM (including warming, salinity changes, and dissolution), we must consider whether there may be factors other than pH that might influence the B proxies.

In culture experiments documenting the sensitivity of planktic foraminiferal $\delta^{11}B$ and B/Ca to pH, no effect was observed with temperature, and for B/Ca only a minor effect with salinity (~2.6 μmol/mol/psu) (Allen et al., 2012). Moreover, culture studies would predict an increase in B/Ca at the PETM onset in response to the local

salinity increase (Zachos et al., 2003), the opposite of what is observed. As for preservation artifacts, Yu et al. (2007) found no correlation between B/Ca in planktic foraminifers and bottom water carbonate saturation state (Ω) in core-top samples, concluding that seafloor dissolution likely does not alter B/Ca. (Coadic et al., 2013), however, found a correlation between depth and planktic B/Ca along a depth transect, suggesting that dissolution may be an issue. The observed dissolution effect of 10-15 μmol/mol between 2,500 and 5,000 m water depth, however, is small compared to the much larger signal in our records, and the paleodepth for Site 1209 was only ~ 1900 m(Takeda and Kaiho, 2007). Similarly, $\delta^{11}B$ records have been observed to be affected by dissolution (Hönisch and Hemming, 2004), and the change is in the same direction as that observed in our PETM records. Importantly, these dissolution artifacts are associated with a concomitant decrease in Mg/Ca (Coadic et al., 2013; Hönisch and Hemming, 2004), whereas our record shows an increase in Mg/Ca, consistent with the global average temperature increase (Dunkley-Jones et al., 2013).

Furthermore, the most extreme phase of dissolution at Site 1209, as reflected in $\%CaCO_3$ and shell fragmentation (Colosimo et al., 2005), occurred over ~5cm during the onset of the event, and dissolution recovered below the $\delta^{11}B$ and B/Ca recoveries. Because $\delta^{11}B$ and B/Ca remain low after recovery of preservation, we do not consider dissolution a likely explanation for the observed trends. Furthermore, the preservation of species-specific offsets in B/Ca suggests that recrystallization/secondary calcification has not altered the primary signal of the shells. Detailed SEM photographs of CIE-interval planktic foraminifera (Colosimo et

al., 2005) provide evidence for some diagenetic carbonate overgrowth and pore infilling, but an overgrowth effect cannot significantly bias our records, given that most of the B in pelagic sediments resides in calcite, pore-water contributes comparably little B, and the B/Ca of inorganic calcite is similar to that of biogenic calcite (Sanyal et al., 2000). A B content similar to that of foraminiferal calcite is most likely in overgrowths, but even if overgrowths contained no B, it would require anomalous carbonate overgrowths of ~30-40% (restricted to only the CIE interval) to explain our B/Ca records, an amount not supported by SEM investigations at Site 1209 (Colosimo et al., 2005). And, if addition of B-free carbonate overgrowth were to account for the B/Ca decrease, then it could not affect the decrease documented in $\delta^{11}B$. Perhaps the strongest evidence against diagenetic alteration of the $\delta^{11}B$ records is the close agreement of resulting pH recorded at 3 different sites with varied lithologies and diagenetic regimes (see section 4.3).

Additionally, photosynthetic activity of symbiotic algae elevates the pH of the mixed layer-dwellers' calcifying microenvironment (Hönisch et al., 2003; Jorgensen et al., 1985; Rink et al., 1998), but severe warming could have led to the loss of symbionts, thus lowered both $\delta^{11}B$ and B/Ca. Symbiont loss has been inferred from a reduced $\delta^{13}C$-shell size relationship during the Middle Eocene Climatic Optimum (Edgar et al., 2013), and culturing studies have documented an effect of symbiont activity on $\delta^{11}B$ (Hönisch et al., 2003). However, the asymbiotic, thermocline-dwelling *Subbotina* also record a B/Ca excursion, which means that potential loss of symbionts cannot explain the entire B/Ca signal.

Additionally, we have measured $\delta^{11}B$ in two size fractions (250-300μm and 300-425μm) below and during the CIE, as well as within the recovery interval, and there is little or no difference between these size fractions (Table S2). Since symbiont activity affects $\delta^{11}B$-size relationships (Hönisch and Hemming, 2004), we conclude that the effects of symbiotic activity or its possible disappearance during the CIE on our $\delta^{11}B$ record is minimal. The mixed-layer species might also have migrated to deeper, cooler waters in response to warming, though this seems unlikely because the +5°C temperature increase recorded by Mg/Ca in the same shells is comparable to the global average (Dunkley-Jones et al., 2013; Sluijs et al., 2006; Zachos et al., 2006; Zachos et al., 2003).

We conclude that symbiont loss and/or depth migration cannot explain the entire trends in our records, but may have amplified the signal in B/Ca and $\delta^{11}B$ in *Morozovella* and *Acarinina*, so that the estimated pH changes should be viewed as maxima if these records are considered complete. However, it is also possible that a short phase of highly acidified conditions at the onset of the CIE is not represented in our B records due to dissolution and chemical erosion. Compared to other pelagic PETM sections, Site 1209 features minimal dissolution, and just a mm-scale clay-rich seam (Colosimo et al., 2005) representing the CIE onset. The time represented by this seam is unknown, but local recovery of carbonate deposition from this initial pulse of emissions would be relatively fast (<10 ky), so most of the main portion of CIE is represented as constrained by the correlation between $\delta^{13}C$ records (Figure S3).

Finally, changes in the Ca budget related to the global carbonate dissolution pulse (Komar and Zeebe, 2011) would produce changes in B/Ca and Mg/Ca much smaller than the analytical uncertainty in the techniques employed in this study. Moreover, the B/Ca signals are much larger than the analytical uncertainty, in contrast to those in studies of much smaller pH variations of the late Cenozoic (Allen and Hönisch, 2012). In sum, the potential contributions of complicating factors are minor compared to the magnitude of the anomalies in both the $\delta^{11}B$ and B/Ca records. We therefore interpret the decreases in both proxies at the onset of the PETM as ocean acidification signals.

4.2 Quantification of ΔpH from $\delta^{11}B$

To constrain the magnitude of the acidification documented by the B proxies, we calculate a range of ΔpH values from the *M. velascoensis* $\delta^{11}B$ record across the CIE onset (pre-PETM values versus CIE values). Computation of absolute pH from foraminiferal $\delta^{11}B$ requires knowledge of $\delta^{11}B_{seawater}$, which is unknown for the Paleogene, and of species-specific vital effects, which are difficult to calibrate in these now extinct species. However, $\delta^{11}B_{seawater}$ can be assumed constant over the ~300 ky time window considered here, because the oceanic residence time of B is >10My (Lemarchand et al., 2000). Furthermore, estimates of ΔpH independent of those parameters can be made by assuming a pre-PETM baseline pH (see supplement for full calculations). Using the magnitude of the $\delta^{11}B$-excursion, we calculate ΔpH for a range of assumed initial pH values between 7.5 and 8.2 (Figure 2). Due to reduced sensitivity in the fractionation of B isotopes at lower pH (Hemming and

Hanson, 1992), the resulting ΔpH is larger at lower assumed initial pH, and smaller at high (near-modern) assumed initial pH. Within the range of estimates of pre-PETM pH given by model simulations (Panchuk et al., 2008; Ridgwell and Schmidt, 2010; Zeebe et al., 2009a), the 0.8‰ decrease in $\delta^{11}B$ at the onset of the event is consistent with a ΔpH of -0.27 units, assuming a pre-PETM pH of 7.80 (total scale, consistent with 750 ppm atmospheric CO_2) (Panchuk et al., 2008), to -0.34 units, assuming a pre-PETM pH of 7.67 (total scale, consistent with 1000 ppm CO_2)(Figure 3).

Propagated uncertainties on ΔpH are calculated for two cases (Figure 2): 1) treating the Paleocene and CIE-interval $\delta^{11}B$ as coherent, normally-distributed populations and using a variance-weighted mean with associated propagated uncertainties, and 2) considering only the two $\delta^{11}B$ data points which span the P-E boundary, and using analytical uncertainty as a source of error (see SI for description of statistics and error propagation). Using the weighted mean allows smaller uncertainty (+/- 0.08 units in the pH=7.8 pre-PETM case, and +/- 0.11 units in the pH=7.67 pre-PETM case) than the second technique (+/- 0.13 units in the pH=7.8 pre-PETM case, and +/- 0.18 units in the pH=7.67 pre-PETM case). The first technique, however, rests on the assumption that the two populations of $\delta^{11}B$ are normally distributed around a coherent mean, which may not be the case, especially within the CIE when pH likely varied over time (Figure 5c). The second technique

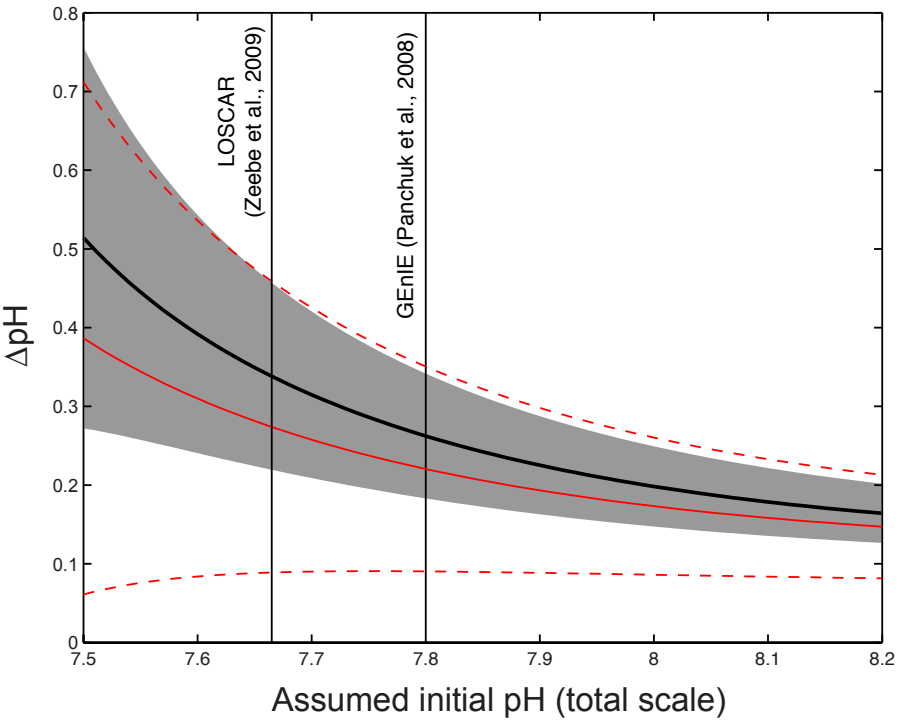
0.8
0.7
0.6
0.5
0.4
0.3
0.2
0.1
0
ΔpH
LOSCAR
(Zeebe et al., 2009)
GEnIE (Panchuk et al., 2008)
7.5
7.6
7.7
7.8
7.9
8
8.1
8.2
Assumed initial pH (total scale)

Figure 2: Calculated ΔpH as a function of assumed initial (pre-PETM) pH. Two sets of calculations are shown: 1) (black line and grey shading) $\delta^{11}B$ data from the Paleocene (n=7) and the CIE interval (n=6) are treated as populations, and calculations are performed on the variance-weighted mean of those populations with associated uncertainty propagated through the ΔpH calculation (pre-CIE $\delta^{11}B$ = 15.51‰ +/- 0.12, CIE $\delta^{11}B$ = 14.71‰ +/- 0.11). 2) (red) Only the two $\delta^{11}B$ data points spanning the P-E boundary are considered (15.35 +/- 0.30 and 14.76 +/- 0.40 for the latest Paleocene and earliest Eocene, respectively), and error is analytical uncertainty of $\delta^{11}B$ analysis propagated through the ΔpH calculation. Vertical lines represent the pre-event pH of two model simulations of the PETM.

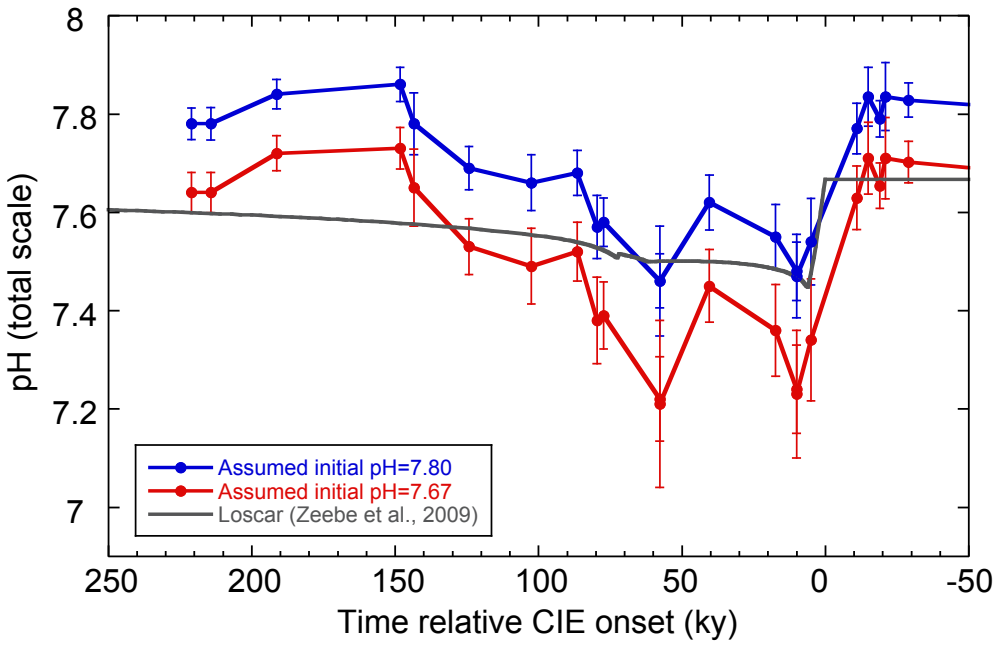
8
7.8
7.6
7.4
7.2
7
pH (total scale)
250
200
150
100
50
0
-50
Time relative CIE onset (ky)
Assumed initial pH=7.80
Assumed initial pH=7.67
Loscar (Zeebe et al., 2009)

Figure 3: Calculated pH versus time after the onset of the PETM. Two scenarios are plotted, one assuming an initial pH of 7.67 (after Zeebe et al., 2009, red) and one assuming initial pH of 7.80 (after Panchuk et al., 2008, blue). Error bars reflect 2 s.e. of individual boron isotope measurements as displayed in Figure 1. For comparison, the grey line shows the evolution of the surface pacific pH in Zeebe et al (2009)'s simulation.

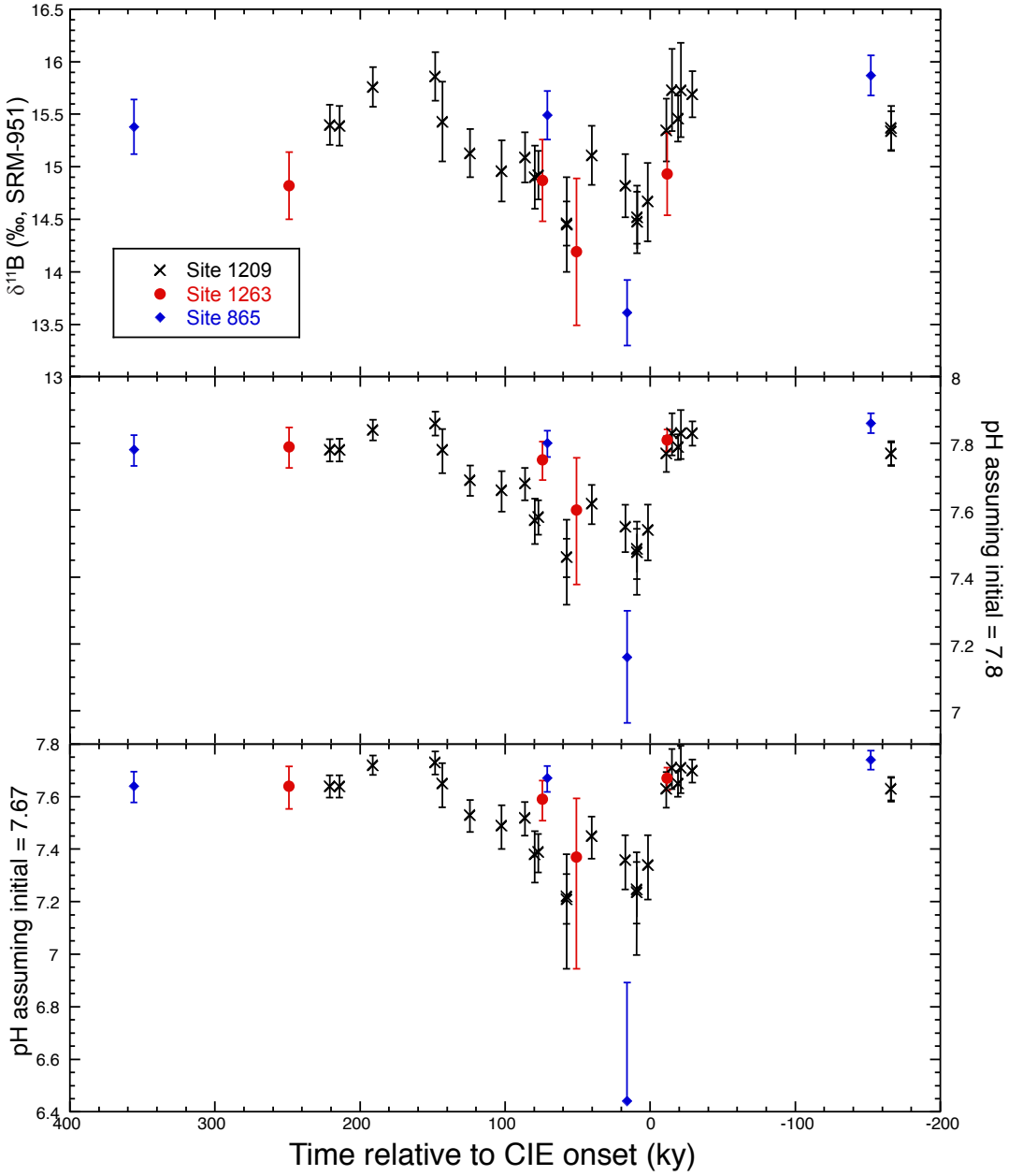
δ11B (‰, SRM-951)
Site 1209
Site 1263
Site 865
pH assuming initial = 7.67
pH assuming initial = 7.8
Time relative to CIE onset (ky)

Figure 4: $\delta^{11}B$ values and two scenarios for pH (total scale) from *M. velascoensis* at all three sites plotted against time. Age models for Sites 1263 and 1209 were produced by correlating the bulk/fine fraction $\delta^{13}C$ excursion to the $\delta^{13}C$ excursion at Site 690 in the age model of (Röhl et al., 2007); for Site 865 the benthic foraminiferal $\delta^{13}C$ record (Zachos et al., 2001) was correlated to that at Site 690, using the same age model. Error bars on $\delta^{11}B$ are 2 s.e. of repeat analyses (n>3), or 2 s.e. of repeat analyses of an in-house vaterite standard given the same n, whichever is larger. pH in the middle and lower panel were calculated by assuming the initial pH for the Site 1209 record of 7.8 and 7.67 (total scale), respectively, and then applying the same $\delta^{11}B$-pH relationship to all sites. Error bars reflect the uncertainty reported for $\delta^{11}B$ analyses. The lower error bar on one point in the CIE from Site 865 is incalculable because the lower error limit on the $\delta^{11}B$ of that point is below the minimum $\delta^{11}B$ in the $\delta^{11}B$-pH relationship.

avoids this assumption, but the two boundary-spanning data points are separated by 16 ky in our age model, so that this comparison does not necessarily capture the full magnitude of the ΔpH across the boundary.

Applying the same vital effect offset and $\delta^{11}B_{seawater}$ values at Sites 1209, 865 and 1263, pre-PETM pH-estimates from $\delta^{11}B$ are within ±0.05 pH units (Figure 4), suggesting that diagenesis is not a major concern, because it would have affected the three sites differently due to different burial depths, carbonate content, bottom water and pore water chemistry. The P-E interval at Site 865 (paleodepth ~1400m) is a winnowed foraminiferal sand (nearly 100% $CaCO_3$), bearing planktic foraminifers with significant overgrowth (Kelly et al., 1996; Kozdon et al., 2013). Site 1209 (paleodepth ~1900m) foraminifers are lightly overgrown (Colosimo et al., 2005) while Site 1263 (paleodepth ~1500m) features clay-rich sediments (~85% $CaCO_3$) with excellent foraminiferal preservation (Kelly et al., 2010) but a larger clay layer indicating more intense dissolution (Zachos et al., 2005). Depending on the initial pH, our Site 1209 $\delta^{11}B$ data allow for a wide range of ΔpH values (i.e., larger if a lower initial pH is assumed and smaller if a higher initial pH is assumed (Figure 2), though an initial pH far outside the range in Figure 2, and assuming realistic values for other carbonate chemistry parameters, would be irreconcilable with independent estimates for Paleocene pCO_2 (Beerling and Royer, 2011).

4.3 Significance of the B/Ca Excursion

The B/Ca data allow us to independently evaluate the magnitude of acidification in surface waters at the onset of the PETM. Based on theoretical and

laboratory studies, a pH decrease as estimated from the anomaly in $\delta^{11}B$ should also lower the B/Ca of foraminifera (Allen et al., 2012), as indeed recorded at Site 1209. In order to estimate changes in pH from B/Ca, however, we must apply calibrations for modern foraminifer species, which, in contrast to $\delta^{11}B$ vs. pH relationships, vary in sensitivity between species. We assume that extinct species shared a similar range of sensitivities as living species, but the approach is complicated by the dual response of planktic B/Ca to varying $[B(OH)_4^-]$ and DIC, where carbonate and borate ion appear to compete for lattice sites during calcification(Allen et al., 2012). Although the concentrations of aqueous borate and carbonate ions are coupled during a rapid ocean acidification event and fall with decreasing pH (Zeebe et al., 2009a), the carbon pulse at the onset of the PETM led to an increase in DIC, which may have amplified the B/Ca decrease through decreasing $B(OH)_4^-$/DIC (Figure 5c). In the later phase of the event (>10 ky after the CIE onset), terrestrial weathering increased the flux of alkalinity and DIC to the ocean which decoupled pH and carbonate ion concentration (Hönisch et al., 2012), leading to slower recovery of $[B(OH)_4^-]$/DIC (and thus B/Ca) than surface ocean carbonate saturation (Figure 5c). As such, a direct, quantitative estimate of carbonate chemistry from raw B/Ca data carries uncertainty at present. Nevertheless, the direction, magnitude and timing of the B/Ca excursions are qualitatively consistent with rapid and sustained reductions in thermocline and surface ocean pH, lasting as long as the peak carbon isotope excursion (>70 ky).

4.4 Model-data comparison

Within the limitations of these uncertainties, we employed a simple strategy to evaluate the magnitude of ocean acidification in our B/Ca record through comparison with modeled environmental parameters. Zeebe et al. (2009a) simulated PETM carbon release with a global carbon cycle model (LOSCAR) constrained by observations of the global CIE and sediment $\%CaCO_3$ which document changes in the position of the CCD. The best fit to available data involves the rapid release of 3,000 Pg C in 6 ky, followed by an additional release of 1480 Pg C over the following 72 ky. This results in an ~700 ppmv CO_2 increase, ~0.18 unit surface pH decrease (Figure 3), and 25% reduction in surface carbonate saturation state. To estimate how modern foraminiferal B/Ca would respond to this scenario, we applied empirical calibrations (Allen et al., 2012; Allen et al., 2011b) that relate B/Ca in the modern species *Globigerinoides ruber, Globigerinoides sacculifer, and Orbulina universa* to ($[B(OH)_4^-]$/DIC). Two interpretations of the culture-based calibrations are used: (a) B/Ca responds to absolute changes in $[B(OH)_4^-]$/DIC, and (b) B/Ca responds to the relative change in $[B(OH)_4^-]$/DIC. The latter may be more appropriate for the PETM because the initial (pre-event) $[B(OH)_4^-]$/DIC predicted by the model is very different from the value in modern seawater in culture experiments (see supplement and Figure S1). In both cases, $[B(OH)_4^-]$/DIC is largely controlled by pH, with additional amplification due to increasing DIC from the carbon input, carbonate dissolution, and enhanced weathering. We then compared these model-derived B/Ca estimates with the measured B/Ca of the PETM mixed layer-dwellers (Figure 5).

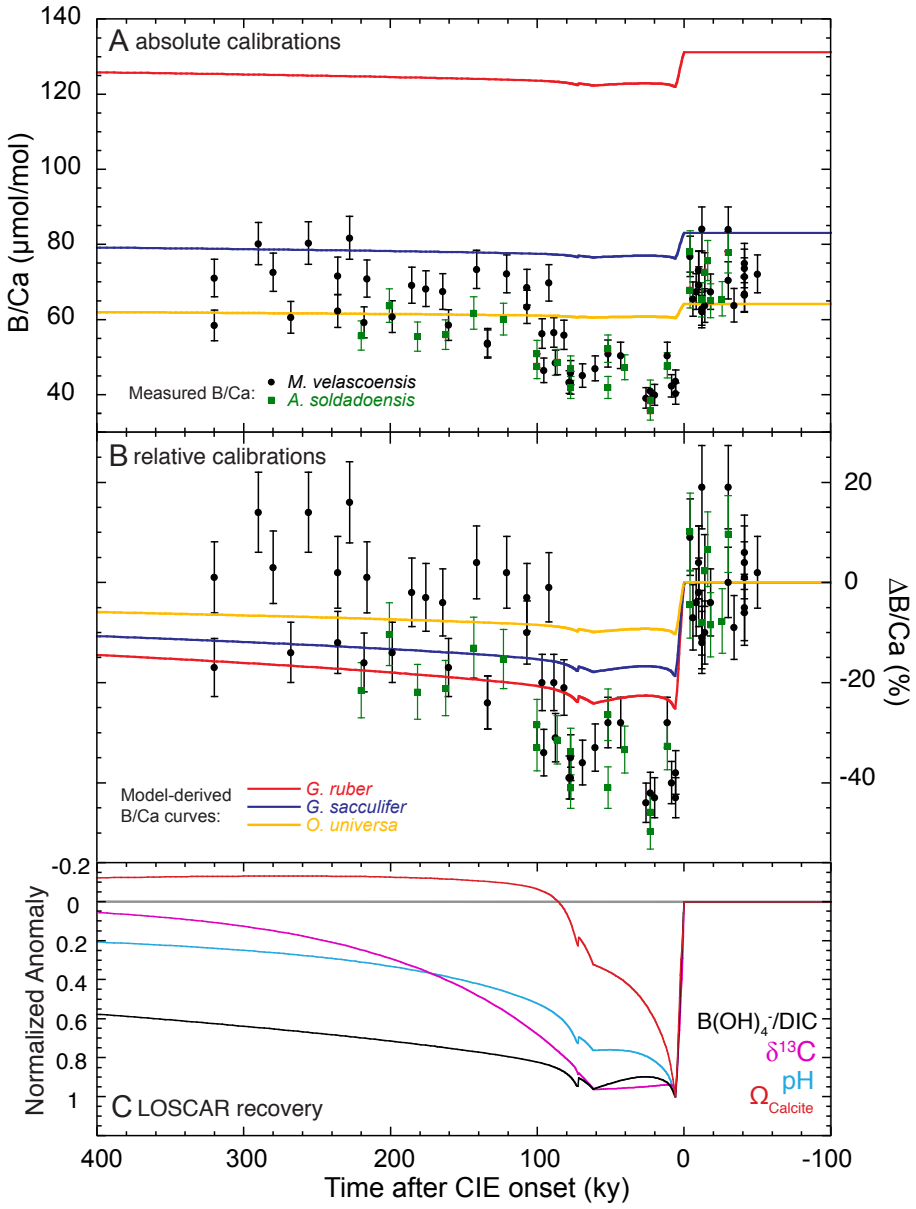
A absolute calibrations
B/Ca (µmol/mol)
Measured B/Ca:
M. velascoensis
A. soldadoensis
B relative calibrations
ΔB/Ca (%)
Model-derived B/Ca curves:
G. ruber
G. sacculifer
O. universa
Normalized Anomaly
B(OH)4-/DIC
δ13C
pH
ΩCalcite
C LOSCAR recovery
Time after CIE onset (ky)

Figure 5: Model-data comparison of the PETM B/Ca anomaly. Symbols with error bars are B/Ca measured in mixed-layer dwelling foraminifers from Core 198-1209B-22H, plotted against a timescale derived from correlating the fine-fraction CIE at that site to the orbitally-tuned age model of ODP Site 690 (Röhl et al., 2007) (see supplementary Figure S3). Note that this age model produces a conservative estimate of the CIE duration (~100 ky) compared to other age models which suggest a duration up to ~200 ky (Murphy et al., 2010), so time after the CIE onset of the B/Ca data should be taken as a minimum. Colored lines are model-derived predictions generated by applying the "absolute" and "relative" cultured B/Ca calibrations of three modern foraminifer species (Allen et al., 2012; Allen et al., 2011b) to the mixed layer water carbonate chemistry conditions calculated for the low-latitude surface Pacific by the best-fit PETM simulation of the LOSCAR carbon-cycle model (Zeebe et al., 2009a) (see SI for discussion of timescale and calibrations). Top panel (A) shows measured B/Ca ratios (μmol/mol) compared with model-derived curves using the absolute calibration. Middle panel (B) expresses the B/Ca anomaly as a % change relative to the Paleocene baseline along with model-derived curves using the relative calibration. Bottom Panel (C) shows normalized excursions in pH, surface Pacific $\delta^{13}C$, $\Omega_{calcite}$, and $B(OH)_4^-$/DIC (where 0 represents initial Paleocene values and 1 represents PETM minima) demonstrating the different timescales of recovery between model parameters. Horizontal grey line represents pre-event conditions for all parameters.

Predicting baseline B/Ca using model-derived pH and DIC constraints combined with modern proxy calibrations yields B/Ca values within the range of observed pre-PETM B/Ca values (Figure 5), implying that the extinct species incorporated boron in roughly the same proportion as some modern species. The model-derived curves also match the overall shape of the B/Ca excursion: a rapid decrease at the CIE onset, followed by an interval of low values that roughly coincides with the duration of the global CIE, and finally a gradual recovery. However, our model-derived B/Ca curves predict a decrease of only 6-8% for the absolute calibrations, 10-25% for the relative calibrations at the onset of the PETM (Figure 5b), as compared to the much larger ~40% decline recorded by fossil shells across the PETM. This suggests that, at face value, the B/Ca data indicate more severe acidification than predicted by the model. Similarly, the LOSCAR best fit simulation (Zeebe et al., 2009a) involves a total ~4500 Pg C input and results in an ~0.18 pH unit decrease, whereas the $\delta^{11}B$ data imply a ΔpH of -0.33 units if calibrated to LOSCAR's initial pH of 7.67 (total scale), also a significantly greater acidification than simulated by the model. There are several potential explanations for the greater acidification implied by both B/Ca and $\delta^{11}B$ than predicted by the model.

In addition to the possible minor amplification of symbiont loss discussed above, the partitioning of B/Ca in extinct species might have been more sensitive to changes in carbonate chemistry than in modern species. This is unlikely, given that their B/Ca values are at the low end of the range reported from modern foraminifera,

thus consistent with what modern foraminifera living in low-pH (Hönisch et al., 2012) and low [B] (Lemarchand et al., 2000) Paleogene seawater might record.

Differences in [B] and $[B(OH)_4^-]$/DIC of Paleogene seawater chemistry from culture calibration conditions (Allen et al., 2012) or the initial boundary conditions of model simulations represent a source of uncertainty. For example, models for the late Paleocene estimate a total [B] of seawater 10% lower than modern (Lemarchand et al., 2000), and [Ca] may have been twice as high as modern (Tyrrell and Zeebe, 2004). Also, the LOSCAR simulations are run from an equilibrium concentration of 1000 ppmv atmospheric CO_2, (Berner and Kothavala, 2001) but Paleocene CO_2 levels may have differed by several hundred ppmv (e.g., Panchuk et al. (2008) use an initial pCO_2 of 750 ppmv), which would affect the initial $[B(OH)_4^-]$/DIC ratio in the model, as well as require a smaller ΔpH based on $\delta^{11}B$ (Figure 2).

A final potential explanation is that the one standard simulation considered in this paper underestimates the mass of carbon released during the PETM, or does not capture the sensitivity of simulated pH changes to variations in model parameters. The large ΔpH estimated from our Site 1209 $\delta^{11}B$ and B/Ca appears more consistent with the upper end of the range of estimates of modeling studies constrained by other observational constraints on ocean carbonate chemistry (i.e., the CCD) (Panchuk et al., 2008; Ridgwell and Schmidt, 2010; Zeebe et al., 2009a). Such comparisons with models, however, hinge on a number of key assumptions, including the initial boundary conditions for ocean chemistry including DIC, pH, initial depth of the CCD, and more. For instance, the simulated ΔpH in the standard run is ~0.18 units at

t = 20 ky after the onset. However, in a simulation including a moderate rise in remineralization of marine organic carbon at intermediate depth in response to the PETM warming (Matsumoto, 2007; Zeebe, 2013) and small changes in the timing of the gradual, additional carbon release, ΔpH is ~0.24 units at t = 20 ky. This number is closer to the ~0.3 units based on $\delta^{11}B$ and illustrates the sensitivity of model-calculated ΔpH to parameters other than carbon input. Similarly, simply initializing LOSCAR to a higher initial surface pH (lower atmospheric pCO_2 concentration) would help reconcile the modeled ΔpH with that based on $\delta^{11}B$ without invoking larger carbon release. Importantly, invoking a larger carbon release during the PETM would have to be reconciled with other observations, specifically the response of the CCD. Records of weight %$CaCO_3$ at Pacific drill sites constrain the initial CCD shoaling in that basin to less than 500m at the onset of the PETM, and modeling simulations invoking a larger carbon release (without compensatory effects such as changing ocean circulation) result in much more pronounced shoaling of the Pacific CCD than observed (Sluijs et al., 2012b).

There are implications for two aspects of the duration and rate of recovery of acidification in our records compared to model simulations. First, the duration of acidified conditions as indicated by the $\delta^{11}B$ and B/Ca record is long, at least 70 ky. Both GENIE (Panchuk et al., 2008) and LOSCAR (Zeebe et al., 2009a) simulations of the PETM are unable to sustain acidified surface ocean conditions for this duration with a single brief (<10 ky) pulse of carbon at the onset of the event. A sustained acidification is more consistent with a scenario of a large, rapid initial pulse of

carbon, followed by a slower, gradual release of carbon, perhaps as a feedback to the initial release (Zeebe, 2013; Zeebe et al., 2009a). Such a gradual release must have persisted as long as the CIE, or a minimum of ~70 ky using our age model (Figure S3). Alternatively, the sustained acidification could result from multiple emission pulses of carbon spaced sufficiently close together (10's of ky apart) that pH does not have time to recover between pules, though there is no obvious evidence for such in marine or continental carbon isotope records. Second, the recovery in $\delta^{11}B$ and B/Ca values is faster (<200 ky) than the >400 ky duration in the LOSCAR simulation, and this is not an artifact of age models. For example, had we used the age model of Murphy et al. (2010), the recovery in our proxies would be more gradual (occurring over ~150 ky rather than the ~100 ky in our age model), but not nearly as prolonged as in the model. This may indicate that B/Ca could actually track a carbonate chemistry parameter other than $B(OH)_4^-$/DIC, or a combination of parameters including Ω, which would be consistent with Ω recovering more quickly than other parameters in our simulation (Figure 5). Alternatively, the recovery may have been accelerated by carbon removal processes not accounted for in the model, such as enhanced organic burial (Bowen and Zachos, 2010). As the simulation of surface saturation is highly sensitive to model-dependent feedbacks (i.e., weathering, export production, etc.) some of which can vary regionally, a full assessment requires data from multiple locations and further analysis.

5. Conclusions

Our records indicate abrupt and sustained acidification of the upper ocean coincident with the onset of the PETM, consistent with a scenario of massive carbon release. The magnitude of acidification (ΔpH of about 0.3 units) appears most consistent with the upper end of carbon release scenarios, although this calculation is subject to significant uncertainties. The timing of the $\delta^{11}B$ and B/Ca excursions is tightly coupled to the Mg/Ca-based temperature excursion (Figure S2), confirming the link between low pH/high pCO_2 and globally elevated temperatures. The total cumulative mass of carbon released during the PETM may have been similar to that anticipated for future anthropogenic carbon emissions of 5,000 Pg C, but the rate of carbon release was likely at least an order of magnitude slower (Zeebe and Zachos, 2012) resulting in significantly more gradual and less severe surface ocean acidification. Calcareous plankton may thus have had the opportunity to adapt, either through migration or possibly through evolution(Hönisch et al., 2012). Therefore, the lack of major extinction of planktic calcifiers during the PETM cannot be taken as evidence that modern calcifiers are insensitive to anthropogenic ocean acidification.

Acknowledgements: I thank Dyke Andreasen, Linda Anderson, Rob Franks, and Jeremy Hourigan for technical support and Steve Bohaty for supplying Site 1209 fine fraction stable isotope data. Andy Ridgwell, Tim Bralower, Tim Lyons and five anonymous reviewers provided productive feedback on different versions of the manuscript. This work was funded by the US National Science Foundation under grants OCE-0903014, OCE09-02869, OCE12-20602, and OCE12-20554.

References

Allen, K. A., and B. Hönisch (2012), The planktic foraminiferal B/Ca proxy for seawater carbonate chemistry: A critical evaluation, *Earth and Planetary Science Letters*, *345–348*(0), 203-211.

Allen, K. A., B. Hönisch, S. M. Eggins, and Y. Rosenthal (2012), Environmental controls on B/Ca in calcite tests of the tropical planktic foraminifer species Globigerinoides ruber and Globigerinoides sacculifer, *Earth and Planetary Science Letters*, *351–352*(0), 270-280.

Allen, K. A., B. Hönisch, S. M. Eggins, J. Yu, H. J. Spero, and H. Elderfield (2011), Controls on boron incorporation in cultured tests of the planktic foraminifer< i> Orbulina universa</i>, *Earth and Planetary Science Letters*, *309*(3), 291-301.

Beerling, D., and D. L. Royer (2011), Convergent Cenozoic CO2 history, *Nature Geoscience*, *4*, 418-420.

Berggren, W. A., and R. D. Norris (1997), Biostratigraphy, phylogeny and systematics of Paleocene trochospiral planktic foraminifera, *Micropaleontol*, *43*, 1-116.

Bowen, G. J., and J. C. Zachos (2010), Rapid carbon sequestration at the termination of the Palaeocene-Eocene Thermal Maximum, *Nature Geoscience*, *3*(12), 866-869.

Bown, P., and P. Pearson (2009), Calcareous plankton evolution and the Paleocene/Eocene thermal maximum event: New evidence from Tanzania, *Marine Micropaleontology*, *71*(1-2), 60-70.

Bralower, T. J., I. Premoli-Silva, M. Malone, and e. al. (2002), *Proc. ODP, Initial Reports*, Ocean Drilling Program, College Station, TX.

Bralower, T. J., J. C. Zachos, E. Thomas, M. Parrow, C. K. Paull, D. C. Kelly, I. P. Silva, W. V. Sliter, and K. C. Lohmann (1995), Late Paleocene to Eocene Paleoceanography of the Equatorial Pacific Ocean - Stable Isotopes Recorded At Ocean Drilling Program Site 865, Allison Guyot, *Paleoceanography*, *10*(4), 841-865.

Coadic, R., F. Bassinot, D. Dissard, E. Douville, M. Greaves, and E. Michel (2013), A core−top study of dissolution effect on B/Ca in Globigerinoides sacculifer from the tropical Atlantic: Potential bias for paleo−reconstruction of seawater carbonate chemistry, *Geochemistry, Geophysics, Geosystems*, *14*(4), 1053-1068.

Colosimo, A. B., T. J. Bralower, and J. C. Zachos (2005), Evidence for lysocline shoaling and methane hydrate dissociation at the Paleocene-Eocene thermal maximum on Shatsky Rise, ODP Leg 198, in *Proc. ODP, Sci. Results*, edited by T. J. Bralower, I. Premoli Silva and M. Malone, Ocean Drilling Program, College Station, TX.

D'Hondt, S., J. C. Zachos, and G. Schultz (1994), Stable Isotopic Signals and Photosymbiosis in Late Paleocene Planktic Foraminifera, *Paleobiology*, *20*(3), 391-406.

Dickens, G. R., M. M. Castillo, and J. C. G. Walker (1997), A blast of gas in the latest Paleocene: Simulating first-order effects of massive dissociation of oceanic methane hydrate, *Geology*, *25*(3), 259-262.

Dunkley-Jones, T., D. J. Lunt, D. N. Schmidt, A. Ridgwell, A. Sluijs, P. J. Valdes, and M. Maslin (2013), Climate model and proxy data constraints on ocean warming across the Paleocene-Eocene Thermal Maximum, *Earth-Science Reviews*, *125*, 123-145.

Edgar, K., S. Bohaty, S. Gibbs, P. Sexton, R. Norris, and P. Wilson (2013), Symbiont 'bleaching'in planktic foraminifera during the Middle Eocene Climatic Optimum, *Geology*, *41*(1), 15-18.

Farley, K. A., and S. F. Eltgroth (2003), An alternative age model for the Paleocene-Eocene thermal maximum using extraterrestrial He-3, *Earth and Planetary Science Letters*, *208*(3-4), 135-148.

Foster, G. L., C. H. Lear, and J. W. Rae (2012), The evolution of pCO2, ice volume and climate during the middle Miocene, *Earth and Planetary Science Letters*, *341*, 243-254.

Gibbs, S. J., H. M. Stoll, P. R. Bown, and T. J. Bralower (2010), Ocean acidification and surface water carbonate production across the Paleocene-Eocene thermal maximum, *Earth and Planetary Science Letters*, *295*(3-4), 583-592.

Gibbs, S. J., P. R. Bown, J. A. Sessa, T. J. Bralower, and P. A. Wilson (2006), Nannoplankton extinction and origination across the Paleocene-Eocene Thermal Maximum, *Science*, *314*(5806), 1770-1773.

Hemming, N. G., and G. N. Hanson (1992), Boron isotopic composition and concentration in modern marine carbonates, *Geochimica et Cosmochimica Acta*, *56*, 537-543.

Hemming, N. G., and G. N. Hanson (1994), A procedure for the isotopic analysis of boron by negative thermal ionization mass spectrometry, *Chem. Geol.*, *114*, 147-156.

Henehan, M. J., et al. (2013), Calibration of the boron isotope proxy in the planktonic foraminifera Globigerinoides ruber for use in palaeo-CO2 reconstruction, *Earth and Planetary Science Letters*, *364*(0), 111-122.

Hönisch, B., and N. G. Hemming (2004), Ground-truthing the boron isotope paleo-*p*H proxy in planktonic foraminifera shells: Partial dissolution and shell size effects, *Paleoceanography*, *19*, doi:10.1029/2004PA001026.

Hönisch, B., and N. G. Hemming (2005), Surface ocean pH response to variations in pCO_2 through two full glacial cycles, *Earth and Planetary Science Letters*, *236*(1-2), 305-314.

Hönisch, B., N. G. Hemming, and B. Loose (2007), Comment on "A critical evaluation of the boron isotope-pH proxy: The accuracy of ancient ocean pH estimates" by M. Pagani, D. Lemarchand, A. Spivack and J. Gaillardet, *Geochimica et Cosmochimica Acta*, *71*(6), 1636-1641.

Hönisch, B., J. Bijma, A. D. Russell, H. J. Spero, M. R. Palmer, R. E. Zeebe, and A. Eisenhauer (2003), The influence of symbiont photosynthesis on the boron isotopic composition of foraminifera shells, *Marine Micropaleontology*, *49*(1-2), 87-96.

Hönisch, B., et al. (2012), The Geological Record of Ocean Acidification, *Science*, *335*(6072), 1058-1063.

Jorgensen, B. B., J. Erez, N. P. Revsbech, and Y. Cohen (1985), Symbiotic photosynthesis in a planktonic foraminiferan, Globigerinoides sacculifer (Brady), studied with microelectrodes, *Limnol. Oceanogr*, *30*(6), 1253-1267.

Kakihana, H., M. Kotaka, S. Satoh, M. Nomura, and M. Okamoto (1977), Fundamental studies on the ion-exchange of boron isotopes, *Bull. Chem. Soc. Japan*, *50*, 158-163.

Kelly, D. C., T. J. Bralower, J. C. Zachos, I. P. Silva, and E. Thomas (1996), Rapid Diversification of Planktonic Foraminifera in the Tropical Pacific (Odp Site 865) During the Late Paleocene Thermal Maximum, *Geology*, *24*(5), 423-426.

Kelly, D. C., T. M. J. Nielsen, H. K. McCarren, J. C. Zachos, and U. Rohl (2010), Spatiotemporal patterns of carbonate sedimentation in the South Atlantic: Implications for carbon cycling during the Paleocene-Eocene thermal maximum, *Palaeogeography Palaeoclimatology Palaeoecology*, *293*(1-2), 30-40.

Kennett, J. P., and L. D. Stott (1991), Abrupt Deep-Sea Warming, Palaeoceanographic Changes and Benthic Extinctions At the End of the Palaeocene, *Nature*, *353*(6341), 225-229.

Koch, P. L., J. C. Zachos, and P. D. Gingerich (1992), Correlation Between Isotope Records in Marine and Continental Carbon Reservoirs Near the Palaeocene Eocene Boundary, *Nature*, *358*(6384), 319-322.

Komar, N., and R. Zeebe (2011), Oceanic calcium changes from enhanced weathering during the Paleocene-Eocene Thermal Maximum: No effect on calcium-based proxies, *Paleoceanography*, *26*, 1-13.

Kozdon, R., D. C. Kelly, N. T. Kita, J. H. Fournelle, and J. W. Valley (2011), Planktonic foraminiferal oxygen isotope analysis by ion microprobe technique suggests warm tropical sea surface temperatures during the Early Paleogene, *Paleoceanography*, *26*(3), 1-17.

Kozdon, R., D. Kelly, K. Kitajima, A. Strickland, J. Fournelle, and J. Valley (2013), In situ δ18O and Mg/Ca analyses of diagenetic and planktic foraminiferal calcite preserved in a deep−sea record of the Paleocene−Eocene thermal maximum, *Paleoceanography*, *28*(3), 517-528.

Lemarchand, D., J. Gaillardet, É. Lewin, and C. J. Allègre (2000), The influence of rivers on marine boron isotopes and implications for reconstructing past ocean *p*H, *Nature*, *408*, 951-954.

Matsumoto, K. (2007), Biology−mediated temperature control on atmospheric pCO2 and ocean biogeochemistry, *Geophysical Research Letters*, *34*(20), 1-5.

McInerney, F. A., and S. Wing (2011), The Paleocene-Eocene Thermal Maximum: A Perturbation of Carbon Cycle, Climate, and Biosphere with Implications for the future, *Annual Review of Earth & Planetary Sciences*, *39*, 489-516.

Murphy, B. H., K. A. Farley, and J. C. Zachos (2010), An extraterrestrial He-3-based timescale for the Paleocene-Eocene thermal maximum (PETM) from Walvis Ridge, IODP Site 1266, *Geochimica Et Cosmochimica Acta*, *74*(17), 5098-5108.

Pagani, M., K. Caldeira, D. Archer, and J. C. Zachos (2006), An ancient carbon mystery, *Science*, *314*(5805), 1556-1557.

Panchuk, K., A. Ridgwell, and L. R. Kump (2008), Sedimentary response to Paleocene-Eocene Thermal Maximum carbon release: A model-data comparison, *Geology*, *36*(4), 315-318.

Pearson, P. N., G. L. Foster, and B. S. Wade (2009), Atmospheric carbon dioxide through the Eocene-Oligocene climate transition, *Nature*, *461*(7267), 1110-1113.

Raffi, I., and B. De Bernardi (2008), Response of calcareous nannofossils to the Paleocene–Eocene Thermal Maximum: Observations on composition, preservation and calcification in sediments from ODP Site 1263 (Walvis Ridge—SW Atlantic), *Marine Micropaleontology*, *69*(2), 119-138.

Raffi, I., J. Backman, and H. Palike (2005), Changes in calcareous nannofossil assemblages across the Paleocene/Eocene transition from the paleo-equatorial Pacific Ocean, *Palaeogeography Palaeoclimatology Palaeoecology*, *226*(1-2), 93-126.

Raffi, I., J. Backman, J. C. Zachos, and A. Sluijs (2009), The response of calcareous nannofossil assemblages to the Paleocene Eocene Thermal Maximum at the Walvis Ridge in the South Atlantic, *Marine Micropaleontology*, *70*(3-4), 201-212.

Raitzsch, M., and B. Hönisch (2013), Cenozoic boron isotope variations in benthic foraminifers, *Geology*, *41*(5), 591-594.

Ridgwell, A., and D. N. Schmidt (2010), Past Constraints on the vulnerability of marine calcifiers to massive carbon dioxide release, *Nature Geoscience*, *3*, 196-200.

Rink, S., M. Kühl, J. Bijma, and H. J. Spero (1998), Microsensor studies of photosynthesis and respiration in the symbiotic foraminifer *Orbulina universa*, *Mar. Biol.*, *131*(4), 583-595.

Röhl, U., T. Westerhold, T. J. Bralower, and J. C. Zachos (2007), On the duration of the Paleocene-Eocene thermal maximum (PETM), *Geochemistry Geophysics Geosystems*, *8*, -.

Sanyal, A., M. Nugent, R. J. Reeder, and J. Bijma (2000), Seawater *p*H control on the boron isotopic composition of calcite: Evidence from inorganic calcite precipitation experiments, *Geochim. Cosmochim. Ac.*, *64*(9), 1551-1555.

Sanyal, A., J. Bijma, H. J. Spero, and D. W. Lea (2001), Empirical relationship between *p*H and the boron isotopic composition of *G. sacculifer*: Implications for the boron isotope paleo-*p*H proxy, *Paleoceanography*, *16*(5), 515-519.

Sanyal, A., N. G. Hemming, W. S. Broecker, D. W. Lea, H. J. Spero, and G. N. Hanson (1996), Oceanic Ph Control on the Boron Isotopic Composition of Foraminifera - Evidence from Culture Experiments, *Paleoceanography*, *11*(5), 513-517.

Simon, L., C. Lecuyer, C. Marechal, and N. Coltice (2006), Modelling the geochemical cycle of boron: Implications for the long-term $\delta^{11}B$ evolution of seawater and oceanic crust, *Chemical Geology*, *22*(1-2), 15.

Sluijs, A., J. C. Zachos, and R. E. Zeebe (2012), Constraints on hyperthermals, *Nature Geosci*, *5*(4), 231-231.

Sluijs, A., et al. (2006), Subtropical arctic ocean temperatures during the Palaeocene/Eocene thermal maximum, *Nature*, *441*(7093), 610-613.

Takeda, K., and K. Kaiho (2007), Faunal turnovers in central Pacific benthic foraminifera during the Paleocene–Eocene thermal maximum, *Palaeogeography, Palaeoclimatology, Palaeoecology*, *251*(2), 175-197.

Thomas, E., and N. J. Shackleton (1996), The Paleocene-Eocene benthic foraminiferal extinction and stable isotope anomalies, in *Correlation of the early Paleogene in Northwest Europe*, edited by R. W. O. B. Knox, R. M. Corfield and R. E. Dunay, pp. 401-441, London.

Tyrrell, T., and R. E. Zeebe (2004), History of carbonate ion concentration over the last 100 million years, *Geochimica Et Cosmochimica Acta*, *68*(17), 3521-3530.

Yu, J., H. Elderfield, and B. Hönisch (2007), B/Ca in planktonic foraminifera as a proxy for surface seawater pH, *Paleoceanography*, *22*(2), 1-17.

Zachos, J., M. Pagani, L. Sloan, E. Thomas, and K. Billups (2001), Trends, rhythms, and aberrations in global climate 65 Ma to present, *Science*, *292*(5517), 686-693.

Zachos, J. C., D. Kroon, P. Blum, and e. al. (2004), *Proc. ODP, Initial Reports*, College Station.

Zachos, J. C., M. W. Wara, S. Bohaty, M. L. Delaney, M. R. Petrizzo, A. Brill, T. J. Bralower, and I. Premoli-Silva (2003), A Transient Rise in Tropical Sea Surface Temperature During the Paleocene-Eocene Thermal Maximum, *Science*, *302*(5650), 1551-1554.

Zachos, J. C., S. Schouten, S. Bohaty, T. Quattlebaum, A. Sluijs, H. Brinkhuis, S. J. Gibbs, and T. J. Bralower (2006), Extreme warming of mid-latitude coastal ocean

during the Paleocene-Eocene Thermal Maximum: Inferences from TEX86 and isotope data, *Geology*, *34*(9), 737-740.

Zachos, J. C., et al. (2005), Rapid Acidification of the Ocean During the Paleocene-Eocene Thermal Maximum, *Science*, *308*(5728), 1611-1615.

Zeebe, R., and J. Zachos (2012), Long-term legacy of massive carbon input to the Earth system: Anthropocene vs. Eocene, *Philosophical Transactions of the Royal Society*, 1-22.

Zeebe, R. E. (2013), What caused the long duration of the Paleocene−Eocene Thermal Maximum?, *Paleoceanography*, *26*, 1-13.

Zeebe, R. E., J. C. Zachos, and G. R. Dickens (2009), Carbon dioxide forcing alone insufficient to explain Palaeocene-Eocene Thermal Maximum warming, *Nature Geoscience*, *2*(8), 576-580.

Supplementary Material for Chapter 1: Rapid and sustained surface ocean acidification during the Paleocene-Eocene Thermal Maximum

Boron isotope analyses:

Sample preparation for boron isotope analyses followed established trace metal cleaning procedures (Barker et al., 2003a), and included crushing 100-220 *M. velascoensis* shells (from the 250-300 and 300-425 μm size fractions, corresponding to ~1-2 mg $CaCO_3$) between two glass slides, clay removal in methanol, oxidative treatment in hot buffered H_2O_2 to remove organic matter, and weak acid leaches to remove any adsorbed contaminants. Samples were then dried, weighed to determine the weight of cleaned samples, and finally dissolved in 2 M suprapure HCl (Fisher Optima, <100 ppt B; ng/kg), using the B concentrations determined by ICP-MS to yield sample solutions with approximately 1 ng B/μl. Immediately following dissolution, samples were centrifuged to separate any insoluble residue, and 1μl of sample solution plus 1μl of boron-free seawater (prepared with Amberlite IRA-743 anion exchange resin) were then loaded onto outgassed zone refined Rhenium filaments, evaporated at an ion current of 0.5A until the load was reduced to a gel, and subsequently mounted into the mass spectrometer. All cleaning and loading procedures were done in PTFE (boron free) filtered laminar flow benches.

Boron isotopes were measured as BO_2^- ions on masses 43 and 42 on a Thermo Scientific Triton multi-collector TIMS. Isotope analyses by TIMS are subject to time-

dependent in-run mass fractionation. Therefore mass fractionation has to be kept minimal, and a strict analytical protocol has to be followed for data collection and acceptance. Mass fractionation can be minimized by heating the sample slowly over a period of 25 minutes, until the analysis temperature of 980°C is reached. The signal intensity is then optimized by repeated ion beam focusing, until a minimum signal intensity of 100 mV is reached, and the signal intensity is stable or slowly rising. This can take 5-10 minutes, and in few cases the temperature has to be increased further (up to 1020°C) to yield 100 mV. In all cases some aliquots are successfully measured at 980°C, and comparison of carbonate data shows no systematic difference in aliquots measured across this temperature range. Data collection starts immediately upon achieving the 100 mV signal. Data are acquired for a minimum of 25 minutes giving 240 ion ratios, and up to 45 min with 400 ratios for small signal intensities. In-run fractionation is considered excessive and unacceptable if the 43/42 ratio of an analysis increases by >0.004 (i.e. 1‰ in $\delta^{11}B$) over the data collection period (25-45 min). Such analyses are excluded from further consideration. In addition, it has been suggested that organic matter can form CNO^- molecules, which could interfere on mass 42 and bias the measured boron isotope ratio (Hemming and Hanson, 1994). At the beginning of each analysis, the presence of potential organic matter interference is monitored by scanning for CN^- on mass 26, using an electron multiplier, and analyses with >2000 counts/sec on mass 26 are rejected. Data rejection based on this second criterion is extremely rare, as the signal on mass 26 is typically very low (60-200

counts/sec). Total procedural blank for boron isotope analysis is 10 ± 3pg B, or ~1% of the B in the sample aliquot.

Boron isotope ratios are reported relative to the boron isotopic composition of SRM 951 boric acid standard, where $\delta^{11}B$ (‰) = $(43/42_{sample} / 43/42_{standard} -1)*1000$. The measurement uncertainty of carbonate samples is estimated as 2se ($2sd/\sqrt{n}$) of repeat measurements of the same sample solution, where a minimum of n=3 acceptable analyses is required. The data population may include up to n=10 analyses to reduce analytical uncertainty. Only those analyses are considered acceptable that neither fractionate excessively nor display significant signal on mass 26. Data are reported as the average of the acceptable data population, and 2se of this population is reported.

In addition to the SRM 951 boric acid standard we also routinely measure an in-house carbonate standard, which is SRM 951 precipitated in $CaCO_3$ (vaterite) and loaded with boron-free seawater, similar to carbonate samples and SRM 951. The long-term reproducibility of this in-house standard provides a measure for the external reproducibility of carbonate analyses by NTIMS. As we average individual sample analyses, reproducibility is given at 2se = 0.34 ‰ (n=3), 0.30 ‰ (n=4), 0.26 ‰ (n=5), 0.23 ‰ (n=6), 0.21 ‰ (n=7), and 0.19 ‰ (n=8 to 10) acceptable analyses. The reported uncertainty is either the 2se estimated from repeat analyses of a particular sample, or the 2se external reproducibility of the in-house carbonate standard for the respective number of repeat analyses, whichever is larger. A recent interlaboratory comparison of $\delta^{11}B$ measurements (Foster et al., 2013) confirmed that

systematic offsets exist between laboratories and between techniques such as NTIMS, as used here, and MC-ICPMS, but relative differences in $\delta^{11}B$ are consistent between the methods. Since relative differences in $\delta^{11}B$ are used in the delta-pH calculation (see below), analytical differences between NTIMS and MC-ICPMS $\delta^{11}B$ are not significant to this contribution, and do not compromise the resulting delta-pH.

Stable isotopes and B/Ca analyses:

Single shells of each species were analyzed for carbon and oxygen stable isotopic composition ($\delta^{13}C$ and $\delta^{18}O$ relative to V-PDB) on a Micromass PRISM stable isotope ratio mass spectrometer using standard dual-inlet techniques. Precision for single shells, based on repeat analysis of a calcite standard, is < 0.1‰ in both $\delta^{13}C$ and $\delta^{18}O$. For trace metal analysis (B/Ca and Mg/Ca), samples consisting of 10 to 20 shells (150-300 μg $CaCO_3$) were crushed and subjected to a full oxidative-reductive cleaning process and analyzed on a Thermo Finnigan Element XR Inductively-Coupled Plasma Mass Spectrometer using the methods of Brown et al. (2011). Briefly, a suite of matrix-matched standards of varying [Ca] and Element/Ca ratios are measured before each sample run, to produce calibration curves for both B/Ca and Mg/Ca, and to monitor for the effect of varying [Ca] between samples. Consistency standards are run every 5 samples to monitor and correct for in-run drift. B/Ca external reproducibility based on repeat analyses of foraminiferal samples is <7% (2 s.d.). Rejection of data was commonly due to unacceptable sample loss during the trace metal cleaning process, resulting in a measured [Ca] lower than the range of calibration standards used to produce B/Ca calibration curves. [Mg] in foraminifers is

2 orders of magnitude higher than [B] and the Mg blank is much lower, so that the [Ca] threshold for Mg/Ca data rejection is much lower than for B/Ca, and some samples have acceptable Mg/Ca data but unacceptable B/Ca analyses, which were omitted from the data table.

ΔpH estimates from $\delta^{11}B$

Translating the boron isotopic composition of carbonate ($\delta^{11}B_{c)}$ to absolute pH would require knowledge of the $\delta^{11}B_c$ versus pH relationship of a specific calcifier, in addition to the boron isotopic composition of seawater ($\delta^{11}B_{sw}$), which likely varies on timescales of 10^7 years (Lemarchand et al., 2000). Numerous studies have shown that the $\delta^{11}B_c$ versus pH relationship in marine carbonates is less sensitive (Henehan et al., 2013; Hönisch et al., 2004; Krief et al., 2010; Reynaud et al., 2004; Sanyal et al., 2001; Sanyal et al., 1996b; Sanyal et al., 2000) than predicted from aqueous boron fractionation in seawater (Klochko et al., 2006), so we use the apparent fractionation factor (α*) that best matches the $\delta^{11}B_c$ versus pH relationship observed in modern carbonates. As a temperature effect on α* is predicted by theory (Rustad et al., 2010; Zeebe, 2005), we apply the temperature correction of Kakihana et al. (1977), (α*= 1.0206-0.000049205*T), with a sensitivity within the range of theoretical studies. Sensitivity to this choice of α* is shown in Figure S5. In addition, different planktic foraminifer species display constant $\delta^{11}B_c$-offsets (*a*) when grown at the same pH, although the $\delta^{11}B_c$ versus pH relationships of different calcifiers are similar across a wide range of pH values (Henehan et al., 2013; Hönisch et al., 2007). Because *M. velascoensis* is now extinct, quantification of the species-specific $\delta^{11}B_c$-offset of this

species would require cross-calibration against co-existing relatives over the past 60 million years, an effort beyond the scope of the present contribution.

However, calculation of the PETM pH excursion (ΔpH, total scale) from $\delta^{11}B$ using an assumed initial pH is independent of the species-specific offset (*a*), and practically independent of the assumed $\delta^{11}B_{sw}$ (Figure S4). The relationship between assumed Paleocene (pre-PETM, denoted by subscript P) and measured pre-event $\delta^{11}B$:

$$pH_P = pKB - \log(-(\delta^{11}B_{sw} - \delta^{11}B_P - a) / (\delta^{11}B_{sw} - \alpha^* \times (\delta^{11}B_P + a) - \varepsilon^*))$$ (Hemming and Hanson, 1992) ,

which contains two unknowns: the species-specific offset *a* and $\delta^{11}B_{sw}$. All other components of the above equation are either constants set by T and S (pKB, α*, ε*), prescribed (pH_P) or measured ($\delta^{11}B_P$). This relationship can thus be solved for *a* as a function of $\delta^{11}B_{sw}$, resulting in:

$$a = \delta^{11}B_{sw} \times (1+10^{pKB-pHp})/(1+\alpha^* \times 10^{pKB-pHp}) + (-\delta^{11}B_P - 10^{pKB-pHp} \times (\varepsilon^* + \alpha^* \times \delta^{11}B_P)/(1+\alpha^* \times 10^{pKB-pHp})$$

which for clarity we simplify to:

$$a = m * \delta^{11}B_{sw} + b,$$

where m and b are set by the constants, prescribed initial pH, and measured $\delta^{11}B_P$:

$$m = (1+10^{pKB-pHp})/(1+\alpha^* \times 10^{pKB-pHp})$$

$$\text{and } b = (-\delta^{11}B_P - 10^{pKB-pHp} * (\varepsilon^* + \alpha^* \times \delta^{11}B_P)/(1+10^{pKB-pHp}).$$

Note that the coefficient m acting on $\delta^{11}B_{sw}$ is in all cases very close to 1, leading to the near insensitivity of these calculations to any assumed $\delta^{11}B_{sw}$ (Figure S4), such that the effect of varying $\delta^{11}B_{sw}$ is insignificant compared with the analytical uncertainty considered in Figure 2. Given this function for *a*, the relationship between CIE-interval (denoted by subscript E for Eocene) $\delta^{11}B$ and pH can be solved for pH:

$$pH_E = pKB\text{-}\log(-(\delta^{11}B_{sw} - \delta^{11}B_E - (m \times \delta^{11}B_{sw} + b))/(\delta^{11}B_{sw} - \alpha^* \times (\delta^{11}B_E + m \times \delta^{11}B_{sw} + b) - \varepsilon^*))$$

For the Pacific Sites 1209 and 865, we use a baseline T=30°C, S=37, similar to other estimates of tropical Paleocene conditions (Kozdon et al., 2011; Pearson et al., 2007), and excursion T=35°C and S=37.5 (Zachos et al., 2003) in calculating the pK_B (a function of T and S) and boron isotopic fractionation factors (a function of T). For Site 1263, pre-event values of T=24°C and S=37, and PETM values of T=28°C and S=38 (Tripati and Elderfield, 2005) are used. Using these values, the pre-PETM pH values for all 3 sites are similar to within 0.1 pH units, consistent with all 3 sites being approximately in equilibrium with atmospheric pCO_2, and suggesting that differential diagenesis between the three sites is not a major issue.

Techniques for assigning pre-event and CIE-interval $\delta^{11}B$ and their associated uncertainties: Method 1 (grey shaded error envelope on Figure 2): the variance ($1/s.d.^2$)-weighted mean of all the $\delta^{11}B$ data points in the pre-event and CIE intervals is calculated; error is the analytical precision of each data point propagated through the variance-weighted mean calculation. This was performed using ISOPLOT (Ludwig, 2003) and resulted in a pre-PETM and CIE-interval $\delta^{11}B$ of 15.51 ± 0.12

and 14.71 ± 0.11 (1 s.d.), respectively. Method 2 (red lines in Figure 2): we consider the two data points spanning the P-E boundary and their analytical uncertainty as described in the boron isotope analytical methods section (15.35 ± 0.30 and 14.76 ± 0.40 for the latest Paleocene and earliest Eocene, respectively).

Figure S5 shows the sensitivity of ΔpH to the choice of α*. We favor the temperature-corrected fractionation factor of Kakihana et al (1977), as this produces a pH vs. $\delta^{11}B$ relationship that most closely matches that observed in a wide range of calcifying organisms (Henehan et al., 2013; Hönisch et al., 2004; Krief et al., 2010; Reynaud et al., 2004; Sanyal et al., 2001; Sanyal et al., 1996b; Sanyal et al., 2000). Using this α*, the central resulting ΔpH is -0.27 units in the intial pH=7.8 case, and -0.34 units in the initial pH=7.67 case. Omitting the temperature correction, ΔpH is reduced to -0.22 units in the initial pH=7.8 case, and -0.26 units in the initial pH=7.67 case. Using an uncorrected α* of Klochko et al. (2006), ΔpH is further lowered to -0.17 units in the initial pH=7.8 case, and -0.20 units in the initial pH=7.67 case. It is important to note, however, that the α* of Klochko et al. (2006) produces a pH vs. $\delta^{11}B$ significantly steeper than observed in calcifying organisms, so those resulting ΔpH values (and the black line in Figure S5) very likely underestimate the acidification at the P-E boundary.

Model-derived B/Ca

To produce the model-derived B/Ca curves from LOSCAR output of Zeebe et al. (2009b), two interpretations of the 3 modern foraminifer B/Ca calibrations

presented by Allen et al. [2011, 2012] are used. In the first (absolute calibration, Figure S1A), B/Ca is calculated directly from a linear relationship to $[B(OH)_4^-]/DIC$, in the form $B/Ca = m * [B(OH)_4^-]/DIC + b$, with slope m and intercept b empirically determined by culturing experiments (Allen et al., 2011a; Allen et al., 2012) for each modern species: *Globigerinoides ruber* (m = 1152, b = 104), *Globigerinoides sacculifer* (m = 853, b = 63), and *Orbulina universa* (m = 473, b = 53). This method assumes the same change in B/Ca for the same *absolute* change in $[B(OH)_4^-]/DIC$ for modern and ancient species. However, these relationships might not be applicable to the PETM. For example, the initial borate/DIC ratio of the model is very different from that in the seawater used in the "ambient" culturing experiments, and there is little certainty about this ratio in the Paleocene due to probable changes in total $[B]_{seawater}$ on multi-million year timescales (Lemarchand et al., 2000). Additionally, to explain the lowest B/Ca values (~40 μmol/mol) recorded during the PETM with the absolute calibration would require negative $[B(OH)_4^-]/DIC$ ratios (see Figure S1A), which is impossible. Another option (relative calibration, Figure S1B) is to assume that the B/Ca of ancient species responds in the same way as modern species to a *relative* change in $[B(OH)_4^-]/DIC$:

$$\Delta B/Ca = m * \Delta[B(OH)_4^-]/DIC * [B(OH)_4^-]/DIC_{modern} / [B(OH)_4^-]/DIC_{Paleocene}$$

Here m values are the same as in the absolute calibrations, $[B(OH)_4^-]/DIC_{modern} = 0.0453$, from the "ambient" experiments of Allen et al. (2012), and $[B(OH)_4^-]/DIC_{Paleocene} = 0.0235$, from the steady-state low-latitude Pacific surface reservoir in the LOSCAR simulation of Zeebe et al. (2009b). Since this equation only generates a

sensitivity (ΔB/Ca) to $[B(OH)_4^-]$/DIC change, an intercept must be chosen to obtain absolute values. We chose an intercept of +70 μmol/mol, so that pre-event values are comparable to the observed data. This approach yields a larger model-derived B/Ca excursion, because the initial $[B(OH)_4^-]$/DIC is approximately half the modern value, so a small change in absolute $[B(OH)_4^-]$/DIC is approximately doubled in relative $[B(OH)_4^-]$/DIC. Given our inability to empirically calibrate extinct foraminifer species, and the uncertainties in the Paleocene $[B(OH)_4^-]$/DIC of the model, we present these two calibrations as a range of possibilities for comparing measured PETM B/Ca data with LOSCAR model output.

Figures:

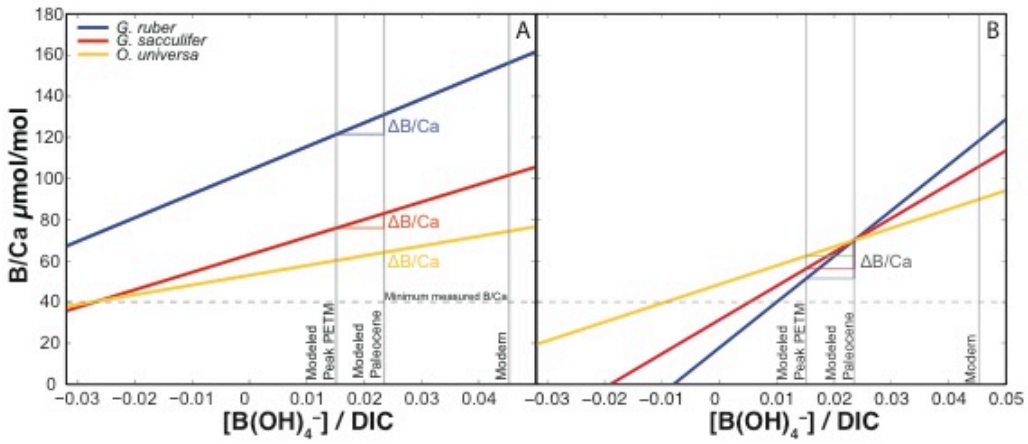

Figure fs01: Calibrations relating B/Ca to $[B(OH)_4^-]$/DIC in modern planktic foraminifers from laboratory culture experiments of Allen et al. [2011, 2012]. These relationships are used to produce model-derived B/Ca curves from LOSCAR model output. In both panels vertical lines represent the $[B(OH)_4^-]$/DIC of modern seawater, model-predicted Paleocene (pre-event) baseline, and minimum $[B(OH)_4^-]$/DIC corresponding to the most acidified conditions of the PETM. The dashed horizontal line represents the minimum values measured on surface dwelling planktic foraminifera. Panel A shows the absolute calibration, taken directly from Allen et al. [2011, 2012]. Using any of these calibrations, a negative $[B(OH)_4^-]$/DIC would be required to generate the minimum measured data. Panel B shows the relative

calibration, in which B/Ca responds as in modern foraminifers to a relative change in $[B(OH)_4^-]$/DIC. The intercept is adjusted to match the pre-event measured data of 70 μmol/mol. For each calibration on both panels the magnitude of the B/Ca shift resulting from a reduction of $[B(OH)_4^-]$/DIC from Paleocene (0.0235) to peak PETM (0.0155) is indicated by the separation of the two vertical lines, and the corresponding ΔB/Ca.

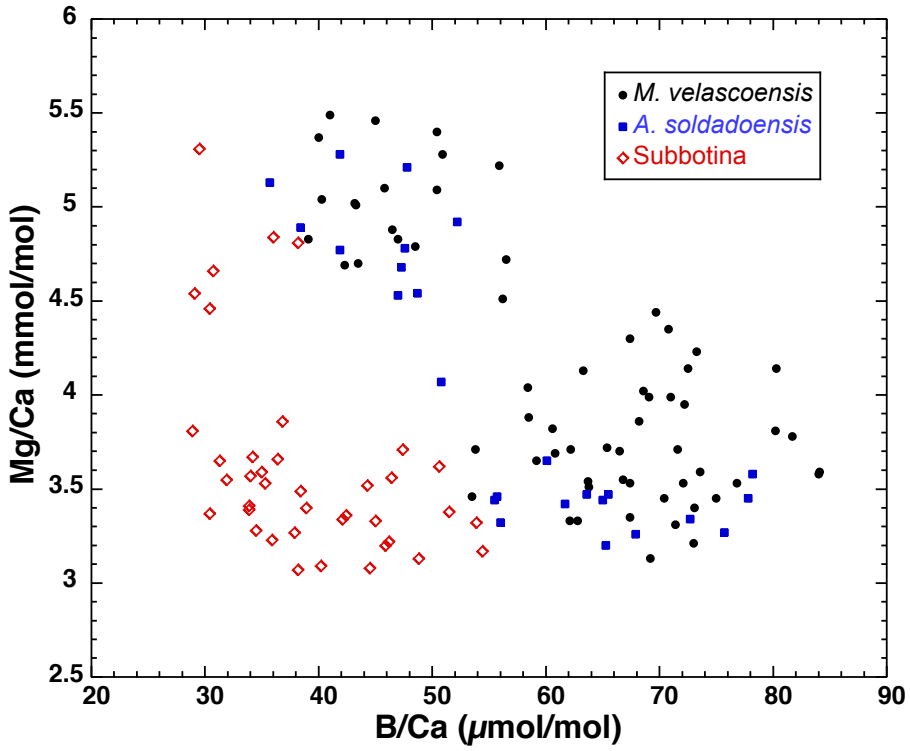

Figure fs02: Cross-plot of Mg/Ca versus B/Ca in PETM planktic foraminifers showing the inverse relationship between Mg/Ca (temperature signal) and B/Ca (acidification signal) in each species. Closed symbols represent surface dwellers, and red open diamonds represent the thermocline-dwelling genus *Subbotina*.

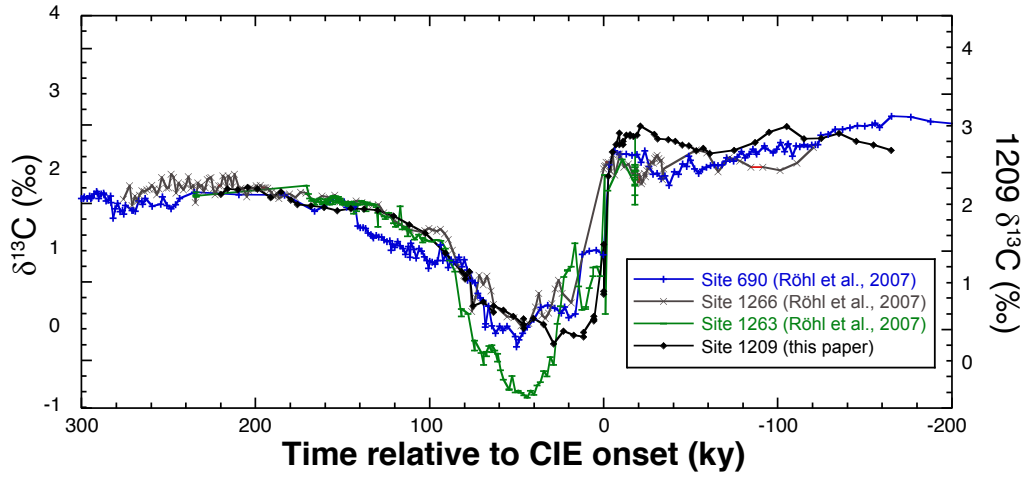

Figure fs03: Comparison of carbon isotope records from pelagic P-E boundary sections. Fine-fraction (<63 μm) and bulk $\delta^{13}C$ records spanning the P-E boundary for ODP Sites 690 (Bains et al., 1999), 1263 and 1266 (Zachos et al., 2005), and 1209 (this study) plotted against time (ky) relative to the P-E boundary. The age models for the first 3 sites are based on orbital-tuning (Röhl et al., 2007). The Site 1209 age model was derived by aligning the carbon isotope record to obtain a "best fit". Given the effects of extensive dissolution on bulk sediment $\delta^{13}C$ (see McCarren et al. (2008a)) and sedimentation rates, and hence relative resolution, the choice of tie points is somewhat subjective. Nevertheless, a reasonably close fit was obtained that yields sensible sedimentation rates consistent with other constraints (i.e., biostratigraphy, modelling). Note that Site 1209 data are slightly more enriched (+0.4‰) in $\delta^{13}C$ relative to other sites throughout the event, presumably because of a higher $\delta^{13}C$ of mixed-layer DIC in the Pacific compared to the Atlantic and Southern

Oceans (similar to modern). In the figure, the Site 1209 record has been offset by -0.4‰ for ease of comparison. No fine fraction isotope data are available for Site 865 due to the unusual nature of carbonate at that site, with a high weight percentage of sand size fraction, possibly due to winnowing. The carbon isotope data on planktic foraminifera and epifaunal benthics do not show a recognizable shape for the CIE so that these data cannot be used for correlation (Bralower et al., 1995). We used the carbon isotope data on the infaunal benthic foraminifer *Bulimina ovula*, which does show a clearly defined CIE, to correlate to the benthic isotope curve at Site 690 (Zachos et al., 2001, Fig. 5), with numerical ages according to (Röhl et al., 2007).

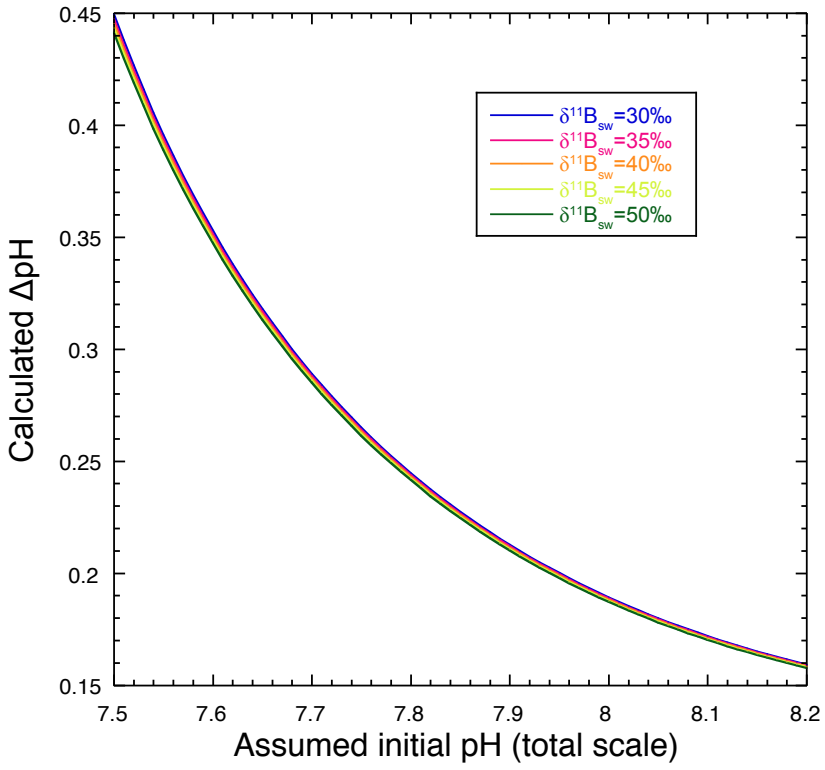

Figure fs04: Delta-pH calculations using a range of assumed $\delta^{11}B_{sw}$ values, demonstrating the near insensitivity of our calculations to that value. The range considered here (30 to 50‰) is far greater than the range of estimates available for

the Paleogene (Lemarchand et al., 2000, Raitzsch and Hönisch, 2013). $\delta^{11}B$ values used are the variance-weighted means of the pre-event and CIE-interval $\delta^{11}B$ populations, equal to 15.47‰ and 14.71‰ respectively.

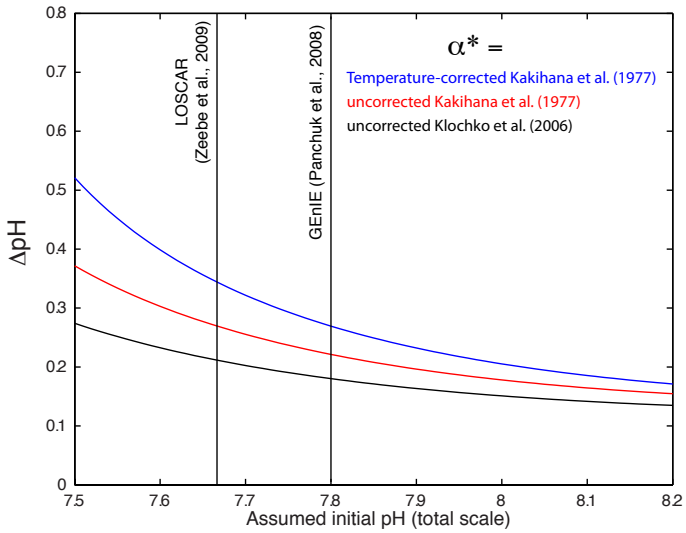

Figure fs05: Sensitivity of ΔpH calculation to choice of apparent boron isotopic fractionation factor (α*). All calculations were made with variance-weighted means for pre-CIE $\delta^{11}B$ (15.47‰) and CIE $\delta^{11}B$ (14.71‰). The blue line uses the temperature-corrected α* of Kakihana et al (1977), the red line omits the temperature correction (α* = 1.0194), and the black line uses the uncorrected fractionation factor of Klochko et al (2006) (α* = 1.027). pK_B is varied with T and S for all cases, as described in the text and in Table 2. Note that all empirical calibrations of the pH - $\delta^{11}B_{carbonate}$ relationship follow a slope similar to Kakihana et al (1977), rather than Klochko et al (2006), so the black line very likely significantly underestimates ΔpH.

References

Agnini, C., Fornaciari, E., Rio, D., Tateo, F., Backman, J., & Giusberti, L. (2007). Responses of calcareous nannofossil assemblages, mineralogy and geochemistry to the environmental perturbations across the Paleocene/Eocene boundary in the Venetian Pre-Alps. *Marine Micropaleontology, 63*(1-2), 19-38.

Allen, K. A., & Hönisch, B. (2012). The planktic foraminiferal B/Ca proxy for seawater carbonate chemistry: A critical evaluation. *Earth and Planetary Science Letters, 345–348*(0), 203-211. doi: 10.1016/j.epsl.2012.06.012

Allen, K. A., Hönisch, B., Eggins, S., Yu, J., Spero, H. J., & Elderfield, H. (2011). Controls on boron incorporation in cultured tests of the planktic foraminifer Orbulina universa. *Earth & Planetary Science Letters*.

Allen, K. A., Hönisch, B., Eggins, S. M., & Rosenthal, Y. (2012). Environmental controls on B/Ca in calcite tests of the tropical planktic foraminifer species Globigerinoides ruber and Globigerinoides sacculifer. *Earth and Planetary Science Letters, 351–352*(0), 270-280. doi: 10.1016/j.epsl.2012.07.004

Allen, K. A., Hönisch, B., Eggins, S. M., Yu, J., Spero, H. J., & Elderfield, H. (2011). Controls on boron incorporation in cultured tests of the planktic foraminifer< i> Orbulina universa</i>. *Earth and Planetary Science Letters, 309*(3), 291-301.

Bains, S., Corfield, R. M., & Norris, R. D. (1999). Mechanisms of climate warming at the end of the Paleocene. *Science, 285*(5428), 724-727.

Bains, S., Norris, R. D., Corfield, R. M., & Faul, K. L. (2000). Termination of global warmth at the Palaeocene/Eocene boundary through productivity feedback. *Nature, 407*(6801), 171-174.

Barker, S., Greaves, M., & Elderfield, H. (2003). A study of cleaning procedures used for foraminiferal Mg/Ca paleothermometry. [Article]. *Geochemistry Geophysics Geosystems, 4*. doi: 10.1029/2003gc000559

Barker, S., Greaves, M., & Elderfield, H. (2003). A study of cleaning procedures used for foraminiferal Mg/Ca paleothermometry. *Geochemistry, Geophysics, Geosystems, 4*(9).

Beerling, D., & Royer, D. L. (2011). Convergent Cenozoic CO2 history. *Nature Geoscience, 4*, 418-420.

Berggren, W. A., & Norris, R. D. (1997). Biostratigraphy, phylogeny and systematics of Paleocene trochospiral planktic foraminifera. *Micropaleontology, 43*, 1-116.

Berner, R. A., & Kothavala, Z. (2001). GEOCARB III: A revised model of atmospheric CO2 over phanerozoic time. *American Journal of Science, 301*(2), 182-204.

Berner, R. A., Lasaga, A. C., & Garrels, R. M. (1983). The carbonate-silicate geochemical cycle and its effects on atmospheric carbon dioxide over the past 100 million years. *American Journal of Science, 283*, 641-683.

Bice, K. L., & Marotzke, J. (2002). Could changing ocean circulation have destabilized methane hydrate at the Paleocene/Eocene boundary? - art. no. 1018. *Paleoceanography, 17*(2), 1018.

Bijma, J., Hönisch, B., & Zeebe, R. E. (2002). Impact of the ocean carbonate chemistry on living foraminiferal shell weight: Comment on "Carbonate ion concentration in glacial-age deep waters of the Caribbean Sea" by W.S. Broecker and E. Clark. *Geochemistry Geophysics Geosystems, 3*(11), 10.1029/2002GC000388.

Bowen, G. J. (2013). Up in smoke: A role for organic carbon feedbacks in Paleogene hyperthermals. *Global and Planetary Change, 109*, 18-29.

Bowen, G. J., Clyde, W. C., Koch, P. L., Ting, S. Y., Alroy, J., Tsubamoto, T., . . . Wang, Y. (2002). Mammalian dispersal at the Paleocene/Eocene boundary. *Science, 295*(5562), 2062-2065.

Bowen, G. J., & Zachos, J. C. (2010). Rapid carbon sequestration at the termination of the Palaeocene-Eocene Thermal Maximum. *Nature Geoscience, 3*(12), 866-869.

Bown, P., & Pearson, P. (2009). Calcareous plankton evolution and the Paleocene/Eocene thermal maximum event: New evidence from Tanzania. [Article]. *Marine Micropaleontology, 71*(1-2), 60-70. doi: 10.1016/j.marmicro.2009.01.005

Bralower, T. J. (2002). Evidence of surface water oligotrophy during the Paleocene-Eocene thermal maximum: Nannofossil assemblage data from Ocean Drilling

Program Site 690, Maud Rise, Weddell Sea (vol 17, pg 1023, 2002) - art. no. 1060. *Paleoceanography, 17*(4), 1060.

Bralower, T. J., Premoli-Silva, I., Malone, M., & al., e. (2002). *Proc. ODP, Initial Reports* (Vol. 198). College Station, TX: Ocean Drilling Program.

Bralower, T. J., Zachos, J. C., Thomas, E., Parrow, M., Paull, C. K., Kelly, D. C., . . . Lohmann, K. C. (1995). Late Paleocene to Eocene Paleoceanography of the Equatorial Pacific Ocean - Stable Isotopes Recorded At Ocean Drilling Program Site 865, Allison Guyot. *Paleoceanography, 10*(4), 841-865.

Brown, R. E., Anderson, L. A., Thomas, E., & Zachos, J. (2011). A core-top calibration of B/Ca in the benthic foraminifers Nuttalides umbonifera and Oridorsalis umbonatus: A proxy for Cenozoic bottom water carbonate saturation. *Earth & Planetary Science Letters, 310*, 360-368.

Coadic, R., Bassinot, F., Dissard, D., Douville, E., Greaves, M., & Michel, E. (2013). A core‐top study of dissolution effect on B/Ca in Globigerinoides sacculifer from the tropical Atlantic: Potential bias for paleo‐reconstruction of seawater carbonate chemistry. *Geochemistry, Geophysics, Geosystems, 14*(4), 1053-1068.

Colosimo, A. B., Bralower, T. J., & Zachos, J. C. (2005). Evidence for lysocline shoaling and methane hydrate dissociation at the Paleocene-Eocene thermal maximum on Shatsky Rise, ODP Leg 198. In T. J. Bralower, I. Premoli Silva

& M. Malone (Eds.), *Proc. ODP, Sci. Results* (Vol. 198). College Station, TX: Ocean Drilling Program.

Cui, Y., Kump, L. R., Ridgwell, A. J., Charles, A. J., Junium, C. K., Diefendorf, A. F., . . . Harding, I. C. (2011). Slow release of fossil carbon during the Palaeocene-Eocene Thermal Maximum. *Nature Geoscience, 4*(7), 481-485.

D'Hondt, S., Zachos, J. C., & Schultz, G. (1994). Stable Isotopic Signals and Photosymbiosis in Late Paleocene Planktic Foraminifera. *Paleobiology, 20*(3), 391-406.

DeConto, R. M., & Pollard, D. (2003). Rapid Cenozoic glaciation of Antarctica induced by declining atmospheric CO2. *Nature, 421*(6920), 245-249.

Depaolo, D. J., & Ingram, B. L. (1985). High-resolution stratigraphy with strontium isotopes. *Science, 227*(4689), 938-941.

Dickens, G. R., Castillo, M. M., & Walker, J. C. G. (1997). A blast of gas in the latest Paleocene: Simulating first-order effects of massive dissociation of oceanic methane hydrate. *Geology, 25*(3), 259-262.

Dickens, G. R., Oneil, J. R., Rea, D. K., & Owen, R. M. (1995). Dissociation of Oceanic Methane Hydrate As a Cause of the Carbon Isotope Excursion At the End of the Paleocene. *Paleoceanography, 10*(6), 965-971.

Dunkley-Jones, T., Lunt, D. J., Schmidt, D. N., Ridgwell, A., Sluijs, A., Valdes, P. J., & Maslin, M. (2013). Climate model and proxy data constraints on ocean warming across the Paleocene-Eocene Thermal Maximum. *Earth-Science Reviews, 125*, 123-145.

Edgar, K., Bohaty, S., Gibbs, S., Sexton, P., Norris, R., & Wilson, P. (2013). Symbiont 'bleaching'in planktic foraminifera during the Middle Eocene Climatic Optimum. *Geology, 41*(1), 15-18.

Farley, K. A., & Eltgroth, S. F. (2003). An alternative age model for the Paleocene-Eocene thermal maximum using extraterrestrial He-3. *Earth and Planetary Science Letters, 208*(3-4), 135-148.

Foster, G. L. (2008). Seawater pH, pCO2 and [CO2-3] variations in the Caribbean Sea over the last 130†kyr: A boron isotope and B/Ca study of planktic foraminifera. *Earth and Planetary Science Letters, 271*(1-4), 254-266.

Foster, G. L., Hönisch, B., Paris, G., Dwyer, G. S., Rae, J. W. B., Elliott, T., . . . Vengosh, A. (2013). Interlaboratory comparison of boron isotope analyses of boric acid, seawater and marine CaCO3 by MC-ICPMS and NTIMS. *Chemical Geology, 358*(0), 1-14. doi: http://dx.doi.org/10.1016/j.chemgeo.2013.08.027

Foster, G. L., Lear, C. H., & Rae, J. W. (2012). The evolution of pCO2, ice volume and climate during the middle Miocene. *Earth and Planetary Science Letters, 341*, 243-254.

Gibbs, S. J., Bown, P. R., Sessa, J. A., Bralower, T. J., & Wilson, P. A. (2006). Nannoplankton extinction and origination across the Paleocene-Eocene Thermal Maximum. *Science, 314*(5806), 1770-1773.

Gibbs, S. J., Stoll, H. M., Bown, P. R., & Bralower, T. J. (2010). Ocean acidification and surface water carbonate production across the Paleocene-Eocene thermal

maximum. [Article]. *Earth and Planetary Science Letters, 295*(3-4), 583-592. doi: 10.1016/j.epsl.2010.04.044

Goodwin, P., & Ridgwell, A. (2010). Ocean‐atmosphere partitioning of anthropogenic carbon dioxide on multimillennial timescales. *Global Biogeochemical Cycles, 24*(2).

Hemming, N. G., & Hanson, G. N. (1992). Boron isotopic composition and concentration in modern marine carbonates. *Geochimica et Cosmochimica Acta, 56*, 537-543.

Hemming, N. G., & Hanson, G. N. (1994). A procedure for the isotopic analysis of boron by negative thermal ionization mass spectrometry. *Chem. Geol., 114*, 147-156.

Henehan, M. J., Rae, J. W. B., Foster, G. L., Erez, J., Prentice, K. C., Kucera, M., . . . Elliott, T. (2013). Calibration of the boron isotope proxy in the planktonic foraminifera Globigerinoides ruber for use in palaeo-CO2 reconstruction. *Earth and Planetary Science Letters, 364*(0), 111-122. doi: http://dx.doi.org/10.1016/j.epsl.2012.12.029

Hönisch, B., Bijma, J., Russell, A. D., Spero, H. J., Palmer, M. R., Zeebe, R. E., & Eisenhauer, A. (2003). The influence of symbiont photosynthesis on the boron isotopic composition of foraminifera shells. *Marine Micropaleontology, 49*(1-2), 87-96.

Hönisch, B., & Hemming, N. G. (2004). Ground-truthing the boron isotope paleo-*p*H proxy in planktonic foraminifera shells: Partial dissolution and shell size effects. *Paleoceanography, 19*, doi:10.1029/2004PA001026.

Hönisch, B., & Hemming, N. G. (2005). Surface ocean pH response to variations in pCO_2 through two full glacial cycles. *Earth and Planetary Science Letters, 236*(1-2), 305-314.

Hönisch, B., Hemming, N. G., Grottoli, A. G., Amat, A., Hanson, G. N., & Bijma, J. (2004). Assessing scleractinian corals as recorders for paleo-*p*H: Empirical calibration and vital effects. *Geochim. Cosmochim. Acta, 68*(18), 3675-3685.

Hönisch, B., Hemming, N. G., & Loose, B. (2007). Comment on "A critical evaluation of the boron isotope-pH proxy: The accuracy of ancient ocean pH estimates" by M. Pagani, D. Lemarchand, A. Spivack and J. Gaillardet. *Geochimica et Cosmochimica Acta, 71*(6), 1636-1641.

Hönisch, B., Ridgwell, A., Schmidt, D. N., Thomas, E., Gibbs, S., Sluijs, A., . . . Williams, B. (2012). The Geological Record of Ocean Acidification. *Science, 335*(6072), 1058-1063.

IPCC. (2007). Climate change 2007

Jorgensen, B. B., Erez, J., Revsbech, N. P., & Cohen, Y. (1985). Symbiotic photosynthesis in a planktonic foraminiferan, Globigerinoides sacculifer (Brady), studied with microelectrodes. *Limnol. Oceanogr, 30*(6), 1253-1267.

Kakihana, H., Kotaka, M., Satoh, S., Nomura, M., & Okamoto, M. (1977). Fundamental studies on the ion-exchange of boron isotopes. *Bull. Chem. Soc. Japan, 50*, 158-163.

Kelly, D. C. (2002). Response of Antarctic (ODP Site 690) planktonic foraminifera to the Paleocene-Eocene thermal maximum: Faunal evidence for ocean/climate change. *Paleoceanography, 17*(4), 1071.

Kelly, D. C., Bralower, T. J., Zachos, J. C., Silva, I. P., & Thomas, E. (1996). Rapid Diversification of Planktonic Foraminifera in the Tropical Pacific (Odp Site 865) During the Late Paleocene Thermal Maximum. *Geology, 24*(5), 423-426.

Kelly, D. C., Nielsen, T. M., & Schellenberg, S. A. (2012). Carbonate saturation dynamics during the Paleocene–Eocene thermal maximum: Bathyal constraints from ODP sites 689 and 690 in the Weddell Sea (South Atlantic). *Marine Geology, 303*, 75-86.

Kelly, D. C., Nielsen, T. M. J., McCarren, H. K., Zachos, J. C., & Rohl, U. (2010). Spatiotemporal patterns of carbonate sedimentation in the South Atlantic: Implications for carbon cycling during the Paleocene-Eocene thermal maximum. *Palaeogeography Palaeoclimatology Palaeoecology, 293*(1-2), 30-40.

Kelly, D. C., Zachos, J. C., Bralower, T. J., & Schellenberg, S. A. (2005). Enhanced terrestrial weathering/runoff and surface ocean carbonate production during the recovery stages of the Paleocene-Eocene thermal maximum. *Paleoceanography, 20*(4), -.

Kennett, J. P., & Stott, L. D. (1991). Abrupt Deep-Sea Warming, Palaeoceanographic Changes and Benthic Extinctions At the End of the Palaeocene. *Nature, 353*(6341), 225-229.

Klochko, K., Kaufman, A. J., Yao, W., Byrne, R. H., & Tossell, J. A. (2006). Experimental measurement of boron isotope fractionation in seawater. *Earth and Planetary Science Letters, 248*(1-2), 261-270.

Koch, P. L., Zachos, J. C., & Gingerich, P. D. (1992). Correlation Between Isotope Records in Marine and Continental Carbon Reservoirs Near the Palaeocene Eocene Boundary. *Nature, 358*(6384), 319-322.

Komar, N., & Zeebe, R. (2011). Oceanic calcium changes from enhanced weathering during the Paleocene-Eocene Thermal Maximum: No effect on calcium-based proxies. *Paleoceanography, 26*, 1-13.

Kozdon, R., Kelly, D., Kitajima, K., Strickland, A., Fournelle, J., & Valley, J. (2013). In situ δ18O and Mg/Ca analyses of diagenetic and planktic foraminiferal calcite preserved in a deep‐sea record of the Paleocene‐Eocene thermal maximum. *Paleoceanography, 28*(3), 517-528.

Kozdon, R., Kelly, D. C., Kita, N. T., Fournelle, J. H., & Valley, J. W. (2011). Planktonic foraminiferal oxygen isotope analysis by ion microprobe technique suggests warm tropical sea surface temperatures during the Early Paleogene. *Paleoceanography, 26*(3), 1-17.

Krief, S., Hendy, E. J., Fine, M., Yam, R., Meibom, A., Foster, G. L., & Shemesh, A. (2010). Physiological and isotopic responses of scleractinian corals to ocean

acidification. [doi: DOI: 10.1016/j.gca.2010.05.023]. *Geochimica et Cosmochimica Acta, 74*(17), 4988-5001.

Lemarchand, D., Gaillardet, J., Lewin, É., & Allègre, C. J. (2000). The influence of rivers on marine boron isotopes and implications for reconstructing past ocean *p*H. *Nature, 408*, 951-954.

Leon-Rodriguez, L., & Dickens, G. R. (2010). Constraints on ocean acidification associated with rapid and massive carbon injections: The early Paleogene record at ocean drilling program site 1215, equatorial Pacific Ocean. *Palaeogeography, Palaeoclimatology, Palaeoecology, 298*(3), 409-420.

Ludwig, K. R. (2003). *User's manual for Isoplot 3.00: A geochronological toolkit for Microsoft Excel*: Kenneth R. Ludwig.

Ma, Z., Gray, E., Thomas, E., Murphy, B., Zachos, J., & Paytan, A. (2014). Carbon sequestration during the Palaeocene-Eocene Thermal Maximum by an efficient biological pump. *Nature Geoscience*.

Maher, K., & Chamberlain, C. (2014). Hydrologic regulation of chemical weathering and the geologic carbon cycle. *Science, 343*(6178), 1502-1504.

Matsumoto, K. (2007). Biology‐mediated temperature control on atmospheric pCO2 and ocean biogeochemistry. *Geophysical Research Letters, 34*(20), 1-5.

McCarren, H., Thomas, E., Hasegawa, T., Rohl, U., & Zachos, J. C. (2008). Depth dependency of the Paleocene-Eocene carbon isotope excursion: Paired benthic and terrestrial biomarker records (Ocean Drilling Program Leg 208, Walvis Ridge). *Geochemistry Geophysics Geosystems, 9*, -.

McCarren, H., Thomas, E., Röhl, U., & Zachos, J. C. (2008). The Paleocene-Eocene Carbon Isotope Excursion: Insights from the benthic record (ODP Leg 208, Walvis Ridge). *Geophysics, Geosystems, Geochemistry*.

McInerney, F. A., & Wing, S. (2011). The Paleocene-Eocene Thermal Maximum: A Perturbation of Carbon Cycle, Climate, and Biosphere with Implications for the future. *Annual Review of Earth & Planetary Sciences, 39*, 489-516.

Murphy, B. H., Farley, K. A., & Zachos, J. C. (2010). An extraterrestrial He-3-based timescale for the Paleocene-Eocene thermal maximum (PETM) from Walvis Ridge, IODP Site 1266. *Geochimica Et Cosmochimica Acta, 74*(17), 5098-5108.

Nunes, F., & Norris, R. D. (2006). Abrupt reversal in ocean overturning during the Palaeocene/Eocene warm period. *Nature, 439*(7072), 60-63.

Pagani, M., Caldeira, K., Archer, D., & Zachos, J. C. (2006). An ancient carbon mystery. *Science, 314*(5805), 1556-1557.

Panchuk, K., Ridgwell, A., & Kump, L. R. (2008). Sedimentary response to Paleocene-Eocene Thermal Maximum carbon release: A model-data comparison. *Geology, 36*(4), 315-318.

Pearson, P. N., Foster, G. L., & Wade, B. S. (2009). Atmospheric carbon dioxide through the Eocene-Oligocene climate transition. *Nature, 461*(7267), 1110-1113.

Pearson, P. N., van Dongen, B. E., Nicholas, C. J., Pancost, R. D., Schouten, S., Singano, J. M., & Wade, B. S. (2007). Stable warm tropical climate through the Eocene Epoch. *Geology, 35*(3), 211-214.

Penman, D. E., Hönisch, B., Zeebe, R. E., Thomas, E., & Zachos, J. C. (2014). Rapid and sustained surface ocean acidification during the Paleocene-Eocene Thermal Maximum. *Paleoceanography*.

Pollard, D., & DeConto, R. M. (2005). Hysteresis in Cenozoic Antarctic ice-sheet variations. *Global and Planetary Change, 45*(1), 9-21.

Raffi, I., Backman, J., & Palike, H. (2005). Changes in calcareous nannofossil assemblages across the Paleocene/Eocene transition from the paleo-equatorial Pacific Ocean. *Palaeogeography Palaeoclimatology Palaeoecology, 226*(1-2), 93-126.

Raffi, I., Backman, J., Zachos, J. C., & Sluijs, A. (2009). The response of calcareous nannofossil assemblages to the Paleocene Eocene Thermal Maximum at the Walvis Ridge in the South Atlantic. *Marine Micropaleontology, 70*(3-4), 201-212.

Raffi, I., & De Bernardi, B. (2008). Response of calcareous nannofossils to the Paleocene–Eocene Thermal Maximum: Observations on composition, preservation and calcification in sediments from ODP Site 1263 (Walvis Ridge—SW Atlantic). *Marine Micropaleontology, 69*(2), 119-138.

Raitzsch, M., & Hönisch, B. (2013). Cenozoic boron isotope variations in benthic foraminifers. *Geology, 41*(5), 591-594.

Ravizza, G., Norris, R. N., Blusztajn, J., & Aubry, M. P. (2001). An osmium isotope excursion associated with the late Paleocene thermal maximum: Evidence of intensified chemical weathering. *Paleoceanography, 16*(2), 155-163.

Reynaud, S., Hemming, N. G., Juillet-Leclerc, A., & Gattuso, J.-P. (2004). Effect of pCO_2 and temperature on the boron isotopic composition of a zooxanthellate coral: *Acropora* sp. *Coral Reefs, 23*, 539-546. doi: 10.1007/s00338-004-0399

Ridgwell, A., & Schmidt, D. N. (2010). Past Constraints on the vulnerability of marine calcifiers to massive carbon dioxide release. *Nature Geoscience, 3*, 196-200.

Rink, S., Kühl, M., Bijma, J., & Spero, H. J. (1998). Microsensor studies of photosynthesis and respiration in the symbiotic foraminifer *Orbulina universa*. *Mar. Biol., 131*(4), 583-595.

Robert, C., & Kennett, J. P. (1994). Antarctic Subtropical Humid Episode At the Paleocene-Eocene Boundary - Clay-Mineral Evidence. *Geology, 22*(3), 211-214.

Röhl, U., Westerhold, T., Bralower, T. J., & Zachos, J. C. (2007). On the duration of the Paleocene-Eocene thermal maximum (PETM). *Geochemistry Geophysics Geosystems, 8*, -.

Rustad, J. R., Bylaska, E. J., Jackson, V. E., & Dixon, D. A. (2010). Calculation of boron-isotope fractionation between B(OH)3(aq) and B(OH)4-(aq). *Geochimica et Cosmochimica Acta, 74*(10), 2843-2850.

Sanyal, A., Bijma, J., Spero, H. J., & Lea, D. W. (2001). Empirical relationship between *p*H and the boron isotopic composition of *G. sacculifer*: Implications for the boron isotope paleo-*p*H proxy. *Paleoceanography, 16*(5), 515-519.

Sanyal, A., Hemming, N. G., Broecker, W. S., Lea, D. W., Spero, H. J., & Hanson, G. N. (1996a). Oceanic Ph Control on the Boron Isotopic Composition of Foraminifera - Evidence from Culture Experiments. *Paleoceanography, 11*(5), 513-517.

Sanyal, A., Hemming, N. G., Broecker, W. S., Lea, D. W., Spero, H. J., & Hanson, G. N. (1996b). Oceanic *p*H control on the boron isotopic composition of foraminifera: Evidence from culture experiments. *Paleoceanography, 11*(5), 513-517.

Sanyal, A., Nugent, M., Reeder, R. J., & Bijma, J. (2000). Seawater *p*H control on the boron isotopic composition of calcite: Evidence from inorganic calcite precipitation experiments. *Geochim. Cosmochim. Ac., 64*(9), 1551-1555.

Simon, L., Lecuyer, C., Marechal, C., & Coltice, N. (2006). Modelling the geochemical cycle of boron: Implications for the long-term $\delta^{11}B$ evolution of seawater and oceanic crust. *Chemical Geology, 22*(1-2), 15.

Sluijs, A., Bowen, G. J., Brinkhuis, H., Lourens, L., & Thomas, E. (2012). The Palaeocene-Eocene Thermal Maximum super greenhouse: biotic and geochemical signatures, age models and mechanisms of global change. In M. Williams, A. M. Haywood, F. J. Gregory & D. N. Schmidt (Eds.), *Deep-Time*

Perspectives on Climate Change: Marrying the Signal from Computer Models and Biological Proxies (pp. 267-293). London: The Geological Society.

Sluijs, A., Schouten, S., Pagani, M., Woltering, M., Brinkhuis, H., Damste, J. S. S., . . . Scientists, E. (2006). Subtropical arctic ocean temperatures during the Palaeocene/Eocene thermal maximum. *Nature, 441*(7093), 610-613.

Sluijs, A., Zachos, J. C., & Zeebe, R. E. (2012). Constraints on hyperthermals. [10.1038/ngeo1423]. *Nature Geosci, 5*(4), 231-231.

Stoll, H. M., & Bains, S. (2003). Coccolith Sr/Ca records of productivity during the Paleocene-Eocene thermal maximum from the Weddell Sea. *Paleoceanography, 18*(2).

Svensen, H., Planke, S., Malthe-Sorenssen, A., Jamtveit, B., Myklebust, R., Eidem, T. R., & Rey, S. S. (2004). Release of methane from a volcanic basin as a mechanism for initial Eocene global warming. *Nature, 429*, 524-527.

Takeda, K., & Kaiho, K. (2007). Faunal turnovers in central Pacific benthic foraminifera during the Paleocene–Eocene thermal maximum. *Palaeogeography, Palaeoclimatology, Palaeoecology, 251*(2), 175-197.

Thomas, D. J., Zachos, J. C., Bralower, T. J., Thomas, E., & Bohaty, S. (2002). Warming the fuel for the fire: Evidence for the thermal dissociation of methane hydrate during the Paleocene-Eocene thermal maximum. *Geology, 30*(12), 1067-1070.

Thomas, E., & Shackleton, N. J. (1996). The Paleocene-Eocene benthic foraminiferal extinction and stable isotope anomalies. In R. W. O. B. Knox, R. M. Corfield

& R. E. Dunay (Eds.), *Correlation of the early Paleogene in Northwest Europe* (Vol. 101, pp. 401-441). London.

Tripati, A., & Elderfield, H. (2005). Deep-Sea Temperature and Circulation Changes at the Paleocene-Eocene Thermal Maximum. *Science, 308*(5730), 1894-1898.

Tyrrell, T., & Zeebe, R. E. (2004). History of carbonate ion concentration over the last 100 million years. *Geochimica Et Cosmochimica Acta, 68*(17), 3521-3530.

Uchikawa, J., & Zeebe, R. E. (2008). Influence of terrestrial weathering on ocean acidification and the next glacial inception. *Geophysical Research Letters, 35*(23).

Walker, J. C. G., Hays, P. B., & Kasting, J. F. (1981). A Negative Feedback Mechanism for the Long-Term Stabilization of Earths Surface-Temperature. *Journal of Geophysical Research-Oceans and Atmospheres, 86*(Nc10), 9776-9782.

Wang, Y., Law, R., & Pak, B. (2010). A global model of carbon, nitrogen and phosphorus cycles for the terrestrial biosphere. *Biogeosciences, 7*(7), 2261-2282.

Wieczorek, R., Fantle, M. S., Kump, L. R., & Ravizza, G. (2013). Geochemical evidence for volcanic activity prior to and enhanced terrestrial weathering during the Paleocene Eocene Thermal Maximum. *Geochimica et Cosmochimica Acta, 119*, 391-410.

Wing, S. L., Harrington, G. J., Smith, F. A., Bloch, J. I., Boyer, D. M., & Freeman, K. H. (2005). Transient floral change and rapid global warming at the Paleocene-Eocene boundary. *Science, 310*(5750), 993-996.

Yu, J., Elderfield, H., & Hönisch, B. (2007). B/Ca in planktonic foraminifera as a proxy for surface seawater pH. *Paleoceanography, 22*(2), 1-17.

Zachos, J., Pagani, M., Sloan, L., Thomas, E., & Billups, K. (2001). Trends, rhythms, and aberrations in global climate 65 Ma to present. *Science, 292*(5517), 686-693.

Zachos, J. C., Dickens, G. R., & Zeebe, R. E. (2008). An early Cenozoic perspective on greenhouse warming and carbon-cycle dynamics. *Nature, 451*(7176), 279-283.

Zachos, J. C., Kroon, D., Blum, P., & al., e. (2004). *Proc. ODP, Initial Reports* (Vol. 208). College Station.

Zachos, J. C., Rohl, U., Schellenberg, S. A., Sluijs, A., Hodell, D. A., Kelly, D. C., . . . Kroon, D. (2005). Rapid acidification of the ocean during the Paleocene-Eocene thermal maximum. *Science, 308*(5728), 1611-1615.

Zachos, J. C., Schouten, S., Bohaty, S., Quattlebaum, T., Sluijs, A., Brinkhuis, H., . . . Bralower, T. J. (2006). Extreme warming of mid-latitude coastal ocean during the Paleocene-Eocene Thermal Maximum: Inferences from TEX86 and isotope data. *Geology, 34*(9), 737-740.

Zachos, J. C., Wara, M. W., Bohaty, S., Delaney, M. L., Petrizzo, M. R., Brill, A., . . . Premoli-Silva, I. (2003). A Transient Rise in Tropical Sea Surface

Temperature During the Paleocene-Eocene Thermal Maximum. *Science, 302*(5650), 1551-1554.

Zeebe, R. (2012). LOSCAR: Long-term ocean-atmosphere-sediment carbon cycle reservoir model v2. 0.4. *Geoscientific Model Development, 5*(1), 149-166.

Zeebe, R., & Zachos, J. (2012). Long-term legacy of massive carbon input to the Earth system: Anthropocene vs. Eocene. *Philosophical Transactions of the Royal Society*, 1-22.

Zeebe, R. E. (2005). Stable boron isotope fractionation between dissolved $B(OH)_3$ and $B(OH)_4^-$. *Geochimica et Cosmochimica Acta, 69*(11), 2753-2766.

Zeebe, R. E. (2013). What caused the long duration of the Paleocene‐Eocene Thermal Maximum? *Paleoceanography, 26*, 1-13.

Zeebe, R. E., Dickens, G. R., Ridgwell, A., Sluijs, A., & Thomas, E. (2014). Onset of carbon isotope excursion at the Paleocene-Eocene thermal maximum took millennia, not 13 years. *Proceedings of the National Academy of Sciences, 111*(12), E1062-E1063.

Zeebe, R. E., & Wolf-Gladrow, D. A. (2001). *CO_2 in seawater: Equilibrium, kinetics, isotopes* (Vol. 65): Elsevier.

Zeebe, R. E., & Zachos, J. C. (2007). Reversed deep-sea carbonate ion basin gradient during Paleocene-Eocene thermal maximum. *Paleoceanography, 22*(3), -.

Zeebe, R. E., & Zachos, J. C. (2013). Long-term legacy of massive carbon input to the Earth system: Anthropocene versus Eocene. *Philosophical Transactions of*

the Royal Society of London A: Mathematical, Physical and Engineering Sciences, 371(2001), 20120006.

Zeebe, R. E., Zachos, J. C., & Dickens, G. R. (2009a). Carbon dioxide forcing alone insufficient to explain Palaeocene-Eocene Thermal Maximum warming. *Nature Geoscience, 2*(8), 576-580.

Zeebe, R. E., Zachos, J. C., & Dickens, G. R. (2009b). Carbon dioxide forcing alone insufficient to explain Palaeocene–Eocene Thermal Maximum warming. *Nature Geoscience, 2*, 576-580.

Appendix to Chapter 1: Records of B/Ca from Sites 689 and 690 confirm global acidification during the Paleocene-Eocene Thermal Maximum

Introduction

Planktic foraminiferal B/Ca and boron isotope records from Site 1209 (North Pacific) feature a rapid decrease coincident with the carbon isotope excursion (CIE) at the onset of the Paleocene-Eocene Thermal Maximum (PETM) (Penman et al., 2014). These decreases were interpreted as evidence for the rapid and sustained acidification of the surface ocean as a result of carbon injection during the PETM. However, it is uncertain to what extent diagenetic processes such as dissolution and recrystallization might affect the B/Ca of foraminifers in sediment, and to what extent the signal at Site 1209 might include a local, rather than global signal which would be expected of ocean acidification. It is therefore important to reproduce the B/Ca results at other sites where local seawater carbonate chemistry and diagenetic regime differ from Site 1209 in order to test the interpretation that those records document a global surface ocean acidification. Towards this end, I measured B/Ca in surface- and thermocline-dwelling foraminifers from two well-studied PETM sections: ODP Sites 689 and 690 in the Weddell Sea (Southern Ocean).

Methods

ODP Site 689 (64° 31.009'S; 3° 05.996'E, depth = 2080 m) and Site 690 (65° 9.629' S; 1° 12.296' E, 2914 m) (Leg 113) are both located on the Maud Rise in the Weddell Sea. The PETM CIE, which is used herein for age model construction and correlation between sites, was first identified at Site 690 by Kennett and Stott (1991)

at a depth of 170.6 meters below seafloor (mbsf), and at Site 689 at 208.2 mbsf (Kelly et al., 2012). Site 690 contains the entire CIE onset, body, and recovery, while Site 689 captures the onset of the CIE at higher sedimentation rate but does not contain the full body or recovery. Samples of the symbiont-bearing surface-dwelling foraminifera *Acaranina soldadoensis* and *Acaranina praepentacamerata* and the thermocline-dwelling genus *Subbotina* were picked from washed sediment samples taken at 1-5 centimeter resolution. Due to foraminiferal species assemblage changes during the PETM (Kelly, 2002) at Sites 689 and 690, *A. soldadoensis* was measured in the Paleocene and *A. praepentacamerata* was used within the CIE interval, however, in overlapping samples very little offset between the two species is evident in B/Ca. Shells were cleaned using established oxidative-reductive cleaning procedures (Barker et al., 2003b) and B/Ca analyses was performed using a ThermoFinnegan Element XR inductively-coupled plasma mass spectrometer (ICP-MS) following the methods of Brown et al. (2011).

Results

B/Ca evidence for acidification in the Southern Ocean

At Southern Ocean Sites 689 and 690, the B/Ca of surface-dwelling Acaraninids fall from a pre-CIE average of ~50 to 55 μmol/mol to an average of ~30 μmol/mol within the PETM while the thermocline-dwelling Subbotinids show a decrease from 40-50 μmol/mol to 20-30 μmol/mol. The B/Ca decreases in both taxa and at both sites are coincident with the CIE and are followed by a plateau of low values and then a gradual recovery at site 690 (the recovery is missing at Site 689 due

to a core gap), in step with the CIE body and recovery. The remarkable similarity of the B/Ca records at Sites 689 and 690 despite their significantly different depths (2080m vs. 2914m) and sedimentation rates suggests that the trends in both records are not the results of dissolution or diagenesis, which would have differed between the two sites, but rather confirms that the signals reflect local surface water conditions. The B/Ca records from the Southern Ocean sites are also quite similar in shape and timing (relative to the CIE) to the B/Ca records from North Pacific Site 1209 (Penman et al., 2014), consistent with a relatively uniform acidification of the surface ocean globally. In addition, absolute B/Ca values between Sites 689/690 and Site 1209 (which shows a B/Ca reduction from ~70 to ~45 μmol/mol in mixed-layer-dwellers and a reduction from ~50 to ~35 μmol/mol in thermocline-dwellers during the PETM) show spatial patterns suggesting surface carbonate chemistry differences between the Southern Ocean and North Pacific, as observed in the modern ocean. Indeed, the variability in e.g. pre-PETM mixed-layer-dweller B/Ca (~55 at Sites 689 and 690 vs. ~70 μmol/mol at Site 1209) is similar to the variability in modern core-top mixed-layer-dwelling foraminiferal B/Ca taken from different oceanographic settings (Foster, 2008). We take the similarity of PETM B/Ca records between sites 689, 690 and 1209 as evidence for global surface ocean acidification in response to rapid carbon injection.

Figures

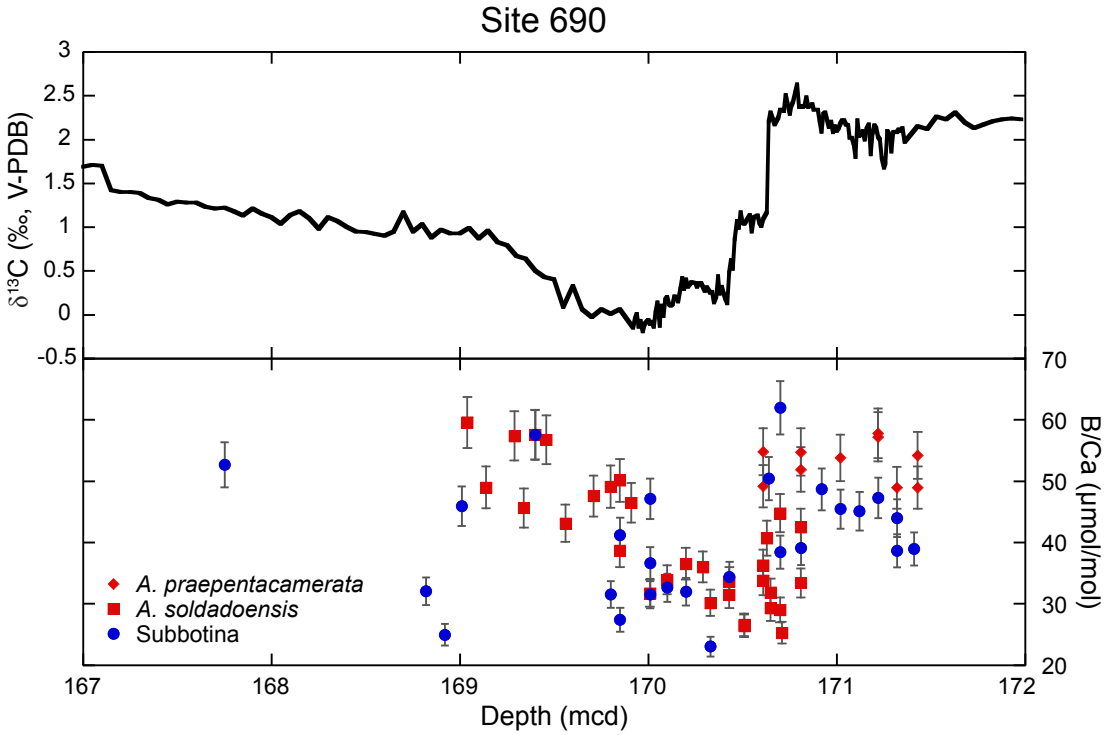

Figure 1: Bulk carbonate $\delta^{13}C$ (Kelly et al., 2012) and B/Ca of planktonic foraminifers from Southern Ocean Site 690 plotted against depth in core. Error bars on B/Ca represent two standard deviations of repeat measurements of an in-house foraminiferal carbonate standard (7%).

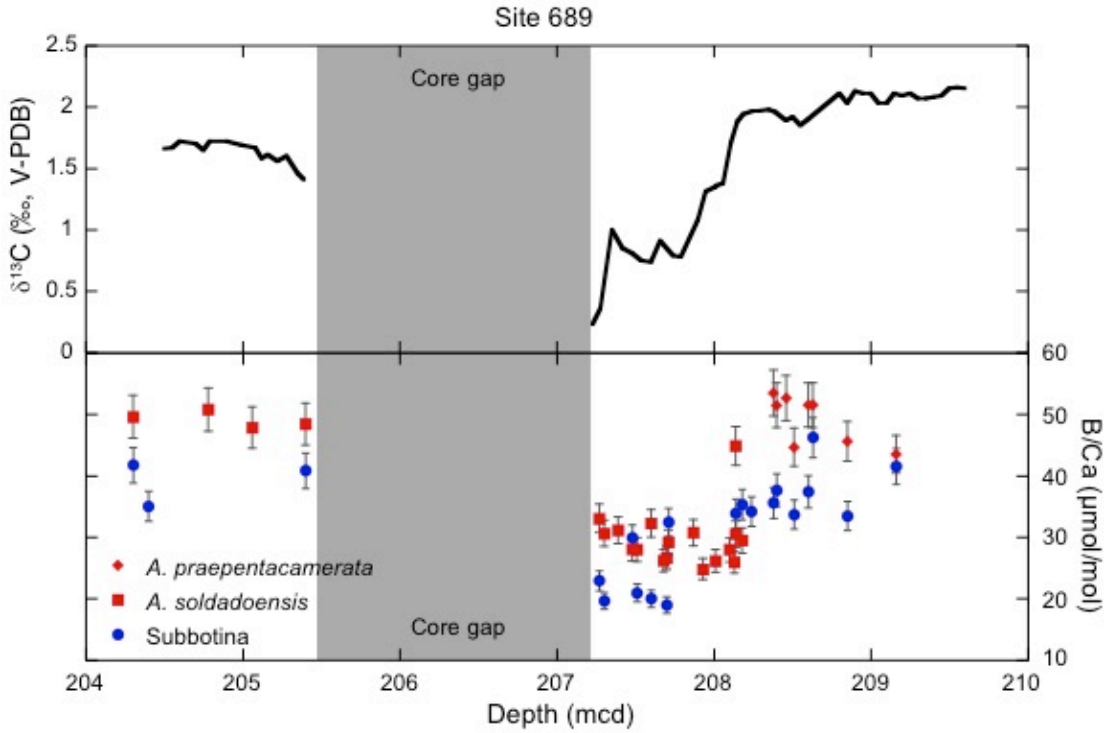

Figure 2: Bulk carbonate $\delta^{13}C$ (Kelly et al., 2012) and B/Ca of planktonic foraminifers from Southern Ocean Site 689 plotted against depth in core. Error bars on B/Ca represent two standard deviations of repeat measurements of an in-house foraminiferal carbonate standard (7%).

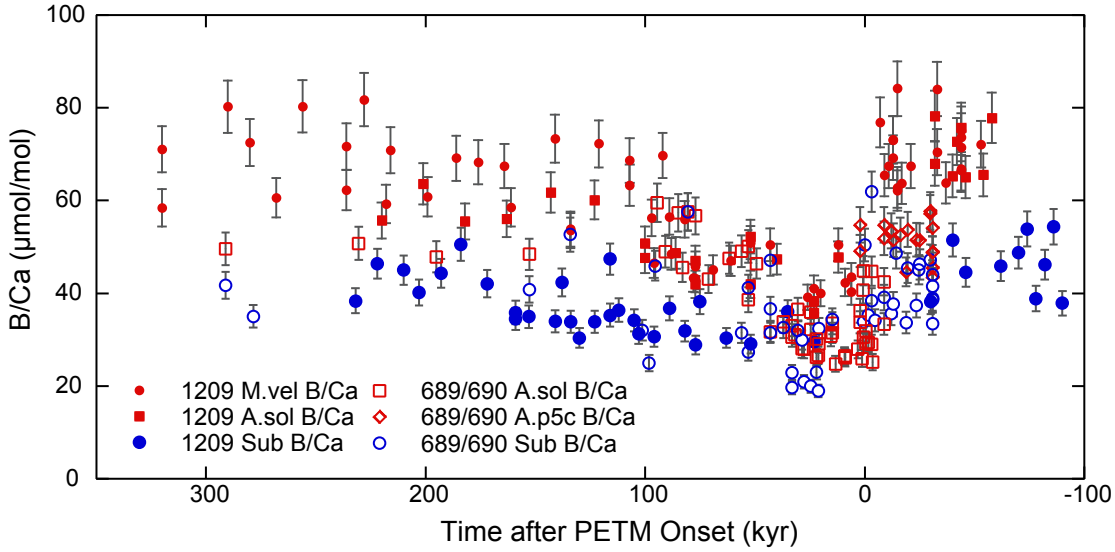

Figure 3: Planktic foraminifer B/Ca from all sites vs. time. Red symbols are surface-dwellers, blue symbols are thermocline dwellers. M.vel = *Morozovella velascoensis*, A.sol = *Acaranina soldadoensis*, A.p5c = *Acaranina praepentacamerata*, Sub = genus Subbotinae. Open symbols are Southern Ocean (Sites 689 and 690), closed symbols are North Pacific (Site 1209) (Penman et al., 2014). Age models were generated for all sites by correlating the fine fraction or bulk carbonate $\delta^{13}C$ of Röhl et al. (2007), and in the case of Sites 689 and 690 used the tie points of Kelly et al. (2012). Error bars on B/Ca represent two standard deviations of repeat measurements of an in-house foraminiferal carbonate standard (7%).

References

Barker, S., Greaves, M., and Elderfield, H., 2003, A study of cleaning procedures used for foraminiferal Mg/Ca paleothermometry: Geochemistry, Geophysics, Geosystems, v. 4, no. 9.

Brown, R. E., Anderson, L. A., Thomas, E., and Zachos, J., 2011, A core-top calibration of B/Ca in the benthic foraminifers Nuttalides umbonifera and Oridorsalis umbonatus: A proxy for Cenozoic bottom water carbonate saturation: Earth & Planetary Science Letters, v. 310, p. 360-368.

Foster, G. L., 2008, Seawater pH, pCO2 and [CO2-3] variations in the Caribbean Sea over the last 130†kyr: A boron isotope and B/Ca study of planktic foraminifera: Earth and Planetary Science Letters, v. 271, no. 1-4, p. 254-266.

Kelly, D. C., 2002, Response of Antarctic (ODP Site 690) planktonic foraminifera to the Paleocene-Eocene thermal maximum: Faunal evidence for ocean/climate change: Paleoceanography, v. 17, no. 4, p. 1071.

Kelly, D. C., Nielsen, T. M., and Schellenberg, S. A., 2012, Carbonate saturation dynamics during the Paleocene–Eocene thermal maximum: Bathyal constraints from ODP sites 689 and 690 in the Weddell Sea (South Atlantic): Marine Geology, v. 303, p. 75-86.

Kennett, J. P., and Stott, L. D., 1991, Abrupt Deep-Sea Warming, Palaeoceanographic Changes and Benthic Extinctions At the End of the Palaeocene: Nature, v. 353, no. 6341, p. 225-229.

Penman, D. E., Hönisch, B., Zeebe, R. E., Thomas, E., and Zachos, J. C., 2014, Rapid and sustained surface ocean acidification during the Paleocene-Eocene Thermal Maximum: Paleoceanography.

Röhl, U., Westerhold, T., Bralower, T. J., and Zachos, J. C., 2007, On the duration of the Paleocene-Eocene thermal maximum (PETM): Geochemistry Geophysics Geosystems, v. 8, p. -.

Chapter 2: Direct evidence for a carbonate compensation depth overshoot in the aftermath of the Paleocene-Eocene Thermal Maximum

Donald E. Penman

with Sandra Kirtland Turner, Philip Sexton, Richard Norris, Alex Dickson, James C. Zachos, Thomas Westerhold, Ursula Röhl, Andy Ridgwell, Richard Zeebe, IODP Expedition 342 Scientists

ABSTRACT

Rapid, global shoaling of the carbonate compensation depth (CCD) at the onset of the Paleocene-Eocene Thermal Maximum (PETM) occurred as a response to the invasion of CO_2 into the oceans. Deep sea sediments show that the CCD gradually recovered as seafloor carbonate dissolution and weathering feedbacks restored ocean carbonate chemistry. Numerical and conceptual models of the long-term carbon cycle predict that these negative feedbacks should have caused a period of carbonate oversaturation (relative to pre-event levels) during the event recovery, wherein the build-up of weathering products in the ocean would have caused an "overshoot" of the CCD. However, direct evidence for a deep ocean depression of the post-PETM CCD has yet to be demonstrated. Here we present two PETM pelagic sections recently recovered by IODP Expedition 342 in the North Atlantic. Site U1409 is similar in character to many previously published pelagic records, featuring a sharp drop in wt% $CaCO_3$ coincident with the PETM carbon isotope excursion. The deeper Site U1403, however, is carbonate-barren in the Late Paleocene (indicating a depth below the pre-PETM CCD), and features a transition to carbonate-bearing sediments in the Early Eocene. Carbonate and organic carbon isotope stratigraphy demonstrate

that the onset of carbonate sedimentation at Site U1403 occurred ~70 kyr after the PETM onset, and is thus the first direct evidence for a post-PETM CCD overshoot. Carbon release experiments using carbon cycle models show that the timing of the CCD overshoot is consistent with a large initial release of carbon as well as a slow, prolonged leak lasting additional tens of thousands of years. The >2 million year persistence of carbonate preservation at the deeper Site U1403 indicates the post-PETM CCD overshoot was superimposed on a well documented global long-term trend toward increased pelagic carbonate preservation.

INTRODUCTION

The Paleocene-Eocene Thermal Maximum (PETM; ~56 million years ago) is one of the largest and most abrupt greenhouse warming events of Earth's past. Marine and terrestrial inorganic and organic carbon isotope records show the event was marked by a pronounced negative carbon isotope excursion (CIE) of >3‰ (Kennett and Stott, 1991; Koch et al., 1992)(McInerney and Wing, 2011), various temperature proxies record global surface warming in excess of 4°C (Dunkley-Jones et al., 2013), and geochemical and sedimentological evidence demonstrates rapid ocean acidification (Penman et al., 2014; Zachos et al., 2005). Collectively, these lines of evidence suggest a geologically rapid (10^3-10^4 years), massive (3,000 to 10,000 PgC) release of ^{13}C-depleted carbon in the form of methane and/or carbon dioxide (CO_2), into the ocean-atmosphere system (Dickens et al., 1995; Panchuk et al., 2008; Zeebe et al., 2009a). The PETM thus offers the opportunity to examine the response of the

long-term global carbon cycle and seawater carbonate chemistry to an ancient CO_2 release similar in magnitude to ongoing anthropogenic fossil fuel combustion (Zeebe and Zachos, 2012).

Our current understanding of long-term carbon cycle processes predicts two phases of ocean carbonate saturation response to carbon injection during the PETM. Over the short term, invasion of CO_2 into seawater lowers pH (Hönisch et al., 2012; Penman et al., 2014; Ridgwell and Schmidt, 2010; Zeebe and Wolf-Gladrow, 2001) and carbonate saturation state (Ω) in tandem, resulting in decreased carbonate production and/or dissolution of both newly deposited and pre-existing carbonate seafloor sediments (Zachos et al., 2005). The result is a dramatic, rapid (within 10^2 – 10^3 years of initial carbon release) shoaling of the carbonate compensation depth (CCD, the depth below which no carbonate is preserved in sediments) (Dickens et al., 1997) which has been well documented at the onset of the PETM (Sluijs et al., 2012b; Zachos et al., 2005; Zeebe and Zachos, 2007). A second phase of carbonate saturation response, arising from increased temperature and pCO_2 levels, is an increase in the rate of terrestrial carbonate and silicate rock chemical weathering, which can be generalized:

$$(1)\ CO_2 + H_2O + CaCO_3 \rightarrow Ca^{2+} + 2HCO_3^-$$

$$(2)\ CaSiO_3 + 2CO_2 + 3H_2O \rightarrow H_4SiO_4 + 2HCO_3^- + Ca^{2+}$$

Speeding up these reactions increases the delivery of dissolved inorganic carbon (DIC) and total alkalinity (TA), the building blocks of carbonate, to the oceans, and thus gradually increases saturation state, decoupling it from pH (Hönisch et al., 2012).

An intensification of continental weathering during the PETM is supported by an increase in the osmium isotopic composition of seawater (Ravizza et al., 2001) and the flux of kaolinite to marine sediments (Robert and Kennett, 1994). The silicate weathering rate responds nearly instantaneously to increased temperature and pCO_2; however, because of the large standing reservoir of DIC and TA this feedback takes $>10^4$ years to gradually overcome the undersaturation associated with the initial acidification phase (Dickens et al., 1997; Goodwin and Ridgwell, 2010). On long timescales ($>10^5$ years), this increased weathering-derived flux of TA and DIC to the oceans must be balanced by carbonate precipitation and burial:

$$(3)\ Ca^{2+} + 2HCO_3^- \rightarrow CaCO_3 + CO_2 + H_2O.$$

The long-term balance of carbonate weathering with subsequent carbonate precipitation and burial has no permanent effect on the ocean's TA or DIC budgets (Equation 1 is the reverse of Equation 3), however, the long-term balance of silicate weathering (Equation 2) with carbonate burial (Equation 3) gives the net reaction (2+3):

$$(4)\ CaSiO_3 + CO_2 + 2H_2O \rightarrow CaCO_3 + H_4SiO_4.$$

Equation 4 represents the general long-term fate of excess carbon released during the PETM; weathering and carbonate burial consumes CO_2 and converts it to carbonate, which becomes buried in deep-sea sediments. This has been proposed as an important long-term negative (stabilizing) feedback on climate throughout Earth history (Berner et al., 1983; Walker et al., 1981) and specifically during the PETM recovery (Dickens et al., 1997). One way in which carbonate burial (Equation 3) can vary to balance

changes in weathering (Equations 1-2) is through fluctuations of the CCD: during the initial acidification phase, carbonate undersaturation leads to a short-term shoaling of the CCD, whereas on longer timescales (>10^5 years), faster weathering rates (equation 1) lead to carbonate oversaturation and increased carbonate burial, which can be accommodated by a deeper CCD (Pälike et al., 2012; Komar et al., 2013). In order to remove the excess carbon (10^3-10^4 PgC) introduced during the PETM and balance long term carbon sources and sinks, carbonate burial during this oversaturation phase must be greater than before the event until pCO_2 recovers to pre-event levels; one way this could be accomplished is through an "overshoot" of the CCD to a position deeper than its pre-event depth (Dickens et al., 1997).

It is possible that additional carbon sequestration processes operated during the PETM recovery; these have the potential to influence the CCD, because removing carbon from the ocean/atmosphere has the effect of simultaneously increasing pH and saturation state (in a sense, the opposite of the PETM acidification phase). The pace of the CIE recovery, ~70 to 150kyr after the onset (Farley and Eltgroth, 2003; Murphy et al., 2010) appears too rapid to be explained by enhanced carbonate burial alone, suggesting preferential removal of ^{12}C is necessary to match the CIE recovery timing (Bowen and Zachos, 2010). Enhanced burial of organic carbon (C_{org}) during the recovery has therefore been suggested as a mechanism to accelerate the PETM recovery, and increased marine productivity has been suggested based on elevated biogenic barium accumulation rates (Bains et al., 2000; Ma et al., 2014) and coccolith Sr/Ca (Stoll and Bains, 2003) during the PETM. If additional burial followed such

elevated productivity, a result would have been a deepening of the CCD. However, just as the CCD shoaling response to carbon addition at the PETM onset was transient (owing to weathering feedbacks), so would be the contribution to CCD deepening by carbon removal – it would last only as long as carbon continued to be removed. Furthermore, with a few minor exceptions, no sufficiently large C_{org}-bearing sediments dating from the PETM recovery are known, and no clear mechanism exists to begin burying C_{org} ~70kyr after the onset and then cease burial once the CIE recovery is complete.

A CCD overshoot is predicted by the silicate weathering feedback, and, indeed, is a feature of carbon cycle model simulations of the PETM that include such a feedback (Dickens et al., 1997; Zeebe et al., 2009a). Given the temperature/CO_2 dependence of the weathering feedback, the magnitude of the resultant CCD overshoot caused by enhanced weathering should scale with the mass of carbon released, and thus could offer crucial constraints on PETM carbon emissions. However, observational evidence for a deeper post-PETM CCD has thus far remained elusive. Post-PETM oversaturation has been suggested by records of increased carbonate mass accumulation rates in sediment cores during the event's recovery phase (Farley and Eltgroth, 2003; Kelly et al., 2005; Murphy et al., 2010; Zachos et al., 2005). However, the cause of these increases is likely linked to surface water processes (as they are accompanied by drastic assemblage shifts dominated by just a few calcifying species (Kelly et al., 2005; Raffi et al., 2009) leading to increased surface carbonate production. Indeed, given the relatively shallow paleodepth of those

sediments it is unlikely that their carbonate accumulation rates are the direct result of changes in deep-water saturation state, and thus while those observations support an increase in global carbonate burial during the PETM recovery, they do not offer direct evidence for the depth of the CCD.

Here we provide new observations from recently recovered sediment cores in the North Atlantic (IODP Sites U1403 and U1409) that further constrain the evolution of the CCD through the PETM, including direct evidence for a CCD overshoot during the PETM recovery.

MATERIALS AND METHODS

During IODP Expedition 342, drilling operations penetrated the P-E boundary at Sites U1403 (39°56.5997N, 51°48.1998W, 4946m depth) and U1409 (41°17.7501N, 49°13.9996W, 3502m depth). Shipboard investigation described lithology, identified the approximate positions of the P-E boundary by nannofossil biostratigraphy, and provided coarse-resolution records of wt.% $CaCO_3$. Cores spanning the PETM were scanned at 1-2 cm-resolution at the IODP Bremen Core Repository and at Scripps Institution of Oceanography using Avaatech X-ray fluorescence (XRF) core scanners. Estimates of the total abundance of calcium (Ca) and iron (Fe) were obtained by scanning cores at an energy level of 10kV, current of 500 uA, and measurement area of 10 x 12 mm. Estimated wt. % $CaCO_3$ records were generated by regressing shipboard wt. % $CaCO_3$ measurements against the natural logarithm of XRF-derived Ca/Fe ratios. For stable isotope analyses, samples were collected at ~5cm resolution from Site U1409 and 10cm resolution from Site U1403,

freeze dried, homogenized with mortar and pestle, and analyzed for $\delta^{13}C_{carb}$ on a ThermoFisher MAT 253 stable isotope mass spectrometer coupled to a Kiel IV carbonate device using standard dual-inlet techniques. In addition, samples from Site U1409 were washed and sieved, and specimens of the benthic foraminifera *Nuttalides truempyi* were picked from the 150-200 and 212-300 μm size fraction. Where possible, 3-8 of these specimens from each sample were run using the $\delta^{13}C_{carb}$ methods described above. For $\delta^{13}C_{org}$ analysis of Site U1403, homogenized sample powders were de-carbonated in 1M HCl and washed in de-ionized water. Wt. % $CaCO_3$ was measured using a Coulormat device. $\delta^{13}C_{org}$ was measured using a Thermo-Finnegan MAT 253 mass spectrometer coupled to a flash HT elemental analyzer, which had been optimized for the measurement of samples with low organic carbon abundances. Analytical reproducibility was monitored using analyses of an IAEA CH-6 sucrose standard and was < ±0.1‰. All $\delta^{13}C$ data are expressed relative to V-PDB.

In order to explore the broader implications of our new CCD constraints for possible PETM emissions scenarios, we also simulated oceanic carbon cycle response to a range of C emission pulses using the global carbon cycle model LOSCAR (Long-term Ocean Sediment CArbon Reservoir) (Zeebe, 2012; Zeebe et al., 2009a). LOSCAR is a numerically-efficient geochemical box model of the marine carbon cycle with realistic interaction with sediments, capable of multi-million year simulations of carbon cycle processes including CCD depth. The only alteration herein from the standard Paleogene LOSCAR v.2.0.4 setup (Zeebe, 2012) is that the

seafloor bathymetry and sediments are more finely subdivided to 100m water depth bins (from the standard 500m resolution) so that CCD evolution can be modeled at a finer scale. In LOSCAR, silicate weathering is parameterized as

$$(5)\ F_w = F_{eq} * ([CO_2]_{atm} / [CO_2]_{eq})^{Nsi}$$

where $[CO_2]_{eq}$ represents equilibrium atmospheric pCO_2 (prescribed as a model boundary condition) and F_{eq} is equal to the volcanic CO_2 flux, such that when $[CO_2]_{atm}$ is equal to $[CO_2]_{eq}$ then volcanic carbon emissions are perfectly balanced by silicate weathering and carbonate burial (Zeebe, 2012). Under this condition pCO_2 is constant over long timescales and the model maintains equilibrium. N_{Si} is a free parameter in the model that sets the strength of the silicate weathering feedback (default $N_{Si} = 0.3$), and governs how quickly silicate weathering rates respond to model pCO_2 that differs from $[CO_2]_{eq}$. We utilize the LOSCAR model in this study in order to qualitatively demonstrate what mechanisms are consistent with the new data, not in an attempt to reconstruct exactly a PETM scenario.

RESULTS

The PETM interval was initially identified at Site U1409 by shipboard biostratigraphy and the CIE was subsequently characterized post-expedition in bulk $\delta^{13}C_{carb}$ (Figure 1A). The CIE occurs in an interval of variously silicified sediments (siliceous claystones, siliceous limestones and cherts) at 182.2–182.5 mcd,

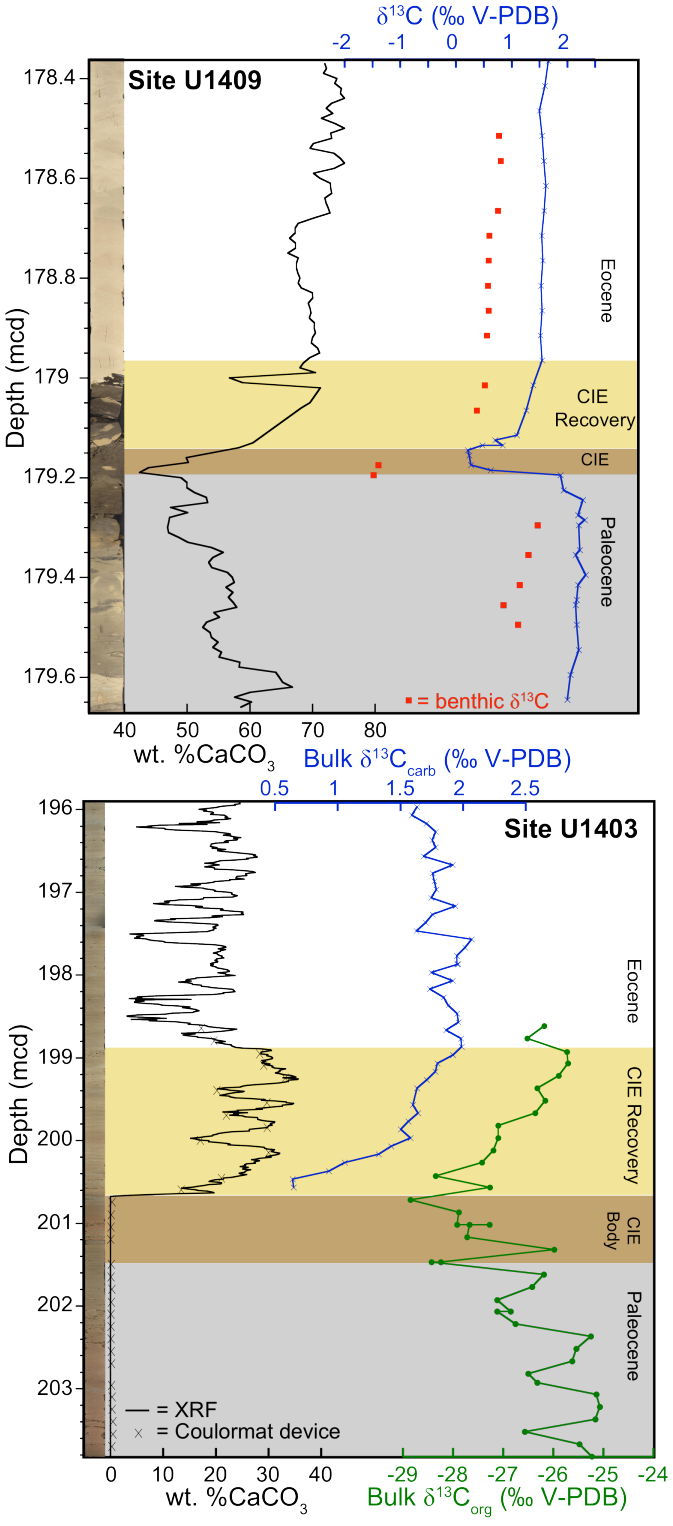
δ13C (‰ V-PDB)
-2
-1
0
1
2
Site U1409
178.4
178.6
178.8
179
179.2
179.4
179.6
Depth (mcd)
Eocene
CIE Recovery
CIE
Paleocene
▪ = benthic δ13C
40
50
60
70
80
wt. %CaCO3
Bulk δ13Ccarb (‰ V-PDB)
0.5
1
1.5
2
2.5
Site U1403
196
197
198
199
200
201
202
203
Depth (mcd)
Eocene
CIE Recovery
CIE Body
Paleocene
— = XRF
× = Coulormat device
0
10
20
30
40
wt. %CaCO3
-29
-28
-27
-26
-25
-24
Bulk δ13Corg (‰ V-PDB)

Figure 1: Lithology and $\delta^{13}C$ of the PETM at sites U1409 (top) and U1403 (bottom) plotted against composite depth (mcd). Each panel shows core photo (stretched in the horizontal), wt. %$CaCO_3$ estimated by XRF (black line), and bulk $\delta^{13}C_{carb}$ (blue line). Bulk $\delta^{13}C_{org}$ (green line) and wt. % $CaCO_3$ measured with a Coulormat device (black X's) are also shown for Site U1403, and benthic foraminifer *Nuttalides truempyi* $\delta^{13}C$ (red squares) is shown for Site U1409. Depth intervals representing the Paleocene, CIE, Recovery, and post-PETM based on $\delta^{13}C$ stratigraphy are highlighted with grey, brown, tan, and white backgrounds, respectively.

contrasting sharply with the nannofossil chalk that characterizes the rest of the Eocene. Although likely slightly condensed, the $\delta^{13}C_{carb}$ record bears the typical PETM CIE pattern of an abrupt decrease of ~2‰ followed by a plateau of low values and then a gradual recovery (Fig. 1A). The Site U1409 benthic foraminiferal $\delta^{13}C$ record is discontinuous due to silicification of sediments at the onset and during most of the recovery, but minimum values in the CIE clay layer show a large (~3‰) excursion, with similar absolute values across the PETM to benthic records generated from Walvis Ridge in the South Atlantic (McCarren et al., 2008b). Above and below this interval carbonate contents are high (~80 wt.%) and within the CIE carbonate content decreases to a minimum of 30 wt.%. This carbonate pattern is similar to other well-studied pelagic PETM sections and allows a similar interpretation of this site's position relative to the CCD: high carbonate content before and after the event indicates the CCD was below Site U1409, while the decrease in carbonate during the PETM documents a transient shoaling of the CCD. The absence of zero wt.% $CaCO_3$ sediment at Site U1409 contrasts with records from the South Atlantic Ocean (Zachos et al., 2005) where cores even shallower than U1409 are completely devoid of carbonate within the CIE. This could be taken as evidence that CCD shoaling in the North Atlantic Ocean was less dramatic than that in the South; however, we note that hiatuses or incomplete recovery of this cherty interval could have resulted in loss of the most severely acidified conditions from this record.

Site U1403 features a pronounced increase in carbonate from <0.5 wt.% in the Upper Paleocene to ~20 wt.% in the lower Eocene (Figure 1B), comprised mostly of

calcareous nannofossils of biostratigraphic zone NP9B. Below this level, Site U1403 sediment is nannofossil claystone, nearly barren of carbonate (<0.5 wt.%) throughout the Upper Paleocene to at least 61Ma. Due to a lack of carbonate to define the CIE, we rely on bulk $\delta^{13}C_{org}$ to define the P-E boundary. The $\delta^{13}C_{org}$ indicates a negative CIE between 200.7 and 201.5 mcd that is superimposed on smaller-scale variations leading up to the first excursion data point. The $\delta^{13}C_{carb}$ record begins at the onset of carbonate sedimentation with low values of ~0.6‰, followed by a gradual 1.4‰ increase over the next ~1.6 m, parallel to the recovery of $\delta^{13}C_{org}$. Given this simultaneous trend to higher $\delta^{13}C$ values in both carbonate and C_{org} and its stratigraphic position in nannofossil zone NP9B, this gradual increase in $\delta^{13}C$ can be unambiguously assigned to the recovery interval of the PETM CIE. The magnitude of the $\delta^{13}C$ increase (1.4‰) is close to the full amplitude of the PETM CIE recovery observed in bulk carbonates globally (Röhl et al., 2007) and at Site U1409 (Figure 2A), so we can constrain the onset of carbonate sedimentation at lower abyssal Site U1403 to the early stages of the PETM recovery.

Age models for Sites U1403 and U1409 were constructed by correlating their $\delta^{13}C_{carb}$ and $\delta^{13}C_{org}$ records to a compilation of bulk and fine fraction $\delta^{13}C_{carb}$ on an orbitally tuned common age model (Röhl et al., 2007) (Figure 2A). Note that this age model produces a shorter duration of the PETM CIE than other estimates (Murphy et al., 2010), so durations here should be taken as minimum estimates. On this time scale, carbonate sedimentation begins at Site U1403 ~70ky after the PETM onset. The initial appearance of carbonate is followed by a period of elevated (20-40) wt. %

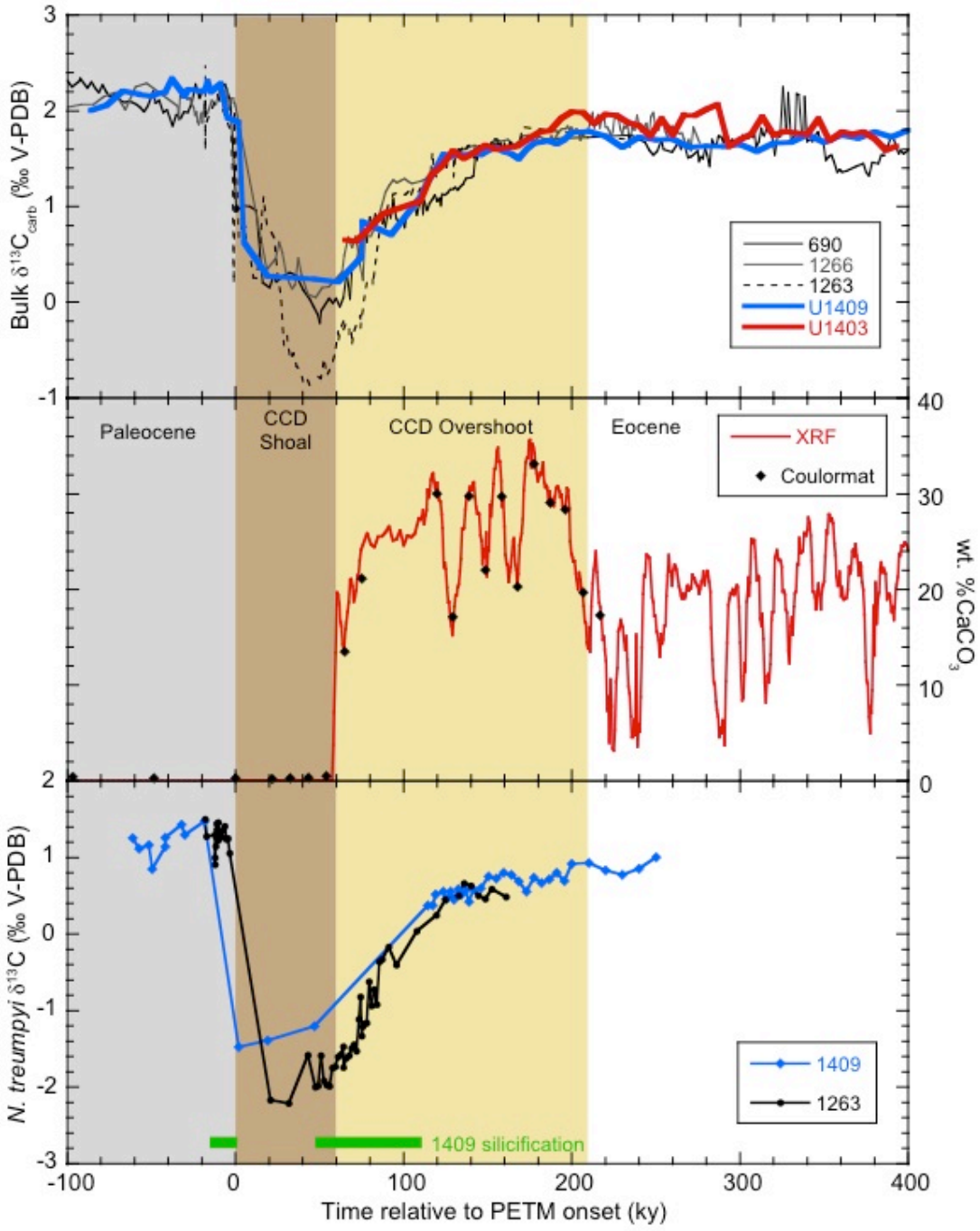
Bulk $\delta^{13}C_{carb}$ (‰ V-PDB)
690
1266
1263
U1409
U1403
Paleocene
CCD Shoal
CCD Overshoot
Eocene
XRF
Coulormat
wt. %$CaCO_3$
N. treumpyi $\delta^{13}C$ (‰ V-PDB)
1409
1263
1409 silicification
Time relative to PETM onset (ky)

Figure 2: A. Bulk $\delta^{13}C_{carb}$ records from sites 690, 1266, 1263 (Röhl et al., 2007), U1403, and U1409 plotted on the age model used in this study. B. $\%CaCO_3$ of site U1403. C. Comparison of benthic $\delta^{13}C$ from South Atlantic Site 1263 (McCarren et al., 2008b) and U1409 demonstrating small and constant North-South aging gradient during the CCD overshoot. Green bars indicate silicified intervals at Site U1409 which precluded measurement of benthic foraminifers.

$CaCO_3$ that persists an additional ~150kyr. Cyclical fluctuations between 5 and 25 wt.% $CaCO_3$ continue throughout the lower Eocene.

DISCUSSION

The pattern of carbonate sedimentation at Site U1403 (carbonate barren in the Paleocene with carbonate appearing during the PETM recovery) has not previously been observed in sedimentary deposits spanning the PETM. The lack of carbonate in the Upper Paleocene and into the earliest Eocene indicates a paleodepth below the CCD before the PETM and through the CIE-onset. The onset of carbonate sedimentation ~70kyr after the PETM onset indicates that the CCD deepened to below the paleodepth of Site U1403 during the early phase of PETM recovery – direct evidence for a post-PETM CCD overshoot. The ~150kyr period of elevated carbonate deposition represents the main phase of the CCD overshoot, and can be correlated to intervals of enhanced carbonate accumulation at shallower paleo-water depths documented by Kelly et al. (2005) and Murphy et al. (2010).

In carbon cycle models of carbon emissions that feature a silicate weathering feedback, the CCD overshoot occurs quickly (within ~10kyr) after carbon emissions cease (Figure 3B) (Dickens et al., 1997; Zeebe et al., 2009a). The delayed (by at least ~70kyr) onset of carbonate sedimentation at Site U1403 is therefore inconsistent with only a short "spike" of carbon released at the onset of the PETM, and is better explained by a sustained release of carbon lasting many tens of kyr after an initial spike (Figure 3B), in accordance with previous studies (Penman et al., 2014; Zeebe et al., 2009a). This prolonged phase of carbon release might have taken place as a

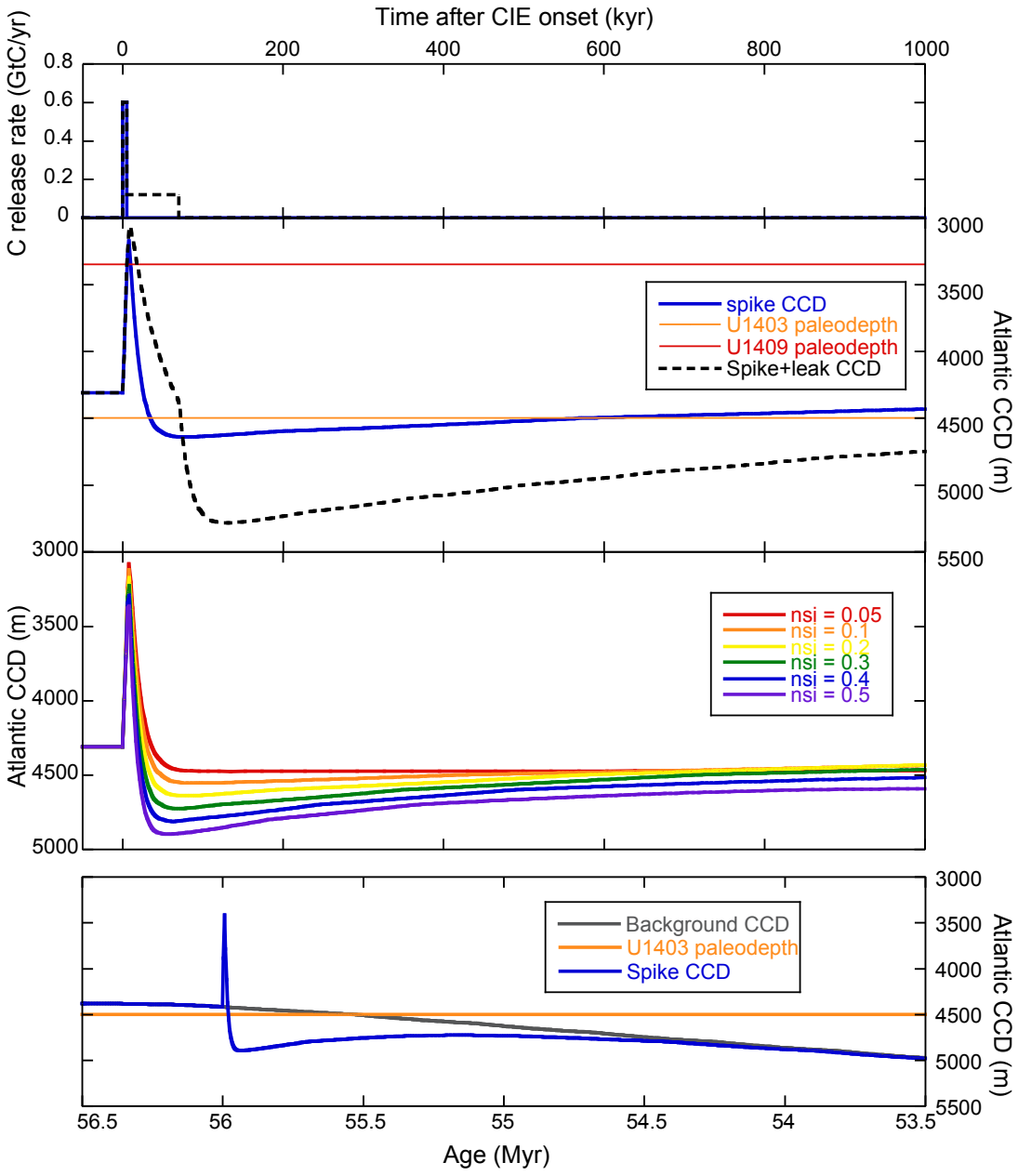
Time after CIE onset (kyr)
0
200
400
600
800
1000
C release rate (GtC/yr)
0.8
0.6
0.4
0.2
0
spike CCD
U1403 paleodepth
U1409 paleodepth
Spike+leak CCD
Atlantic CCD (m)
3000
3500
4000
4500
5000
5500
nsi = 0.05
nsi = 0.1
nsi = 0.2
nsi = 0.3
nsi = 0.4
nsi = 0.5
Background CCD
U1403 paleodepth
Spike CCD
56.5
56
55.5
55
54.5
54
53.5
Age (Myr)

Figure 3: LOSCAR modeling of the CCD overshoot. A: Carbon emissions forcing for spike (0.6PgC/yr for 5kyr) and spike + leak (0.11PgC/yr for an additional 65kyr) scenarios. B: Evolution of the modeled Atlantic CCD in response to spike and spike + leak scenarios. Without a sustained leak, the CCD overshoots within ~15kyr, in contrast to the U1403 record C: Large sensitivity of the CCD overshoot magnitude, timing, and duration to the strength of the weathering feedback, which is poorly constrained. Weathering flux is parameterized in LOSCAR as $F_w = F_{eq} * ([CO_2]_{atm} / [CO_2]_{eq})^{Nsi}$, where F_{eq} and $[CO_2]_{eq}$ are equilibrium weathering flux and atmospheric pCO_2 at which volcanic carbon emissions are perfectly balanced by silicate weathering and carbonate burial (Zeebe, 2012). N_{Si} is a free parameter in the model which sets the strength of the silicate weathering feedback (default $N_{Si} = 0.3$). All scenarios are spike only. D: Atlantic CCD evolution of a spike scenario superimposed on a long-term CCD deepening trend forced by increasing volcanic carbon flux by 15% over 3Ma. Note separate time axis for panel D. All LOSCAR models are provided to qualitatively demonstrate mechanisms that are consistent with the new CCD constraints, not as an attempt to precisely reconstruct a PETM scenario.

positive feedback response to warming either as methane or organic carbon (Bowen, 2013; Zeebe, 2013).

(Penman et al., 2014; Zeebe et al., 2009a). This prolonged phase of carbon release might have taken place as a A notable and unexpected aspect of the Site U1403 carbonate record is that following the main phase of the CCD overshoot featuring the highest carbonate contents, wt.% $CaCO_3$ does not return to near 0% (its pre-event level) before the next hyperthermal (ETM-2, ~2.4Ma later), indicating that the post-PETM CCD overshoot was long-lasting at this site. This represents a component of the carbon cycle (the North Atlantic CCD) that never recovered to its pre-PETM equilibrium state. That this was likely a global phenomena is supported by carbonate records (e.g., %$CaCO_3$) from other locations in the Atlantic and Pacific (Zachos et al., 2005; Kelly et al. 2010; Hancock and Dickens 2005; Hancock et al. 2007) which also show long-term trends across the Late Paleocene – Early Eocene. As such, only two possible explanations exist for this observation. First, negative feedbacks could have been slow to re-establish equilibrium. This is unlikely, given that all other records of environmental perturbation during the PETM (such as temperature, pH, and the CIE) recovered in hundreds of thousands of years, not millions. Second, the carbon cycle, and the CCD, may have recovered to a new equilibrium that had shifted from its pre-PETM baseline. This could have arisen from changes in boundary conditions (either unrelated to, or caused by, the PETM itself), or the system could exhibit threshold behavior with multiple equilibria.

Several mechanisms may help explain the long duration of the CCD overshoot. First, the PETM CCD evolution may have been superimposed on a long-term (multi-million year), baseline CCD deepening trend (Depaolo and Ingram, 1985;

Kelly et al., 2012). Increasing pCO_2 across the Late Paleocene-Early Eocene from greater volcanic CO_2 release or an imbalance between terrestrial C_{org} oxidation and marine C_{org} burial could have caused increasing weathering rates and thus higher seawater carbonate saturation and a deepening CCD from ~58 to ~52Ma, independently of the PETM (Kelly et al., 2012). Indeed, our LOSCAR simulations of a carbon release superimposed on a long-term CCD deepening (forced in this case by long-term increasing volcanic CO_2 flux, Figure 3D) agree well with our observations from Site U1403, including the persistence of the 'overshoot'. Alternatively, a reorganization of ocean circulation during the PETM would have had a significant effect on the regional CCD (note that the permanence of the CCD overshoot was not necessarily global). Indeed, profound circulation changes during the PETM have been proposed (Bice and Marotzke, 2002; Nunes and Norris, 2006; Zeebe and Zachos, 2007; Zeebe et al., 2009a) that would have been expected to affect the evolution of the North Atlantic CCD. Weakened North Atlantic-sourced overturning during the acidification phase and enhanced overturning during the oversaturation phase could have produced the large CCD shoaling documented at Walvis Ridge (Zachos et al., 2005) and enhanced the CCD overshoot at Site U1403. If these circulation changes persisted for several Myr, they could have produced a persistently deeper post-PETM CCD in the North Atlantic, consistent with the Site U1403 record.

Examining spatial benthic $\delta^{13}C$ gradients can shed light on circulation changes (Nunes and Norris, 2006), because the accumulation of DIC from respired organic carbon reduces the $\delta^{13}C$ of deep water DIC as it ages. Unfortunately, Site U1403 is

nearly barren of benthic foraminifera throughout the PETM and its recovery (perhaps unsurprisingly, given its low wt. %$CaCO_3$ and inferred position near the CCD). However, comparing the Site U1409 benthic $\delta^{13}C$ record to other sites could diagnose large-scale circulation changes that might affect the local CCD. Site U1409 benthic $\delta^{13}C$ overlaps in its variability with Site 1263 in the South Atlantic during intervals before the PETM and during the later stages of the recovery, including a time interval (>110kyr after the event) where Site U1403 documents a CCD overshoot. Therefore, benthic gradients between the South and North Atlantic do not show any evidence for large-scale changes in Atlantic overturning circulation during the PETM recovery. The fact that the sites in the S. Atlantic and Pacific show evidence of a permanent, long-term increase in carbonate deposition also support this conclusion.

Our finding of a post-PETM CCD overshoot represents an important additional constraint on quantifying carbon emissions during the PETM and the processes responsible for restoring steady-state conditions in the oceanic carbonate system (Figure 3). In theory, one could directly calculate the mass of carbon released during the PETM, as the extent of the overshoot should scale with the mass of carbon released. However, in practice, one site does not fully constrain the global extent of the overshoot, nor its absolute magnitude (strictly, we can only determine that the North Atlantic CCD deepened to below its pre-PETM depth ~70kyr after the CIE onset). Further constrains on the CCD overshoot from deeper water depths and additional ocean basins are therefore an essential target for future scientific drilling. Additionally, uncertainty in the parameterization and strength of the silicate

weathering feedback (Figure 3C) (Uchikawa and Zeebe, 2008) as well as the potential influences of initial conditions, circulation changes, C_{org} burial, and changing clay flux preclude direct calculation of carbon release. Many combinations of mass of carbon release, weathering feedback strength, and C_{org} burial are possible that are consistent with the new observations described here. Nevertheless, the Newfoundland carbonate records provide a novel constraint on PETM carbon cycling that must be reproduced by carbon cycle model simulations of the PETM if we are to significantly advance our understanding of Earth system processes and feedbacks during a major global warming event driven by large-scale perturbations to the carbon cycle.

References

Bains, S., Norris, R. D., Corfield, R. M., and Faul, K. L., 2000, Termination of global warmth at the Palaeocene/Eocene boundary through productivity feedback: Nature, v. 407, no. 6801, p. 171-174.

Berner, R. A., Lasaga, A. C., and Garrels, R. M., 1983, The carbonate-silicate geochemical cycle and its effects on atmospheric carbon dioxide over the past 100 million years: American Journal of Science, v. 283, p. 641-683.

Bice, K. L., and Marotzke, J., 2002, Could changing ocean circulation have destabilized methane hydrate at the Paleocene/Eocene boundary? - art. no. 1018: Paleoceanography, v. 17, no. 2, p. 1018.

Bowen, G. J., 2013, Up in smoke: A role for organic carbon feedbacks in Paleogene hyperthermals: Global and Planetary Change, v. 109, p. 18-29.

Bowen, G. J., and Zachos, J. C., 2010, Rapid carbon sequestration at the termination of the Palaeocene-Eocene Thermal Maximum: Nature Geoscience, v. 3, no. 12, p. 866-869.

Depaolo, D. J., and Ingram, B. L., 1985, High-resolution stratigraphy with strontium isotopes: Science, v. 227, no. 4689, p. 938-941.

Dickens, G. R., Castillo, M. M., and Walker, J. C. G., 1997, A blast of gas in the latest Paleocene: Simulating first-order effects of massive dissociation of oceanic methane hydrate: Geology, v. 25, no. 3, p. 259-262.

Dickens, G. R., Oneil, J. R., Rea, D. K., and Owen, R. M., 1995, Dissociation of Oceanic Methane Hydrate As a Cause of the Carbon Isotope Excursion At the End of the Paleocene: Paleoceanography, v. 10, no. 6, p. 965-971.

Dunkley-Jones, T., Lunt, D. J., Schmidt, D. N., Ridgwell, A., Sluijs, A., Valdes, P. J., and Maslin, M., 2013, Climate model and proxy data constraints on ocean warming across the Paleocene-Eocene Thermal Maximum: Earth-Science Reviews, v. 125, p. 123-145.

Farley, K. A., and Eltgroth, S. F., 2003, An alternative age model for the Paleocene-Eocene thermal maximum using extraterrestrial He-3: Earth and Planetary Science Letters, v. 208, no. 3-4, p. 135-148.

Goodwin, P., and Ridgwell, A., 2010, Ocean-atmosphere partitioning of anthropogenic carbon dioxide on multimillennial timescales: Global Biogeochemical Cycles, v. 24, no. 2.

Hönisch, B., Ridgwell, A., Schmidt, D. N., Thomas, E., Gibbs, S., Sluijs, A., Zeebe, R., Kump, L., Martindale, R. C., Greene, S., Kiessling, W., Ries, J. B., Zachos, J., Royer, D. L., Barker, S., Marchitto, T., Moyer, R., Pelejero, C., Ziveri, P., Foster, G. L., and Williams, B., 2012, The Geological Record of Ocean Acidification: Science, v. 335, no. 6072, p. 1058-1063.

Kelly, D. C., Nielsen, T. M., and Schellenberg, S. A., 2012, Carbonate saturation dynamics during the Paleocene–Eocene thermal maximum: Bathyal constraints from ODP sites 689 and 690 in the Weddell Sea (South Atlantic): Marine Geology, v. 303, p. 75-86.

Kelly, D. C., Zachos, J. C., Bralower, T. J., and Schellenberg, S. A., 2005, Enhanced terrestrial weathering/runoff and surface ocean carbonate production during the recovery stages of the Paleocene-Eocene thermal maximum: Paleoceanography, v. 20, no. 4, p. -.

Kennett, J. P., and Stott, L. D., 1991, Abrupt Deep-Sea Warming, Palaeoceanographic Changes and Benthic Extinctions At the End of the Palaeocene: Nature, v. 353, no. 6341, p. 225-229.

Koch, P. L., Zachos, J. C., and Gingerich, P. D., 1992, Correlation Between Isotope Records in Marine and Continental Carbon Reservoirs Near the Palaeocene Eocene Boundary: Nature, v. 358, no. 6384, p. 319-322.

Ma, Z., Gray, E., Thomas, E., Murphy, B., Zachos, J., and Paytan, A., 2014, Carbon sequestration during the Palaeocene-Eocene Thermal Maximum by an efficient biological pump: Nature Geoscience.

McCarren, H., Thomas, E., Röhl, U., and Zachos, J. C., 2008, The Paleocene-Eocene Carbon Isotope Excursion: Insights from the benthic record (ODP Leg 208, Walvis Ridge): Geophysics, Geosystems, Geochemistry.

Murphy, B. H., Farley, K. A., and Zachos, J. C., 2010, An extraterrestrial He-3-based timescale for the Paleocene-Eocene thermal maximum (PETM) from Walvis Ridge, IODP Site 1266: Geochimica Et Cosmochimica Acta, v. 74, no. 17, p. 5098-5108.

Nunes, F., and Norris, R. D., 2006, Abrupt reversal in ocean overturning during the Palaeocene/Eocene warm period: Nature, v. 439, no. 7072, p. 60-63.

Panchuk, K., Ridgwell, A., and Kump, L. R., 2008, Sedimentary response to Paleocene-Eocene Thermal Maximum carbon release: A model-data comparison: Geology, v. 36, no. 4, p. 315-318.

Penman, D. E., Hönisch, B., Zeebe, R. E., Thomas, E., and Zachos, J. C., 2014, Rapid and sustained surface ocean acidification during the Paleocene-Eocene Thermal Maximum: Paleoceanography.

Raffi, I., Backman, J., Zachos, J. C., and Sluijs, A., 2009, The response of calcareous nannofossil assemblages to the Paleocene Eocene Thermal Maximum at the Walvis Ridge in the South Atlantic: Marine Micropaleontology, v. 70, no. 3-4, p. 201-212.

Ravizza, G., Norris, R. N., Blusztajn, J., and Aubry, M. P., 2001, An osmium isotope excursion associated with the late Paleocene thermal maximum: Evidence of intensified chemical weathering: Paleoceanography, v. 16, no. 2, p. 155-163.

Ridgwell, A., and Schmidt, D. N., 2010, Past Constraints on the vulnerability of marine calcifiers to massive carbon dioxide release: Nature Geoscience, v. 3, p. 196-200.

Robert, C., and Kennett, J. P., 1994, Antarctic Subtropical Humid Episode At the Paleocene-Eocene Boundary - Clay-Mineral Evidence: Geology, v. 22, no. 3, p. 211-214.

Röhl, U., Westerhold, T., Bralower, T. J., and Zachos, J. C., 2007, On the duration of the Paleocene-Eocene thermal maximum (PETM): Geochemistry Geophysics Geosystems, v. 8, p. -.

Sluijs, A., Zachos, J. C., and Zeebe, R. E., 2012, Constraints on hyperthermals: Nature Geosci, v. 5, no. 4, p. 231-231.

Stoll, H. M., and Bains, S., 2003, Coccolith Sr/Ca records of productivity during the Paleocene-Eocene thermal maximum from the Weddell Sea: Paleoceanography, v. 18, no. 2.

Uchikawa, J., and Zeebe, R. E., 2008, Influence of terrestrial weathering on ocean acidification and the next glacial inception: Geophysical Research Letters, v. 35, no. 23.

Walker, J. C. G., Hays, P. B., and Kasting, J. F., 1981, A Negative Feedback Mechanism for the Long-Term Stabilization of Earths Surface-Temperature: Journal of Geophysical Research-Oceans and Atmospheres, v. 86, no. Nc10, p. 9776-9782.

Zachos, J. C., Rohl, U., Schellenberg, S. A., Sluijs, A., Hodell, D. A., Kelly, D. C., Thomas, E., Nicolo, M., Raffi, I., Lourens, L. J., McCarren, H., and Kroon, D., 2005, Rapid acidification of the ocean during the Paleocene-Eocene thermal maximum: Science, v. 308, no. 5728, p. 1611-1615.

Zeebe, R., 2012, LOSCAR: Long-term ocean-atmosphere-sediment carbon cycle reservoir model v2. 0.4: Geoscientific Model Development, v. 5, no. 1, p. 149-166.

Zeebe, R., and Zachos, J., 2012, Long-term legacy of massive carbon input to the Earth system: Anthropocene vs. Eocene: Philosophical Transactions of the Royal Society, p. 1-22.

Zeebe, R. E., 2013, What caused the long duration of the Paleocene-Eocene Thermal Maximum?: Paleoceanography, v. 26, p. 1-13.

Zeebe, R. E., and Wolf-Gladrow, D. A., 2001, CO_2 in seawater: Equilibrium, kinetics, isotopes, Elsevier, Elsevier Oceanography Series, 346 p.:

Zeebe, R. E., and Zachos, J. C., 2007, Reversed deep-sea carbonate ion basin gradient during Paleocene-Eocene thermal maximum: Paleoceanography, v. 22, no. 3, p. -.

Zeebe, R. E., Zachos, J. C., and Dickens, G. R., 2009, Carbon dioxide forcing alone insufficient to explain Palaeocene-Eocene Thermal Maximum warming: Nature Geoscience, v. 2, no. 8, p. 576-580.

New constraints on carbon release and recovery processes during the Paleocene-Eocene Thermal Maximum

Donald Penman, James Zachos

Abstract

Recent geochemical and sedimentological evidence has provided novel constraints on the response of seawater chemistry to massive carbon injection during the Paleocene-Eocene Thermal Maximum (PETM), providing an opportunity to re-evaluate scenarios of carbon release and the feedbacks involved in terminating the event. Records of the carbonate chemistry proxy B/Ca in planktic foraminifera document global ocean acidification that persisted for the duration of the carbon isotope excursion (CIE). Complementary records of $\delta^{11}B$ in some of the same cores allow quantification of this acidification. A recently drilled sediment core (IODP Site U1403) from the North Atlantic documents a carbonate compensation depth (CCD) over-shoot during the recovery phase of the event, a feature that had been predicted by carbon cycle models in association with the negative feedback processes that restored carbonate saturation state during the PETM recovery. These new lines of evidence are used to constrain simulations using the carbon cycle model LOSCAR to examine first the onset of, and then recovery from the PETM. In order to constrain the event's onset, we systematically varied the mass of carbon, duration of injection, initial atmospheric pCO_2, ocean circulation patterns, and location of carbon injection, then evaluated which combinations of those parameters were consistent with the

magnitude of initial acidification as well as basin-specific constraints on the shoaling of the CCD. A range of input parameters produced output that successfully conformed to available constraints on the event onset, however none of the successful scenarios featured aragonite or carbonate undersaturation at even peak PETM conditions (consistent with the general lack of calcifier extinction, and in contrast to simulations of future anthropogenic carbon release) and most runs featured approximately a doubling of pCO_2 relative to pre-event conditions (suggesting a PETM climate sensitivity at the higher end of modern estimates). For the body and recovery of the PETM, further LOSCAR runs were carried out to test the compatibility of scenarios with the new constraints of sustained acidification and rapid recovery suggested by new boron records as well as the timing and depth of the CCD overshoot at Site U1403. Successful scenarios all include a sustained release of carbon throughout the CIE (in some cases comparable in mass to that released during the onset) perhaps as a feedback to initial warming, and removal of carbon (likely as burial of organic carbon) during the recovery.

Introduction

The Paleocene-Eocene Thermal Maximum (PETM, ~56Ma) involved the geologically rapid release of thousands of petagrams of ^{12}C-enriched [^{13}C-depleted] carbon (Kennett and Stott, 1991) into the ocean-atmosphere system, resulting in global warming (Dunkley-Jones et al., 2013; Zachos et al., 2003), ocean acidification (Penman et al., 2014; Zachos et al., 2005), and varied yet pronounced impacts on marine and terrestrial biota (Agnini et al., 2007; Bowen et al., 2002; Bralower, 2002;

Thomas and Shackleton, 1996; Wing et al., 2005). The event has thus been proposed as an Earth history analogue for the current anthropogenic release of fossil fuel-derived CO_2 into the atmosphere, with the potential to improve our understanding of the response of climate, biota, and the exogenic carbon cycle to rapid carbon injection. However, in order to evaluate how the PETM compares to forecasts of future emissions, accurate estimates of the mass and rate of carbon release during the PETM, as well as the strength of feedback processes responsible for terminating the event, are necessary. Recently, geochemical and sedimentological evidence from new records of the PETM have placed improved constraints on the response of seawater carbonate chemistry during the PETM, which allow the re-evaluation and refinement of scenarios of the event using carbon cycle modeling.

Recently, boron-based proxies of carbon chemistry were applied to planktic foraminifera spanning the PETM to document and quantify ocean acidification during the event (Penman et al., 2014) ; Appendix 1). The B/Ca proxy, which herein is interpreted as a qualitative proxy for acidification, demonstrates at several sites (Figure 1) a rapid decrease at the event onset, followed by a plateau of low values and finally a recovery to near pre-event levels in step with the carbon isotope excursion (CIE, Figure 2). This is interpreted as rapid (of a similar rate to the CIE onset), global, and sustained (of a similar duration to the CIE body) acidification of the surface ocean. At ODP Sites 1209, 865, and 1263, a record of the boron isotopic composition ($\delta^{11}B$, a direct proxy for seawater pH) of surface-dwelling planktic foraminifers corroborates the acidification suggested by B/Ca records, and allows for its

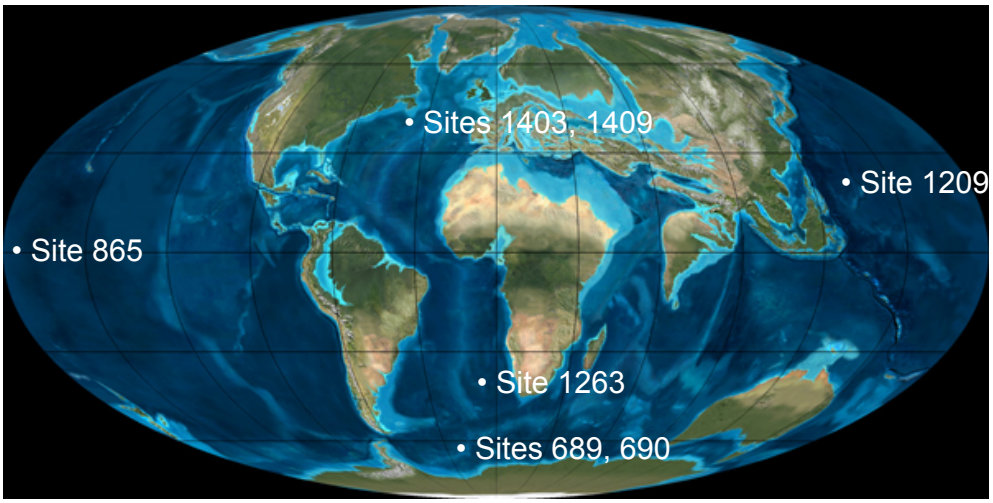

Figure 1: Map of all sites providing data for carbonate chemistry constraints placed on PETM simulations on Eocene geography by Colorado Plateau Geosystems (http://cpgeosystems.com/index.html).

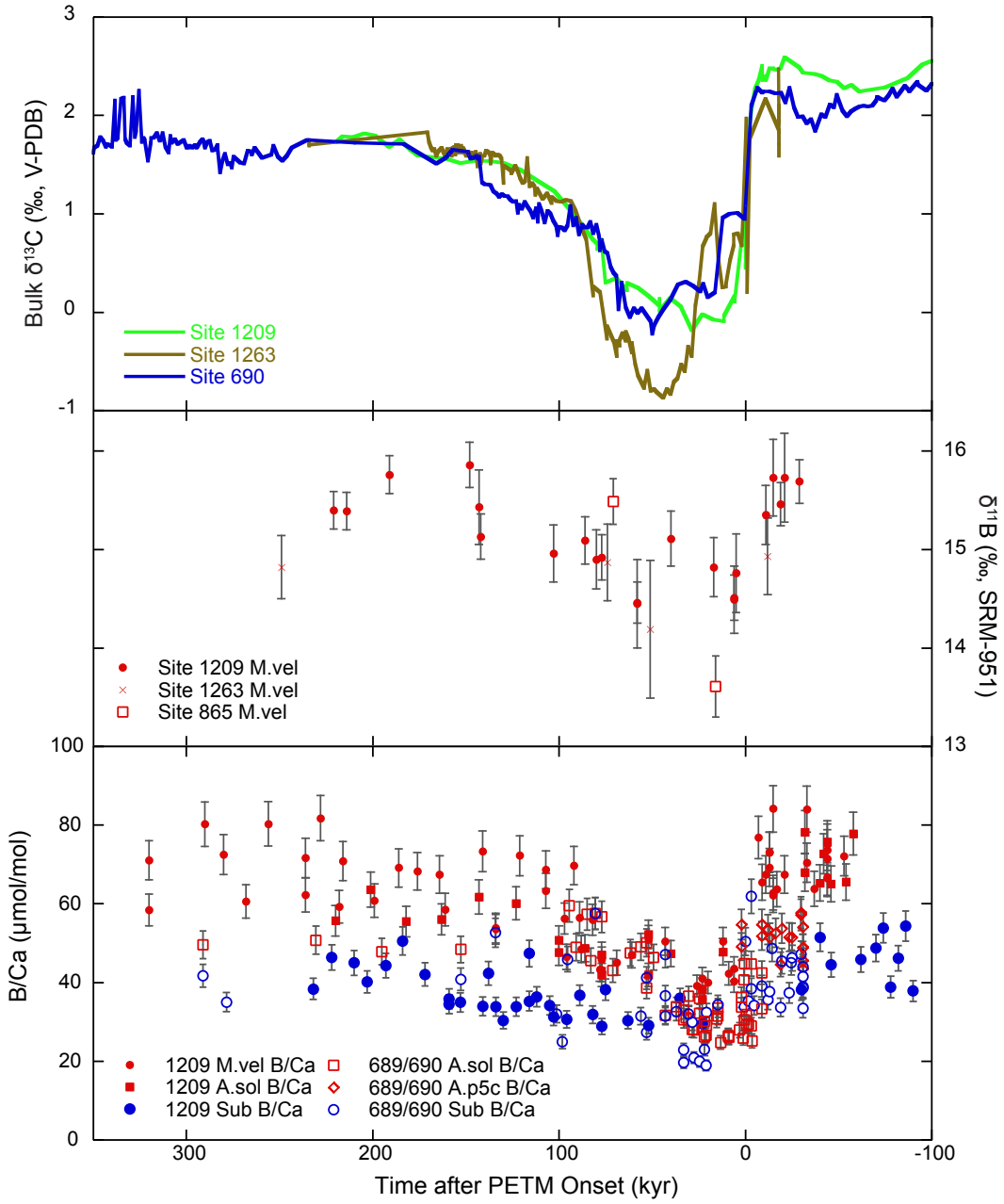
Bulk δ13C (‰, V-PDB)
Site 1209
Site 1263
Site 690
δ11B (‰, SRM-951)
Site 1209 M.vel
Site 1263 M.vel
Site 865 M.vel
B/Ca (µmol/mol)
1209 M.vel B/Ca
1209 A.sol B/Ca
1209 Sub B/Ca
689/690 A.sol B/Ca
689/690 A.p5c B/Ca
689/690 Sub B/Ca
Time after PETM Onset (kyr)

Figure 2: Bulk carbonate $\delta^{13}C$ (Colosimo et al., 2005; Kelly et al., 2012; McCarren et al., 2008a), planktic foraminifer $\delta^{11}B$ (Penman et al., 2014), and planktic foraminifer B/Ca from all sites vs. time. Red symbols are surface-dwellers, blue symbols are thermocline dwellers. M.vel = *Morozovella velascoensis*, A.sol = *Acaranina soldadoensis*, A.p5c = *Acaranina praepentacamerata*, Sub = genus Subbotinae. For B/Ca, open symbols are Southern Ocean (Sites 689 and 690), closed symbols are North Pacific (Site 1209). Age models were generated for all sites by correlating the fine fraction or bulk carbonate $\delta^{13}C$ of Röhl et al. (2007), and in the case of Sites 689 and 690 used the tie points of Kelly et al. (2012). Error bars on $\delta^{11}B$ represent 2 standard errors of repeat measurements. Error bars on B/Ca represent two standard deviations of repeat measurements of an in-house foraminiferal carbonate standard (7%).

quantification. Due to the differing sensitivity of $\delta^{11}B$ at different pH, the estimate for ΔpH across the PETM is a function of assumed initial pH, but for a reasonable assumption of pre-event (Paleocene) pH the acidification across the P-E boundary is approximately 0.3 pH units on the total scale (Penman et al., 2014). This falls within the range of pH declines simulated by models assuming various carbon inputs (Panchuk et al., 2008; Ridgwell and Schmidt, 2010; Zeebe et al., 2009a) although toward the higher end. Constraining model scenarios with boron-based estimates of the magnitude and timing of pH change through the PETM, as well as existing constraints like the magnitude and timing of the CIE and the basin-specific pattern of CCD shoaling, promises to improve the accuracy of scenarios of PETM carbon release and recovery.

Indirect evidence for the response of carbonate chemistry to rapid carbon injection during the PETM comes from sedimentological records of carbonate content, which constrain the evolution of the CCD throughout the event. The first evidence for ocean acidification during the PETM was the decrease in $\%CaCO_3$ content in sediment cores globally (Kennett and Stott, 1991; Thomas et al., 2002; Zachos et al., 2005; Zeebe and Zachos, 2007), documenting a rapid shoaling of the CCD as the injection of CO_2 into the oceans decreases pH and carbonate saturation state in tandem (Hönisch et al., 2012), resulting in decreased carbonate production and/or dissolution of seafloor carbonate. Deep sea sedimentary evidence (Zachos et al., 2005) suggests that the CCD gradually recovered as seafloor carbonate dissolution and weathering feedbacks restored ocean carbonate saturation. Numerical

and conceptual models of the long-term carbon cycle predict that these negative feedbacks should have caused a period of carbonate oversaturation (relative to pre-event levels) during the event recovery, wherein the build-up of weathering products in the ocean would have caused an "overshoot" of the CCD (Dickens et al., 1997; Zeebe and Zachos, 2012; Zeebe and Zachos, 2013). Evidence for this hypothesized CCD overshoot remained elusive until Site U1403 was drilled during IODP Expedition 342. The sedimentary record across the P-E boundary at this site features a transition from Paleocene carbonate-barren clay to Eocene sediments containing 10-40% carbonate. Post-cruise bulk carbonate stable isotope analysis confirmed that the first appearance of this carbonate dates to the recovery interval of the PETM, thus providing the first evidence of a CCD overshoot. The presence of this overshoot correlates well with existing records of elevated $\%CaCO_3$ (Figure 3) during the PETM recovery (Farley and Eltgroth, 2003; Kelly et al., 2005; Murphy et al., 2010; Zachos et al., 2005), and its depth, timing and magnitude provide further evidence for the evolution of the CCD during the PETM which can be used to constrain model simulations of the event.

This study aims to estimate carbon fluxes utilizing the latest observations on changes in ocean carbonate chemistry during the PETM. To this end, we use the global carbon cycle model LOSCAR (Long-term Ocean-atmosphere-Sediment CArbon Reservoir) to test which scenarios for carbon release and sequestration are

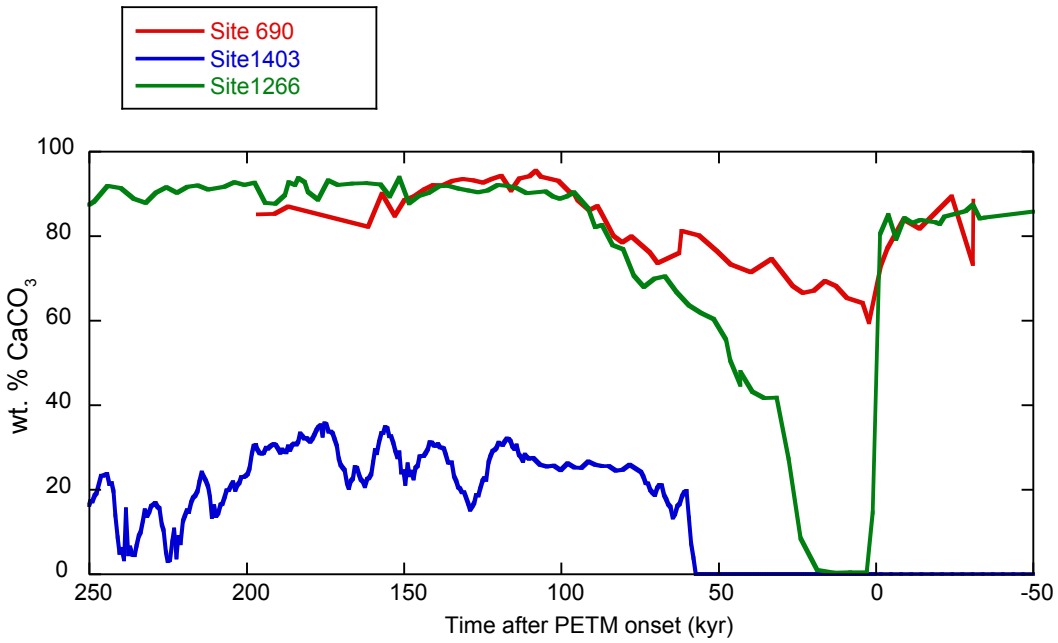

Figure 3: %$CaCO_3$ records over the PETM vs. time (1403, 1266, 690) (Kelly et al., 2012; Murphy et al., 2010)(Site 1403 data and age model from Chapter 2 of this Dissertation). Age models for all sites were constructed by correlating the fine-fraction or bulk $\delta^{13}C$ to the CIE of (Röhl et al., 2007).

consistent with these new constraints on the magnitude of acidification and the overshoot of the CCD.

Methods

Carbon cycle modeling

In order to test which scenarios are consistent with constraints on ocean acidification and basin-specific CCD shoaling, we performed a suite of experiments using LOSCAR, a numerically efficient box model of the exogenic carbon cycle that calculates fluxes of carbon between atmosphere, oceans, and sediments on timescales from decades to millions of years. In the Paleogene configuration (Zeebe, 2012), the ocean model contains surface, intermediate, and deep reservoirs for all modern ocean basins as well as a Tethys basin. The interaction between ocean and sediment modules includes bioturbation and realistic calculations of $CaCO_3$ dissolution and carbonate compensation, which is crucial for modeling the evolution of the CCD. LOSCAR also includes a parameterization of the weathering response to elevated pCO_2, which is important for carbon cycle perturbations on timescales greater than 10^3 years such as the PETM. Two sets of experiments were performed aiming to first constrain the PETM onset, and then the body and recovery from the event.

Observations:

The primary observational constraints on ocean carbonate chemistry during the PETM include constraints on deep sea saturation and surface ocean pH. The deep sea saturation state is constrained by reconstructions of the CCD, whereas the changes in surface ocean pH are constrained by the B concentration and isotopic

composition of planktonic foraminifer from several cores spanning the tropical to sub-polar oceans (Penman et al., 2014; Appendix A). At all sites B/Ca ratios of mixed-layer planktonic foraminifera decline by 30 to 40%, and the B isotope ratios by ~1‰. The similarity of the changes in B proxies between sites demonstrates that the signals are global and thus reflecting on changes in surface ocean pH/saturation state.

PETM Onset Experiment

In order to determine what combinations of boundary conditions and carbon release scenarios are consistent with the magnitude of initial ocean acidification as well as constraints on the global CCD shoal, we performed a suite of experiments in which input parameters (i.e. mass and rate of C input as well as boundary conditions) were varied systematically. In contrast to previous modeling efforts, for the present experiment we ignore the $\delta^{13}C$ of carbon released, relying on carbonate chemistry constraints with the expectation that $\delta^{13}C$ could be altered for any carbon emission scheme *post-hoc* to match records of the CIE. This experiment only considers the magnitude of the event onset; the body and recovery is modeled in later sections.

Mass of carbon input

Past estimates of the mass of carbon release range from 1200 to 10000 PgC (Cui et al., 2011; Dickens et al., 1997; Panchuk et al., 2008; Zeebe et al., 2009a). In order to encompass these existing estimates of the magnitude of C release, the mass of carbon release in the PETM onset experiment was varied between 1,000 and 15,000 GtC in increments of 1,000 GtC. While we do not attempt to use $\delta^{13}C$ as a constraint on the PETM onset, we note that this range of carbon mass would, using mass balance

calculations of the CIE magnitude, encompass the range of methane, organic carbon, and volcanic input $\delta^{13}C$ values (McInerney and Wing, 2011; Sluijs et al., 2012a).

Duration of carbon input

The duration of carbon release for the initial onset was varied from 1,000 to 10,000 years by increments of 1,000 years, which encompasses and exceeds the range of realistic estimates of carbon release (Beerling and Royer, 2011; Farley and Eltgroth, 2003; Murphy et al., 2010; Zachos et al., 2008; Zeebe et al., 2014; Zeebe and Zachos, 2013).

Initial (pre-event) atmospheric pCO_2

Estimates of pre-event (Paleogene) atmospheric pCO_2 vary considerably (Beerling and Royer, 2011) and represent a large source of uncertainty in PETM scenarios constrained by boron isotope data, owing to the changing sensitivity of $\delta^{11}B$ at different initial pH (and thus initial pCO_2). Experiments were initiated at initial (steady-state) atmospheric pCO_2 levels of 500, 750, 1000, 1250, and 1500ppm. 500ppm represents an extreme lower limit, because it can be argued that Paleocene climate is inconsistent with such low pCO_2 levels, specifically due to the absence of large Antarctic ice sheets, which have been argued (DeConto and Pollard, 2003; Pollard and DeConto, 2005) to form at pCO_2 levels lower than 700ppm.

Strength of the weathering feedback

While it is of much greater importance on longer timescales, the sensitivity of silicate and carbonate weathering flux to elevated pCO_2 can have a significant impact on ocean acidification and carbonate preservation during the onset of the event in long-

duration (>5,000 kyr) carbon release experiments. The silicate and carbonate weathering feedbacks are parameterized in LOSCAR as

$F_{si} = F_{eq\_si} * ([CO_2]_{atm} / [CO_2]_{eq})^{Nsi}$

$F_{cc} = F_{eq\_cc} * ([CO_2]_{atm} / [CO_2]_{eq})^{Ncc}$

where F_{eq} and $[CO_2]_{eq}$ are equilibrium weathering flux and atmospheric pCO_2 at which volcanic carbon emissions are perfectly balanced by silicate weathering and carbonate burial (Zeebe, 2012). Exponents N_{Si} and N_{cc} are free parameters in the model that set the strength of the silicate and carbonate weathering feedbacks. (default $N_{Si} = 0.2$, $N_{cc} = 0.4$). The PETM onset was modeled at default, double ($N_{Si} = 0.4$, $N_{cc} = 0.8$), and half ($N_{Si} = 0.1$, $N_{cc} = 0.2$) weathering exponents.

Circulation change and deep Atlantic injection

An interesting feature of the carbonate dissolution response during the PETM is the large difference in initial CCD shoaling between ocean basins. The Atlantic experienced the largest shoaling of the CCD, constrained by a depth transect at Walvis Ridge to >2km (Zachos et al., 2005). This is in sharp contrast to the Pacific (which is and was the largest ocean basin during the Paleogene), where depth transects suggest a CCD shoal of ~500m or less (Colosimo et al., 2005; Leon-Rodriguez and Dickens, 2010; Zeebe and Zachos, 2007; Zeebe et al., 2009a). In order to reproduce this pattern, Zeebe et al. (2009a) included a slowdown of circulation as well as a switch from only Southern Ocean-sourced to Southern Ocean plus North Pacific-sourced deep water formation during the PETM following the ocean physics modeling of Bice and Marotzke (2002) as well as an injection of a fraction of the

carbon release directly into the deep Atlantic reservoir, which could be interpreted as representing a local release of carbon in the form of e.g. methane hydrates. For the present experiment, the model was run both with and without the circulation slowdown and switch as prescribed by (Zeebe et al., 2009a) and with 0%, 25%, 50%, or 100% of the carbon release injected directly into the deep Atlantic, with the remainder being released into the atmosphere.

All possible combinations of the above parameters were run, totaling 18,000 different model permutations. All model runs that featured differences in boundary conditions (initial pCO_2, weathering strength) were run to steady-state before beginning PETM perturbation experiments, which subtly changes some of the initial conditions such as CCD depth. Global temperature increase (which effects carbonate chemistry equilibrium and solubility constants, among others) was parameterized with a simple (fast) climate sensitivity of 3.0 °C per doubling of pCO_2.

Criteria for successful run

For each run, limits of acceptable ΔpH were calculated from Site 1209 planktic foraminifer boron isotope data as a function of initial surface pH (the "population statistics" method of Penman et al., 2014). This site was located in an oligotrophic portion of the North Pacific gyre, and thus the mixed-layer pCO_2 would have been at or in near equilibrium with the atmospheric pCO_2. Runs were deemed consistent with records of seawater carbonate chemistry if the Pacific surface pH decline during the event onset (minimum low-latitude Pacific surface pH subtracted from pre-event low-latitude Pacific surface pH) fell within those run-specific limits,

and if the initial CCD shoaling (minimum CCD subtracted from pre-event CCD) exceeded 2 km in the Atlantic and was restricted to less than 500m in the Pacific, in accordance with existing records of the CCD (Colosimo et al., 2005; Leon-Rodriguez and Dickens, 2010; Sluijs et al., 2012b; Zachos et al., 2005; Zeebe and Zachos, 2007; Zeebe et al., 2009a).

LOSCAR modeling of the PETM body and recovery

The above experiment only considers carbonate chemistry constraints on the onset of the PETM. However, the event lasted at least an additional 100,000 years (Murphy et al., 2010; Röhl et al., 2007) and observations of carbonate chemistry during the sustained body of the CIE and the recovery can be used to constrain an emissions schedule and recovery processes for a full PETM scenario using LOSCAR. Three sets of observations argue for a sustained "leak" of carbon after the initial large carbon release: the prolonged body of the CIE in most records (Zeebe et al., 2009a), the sustained acidifications in records of planktic foraminifer $\delta^{11}B$ and B/Ca globally (Penman et al., 2014), both of which would otherwise begin to recover immediately following emissions cessation, and the delayed CCD overshoot at Site 1403, which would occur shortly (within tens of thousands of years) after the cessation of carbon emissions in the absence of a sustained leak.

For LOSCAR modeling of the body and recovery of the PETM, the model was modified slightly from the standard Paleogene LOSCAR setup (Zeebe, 2012; Zeebe et al., 2009a) in that the seafloor bathymetry and sediments are more finely subdivided to 100m water depth bins (from the default 500m resolution) so that CCD

evolution could be modeled at a finer scale. Three scenarios of the PETM onset were selected representing low (initial pCO_2 = 500ppm, initial carbon input = 2,000GtC over 1,000 years, 50% injected into deep Atlantic, circulation switch = on, weathering = default), intermediate (initial pCO_2 = 750ppm, initial carbon input = 3,300GtC over 5,000 years, 0% injected into deep Atlantic, circulation switch = on, weathering = default), and high (initial pCO_2 = 1500ppm, initial carbon input = 7,000GtC over 10,000 years, 25% injected into deep Atlantic, circulation switch = on, weathering = 2*default) (Table 1) carbon releases that all satisfied the carbonate chemistry constrains on the onset of the event, and introduced a sustained leak of carbon lasting 70 kyr (the approximate duration of the CIE body following the age model of Röhl et al. (2007)). The rate of the leak was adjusted in order to achieve a plateau of decreased pH in accordance with the shape of $\delta^{11}B$ and B/Ca records.

A key feature of the PETM that reflects on the process of carbon sequestration and needs to be considered in model simulations of the event is the rate of the recovery. After the body of the CIE, $\delta^{13}C$ recovers within approximately 50 kyr, which is thought to be too rapid to be explained by the long-term negative carbon cycle feedbacks (e.g. silicate weathering plus carbonate burial) alone (Bowen and Zachos, 2010). The $\delta^{11}B$ and B/Ca records of ocean acidification (Figure 2) also recover within a similar time frame, far more quickly than carbon cycle models of the PETM (e.g. Zeebe et al. (2009a)) which rely on silicate weathering alone as the long-term sequestration process for excess carbon. These two corroborating lines of evidence lead to the conclusion that some process for removing ^{13}C-depleted carbon

from the exogenic carbon cycle (e.g. marine or terrestrial organic burial) must have operated during the PETM recovery. In order to replicate the rapidity of the pH (and $\delta^{13}C$) recovery, carbon removal from the atmosphere was introduced to those same three simulations of the PETM onset and body. The length of carbon removal was set as the duration of the $\delta^{13}C$ recovery in Röhl et al. (2007) (an additional 50,000 years after the body) and the $\delta^{13}C$ of carbon removed was set at -25 ‰, consistent with terrestrial organic carbon burial. The amount of carbon removed was adjusted obtain a pH recovery consistent with the Site 1209 $\delta^{11}B$ record.

Results

LOSCAR modeling of the PETM onset

Characteristics of successful runs

363 combinations of input parameters (~2% of total runs) resulted in runs that satisfied the criteria for a successful run, the primary constraints on acidification and basin-specific CCD shoaling. An example plot of $\delta^{11}B$ -consistent ΔpH for a given set of boundary conditions (initial pCO_2, circulations schemes, and weathering rates) is shown in Figure 4. For most (but not all) sets of boundary conditions, some combinations of carbon input and input duration were found that satisfied both $\delta^{11}B$ -based and CCD-based constraints on carbonate chemistry response. However, in order to satisfy basin-specific CCD shoal constraints, all successful runs required either Deep Atlantic injection, the circulation switch of Zeebe et al. (2009), or both. The mass of carbon inputs in successful scenarios ranged from 2,000 (which in order

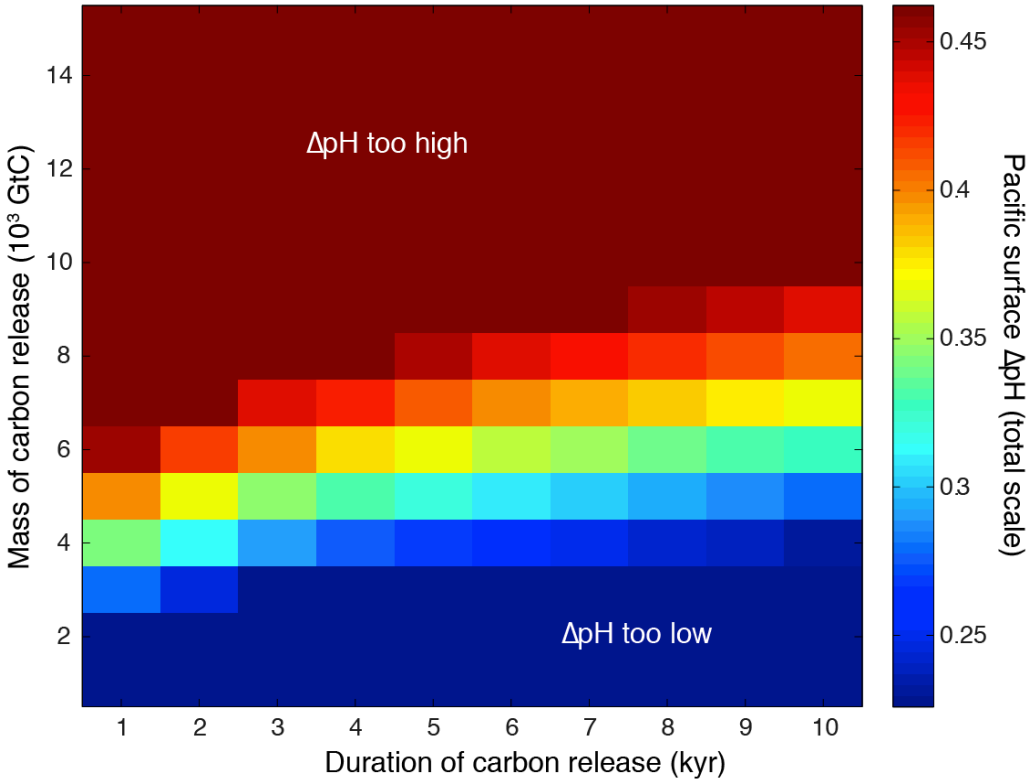

Figure 4: Example of LOSCAR ΔpH output from the PETM onset experiment for a given set of boundary conditions. All runs were started from steady state atmospheric pCO_2 = 1000ppm, weathering at LOSCAR default values, 0% injected into the deep Atlantic, with the circulation switch of Zeebe et al. (2009a) during the carbon release phase. The ΔpH color scale is adjusted to the limits of consistent delta-pH based on boron isotopes, so that results that are blue or red are inconsistent with boron records.

to achieve a CIE of -3.5 ‰ would require a source $\delta^{13}C$ lower than -50 ‰, e.g. methane) to 7,000 GtC (which would require a source $\delta^{13}C$ ~= -25 ‰, e.g. organic carbon), and all timescales of input considered here (1,000 to 10,000 years) generated successful runs when combined with specific boundary conditions and carbon inputs.

Saturation state decline in successful runs

All successful PETM onset simulations featured a decline in seawater carbonate saturation (Ω) state in response to rapid carbon injection, reaching minimum values shortly after the cessation of carbon injection. Minimum low-latitude surface Ω values are shown in Figure 5, and range from 1.4 to 2.2 for aragonite, and from 3.1 to 4.7 for calcite. The lack of under-saturated conditions in any of the successful PETM simulations is consistent with the general lack of extinctions amongst pelagic surface calcifiers and suggests that marine calcifiers can cope with reductions in saturation state in the above range through geographic migration, adaptation, and evolution as long as this acidification occurs over thousands of years. The magnitude and rate of saturation state reduction in successful PETM simulations stands in contrast to future simulations of anthropogenic ocean acidification, which is currently occurring much faster than the PETM and is projected to reach a more severe minimum in coming centuries (Zeebe and Zachos, 2013).

CO_2 increase in successful runs

Comparing the range of pCO_2 increase (maximum pCO_2 versus initial pCO_2) in successful scenarios of the PETM with existing estimates of the global temperature

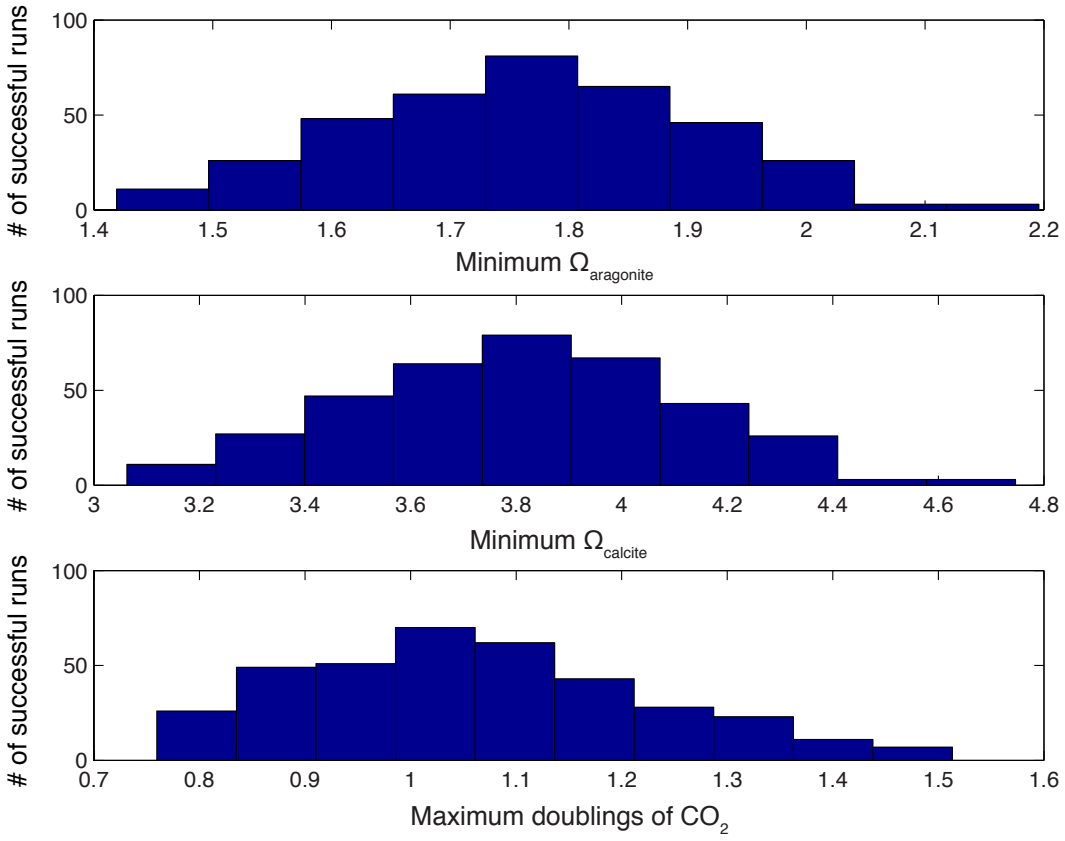

Figure 5: Histograms of output from all successful LOSCAR runs from the PETM onset experiment: minimum aragonite saturation state (Ω_{arag}) of the low-latitude surface Pacific, minimum calcite saturation state (Ω_{calc}) of the low-latitude surface Pacific, and maximum atmospheric pCO_2 expressed as doublings of pre-event (initial, equilibrium) pCO_2. Doublings = $\log_2$(maximum pCO_2 / initial pCO_2).

increase during the PETM (Dunkley-Jones et al., 2013) can be used to constrain climate sensitivity (expressed as the global temperature increase in response to a doubling of pCO_2) on 10^3 year timescales during the PETM onset. Due to the wide range (500 to 1500ppm) in initial atmospheric pCO_2 in successful runs, the absolute pCO_2 increase is highly variable (from a minimum increase of ~350ppm in runs started from an initial pCO_2 of 500ppm to a maximum increase of ~1700ppm in runs started at 1500ppm). However, the pCO_2 increase expressed as the number of doublings of initial pCO_2 (doublings = $\log_2$(maximum pCO_2 / initial pCO_2)) is much more similar among successful runs, limited to the range of 0.8 to 1.5 doublings of pCO_2. Combined with a recent estimate of 4-5 °C of global temperature increase during the PETM (Dunkley-Jones et al., 2013), this range in pCO_2 increase is consistent with 10^3 year climate sensitivities of 2.7 to 6.2 °C per doubling of pCO_2 during the PETM onset. This range overlaps with the high end of climate sensitivities considered by the Intergovernmental Panel on Climate Change (IPCC, 2007) for anthropogenic warming (1.5 to 4.5 °C per doubling of pCO_2).

LOSCAR modeling of sustained acidification

Sustaining acidified conditions for 70 kyr requires a continuous input (leak) of carbon in all scenarios, but the total mass of leaked carbon required varies considerably depending on the mass of the initial C release during the onset of the event. In the case of the low initial C release scenario (Figure 6, a spike of 2,000 GtC in 1,000 years), an additional 6,100 GtC over the following 69,000 years are needed to sustain surface acidification, an amount that far surpasses the initial release. This is

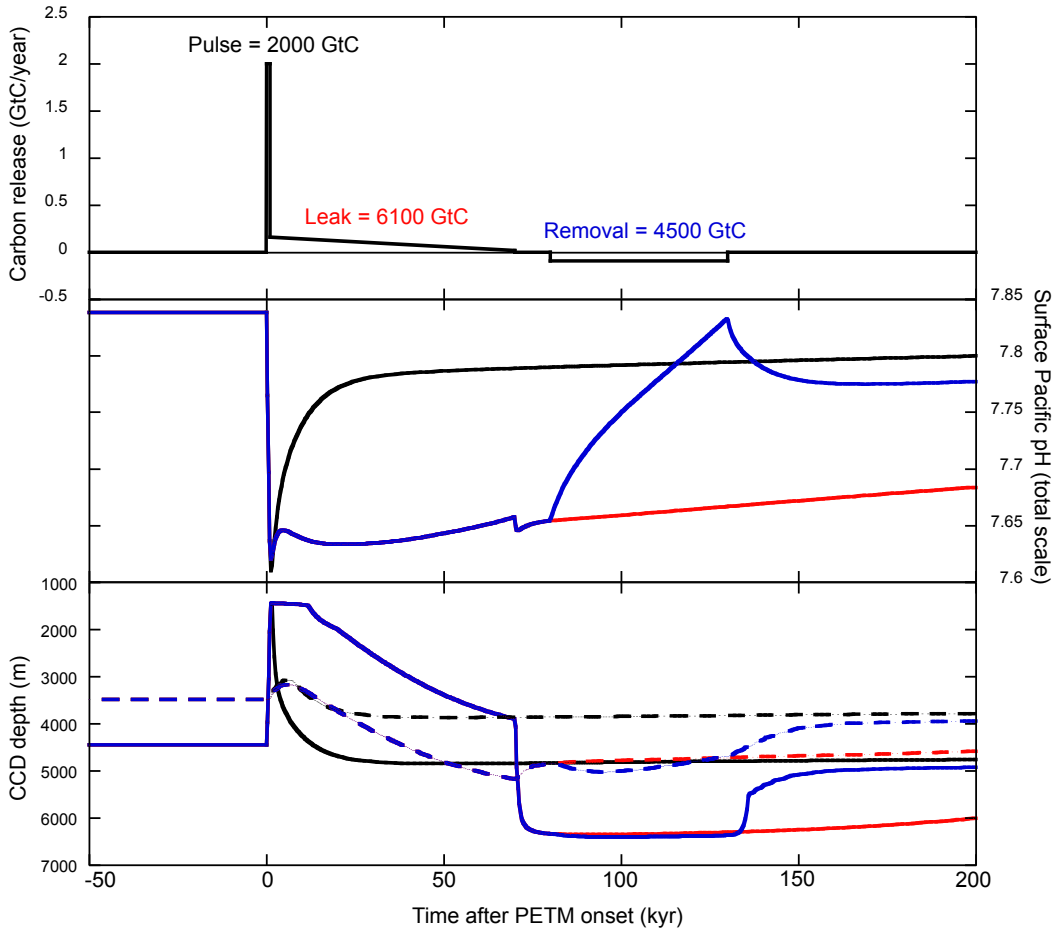

Figure 6: Low C release PETM scenario. Black lines = only the initial C pulse, red lines = Pulse leak C, blue lines = pulse, leak, and removal. Dashed CCD lines represent the Pacific, solid lines represent the Atlantic.

a consequence of the brief input duration (1,000 years) which is shorter than a full ocean mixing time. The small carbon injection (2,000 GtC) is enough to depress surface ocean pH in accordance with $\delta^{11}B$ estimates at t=1,000 years, however on longer timescales this carbon will be mixed into the deep ocean, so more emissions are needed to keep the surface acidified. A large sustained leak would seem to be required of any PETM scenario that invoked a carbon release shorter than the ocean mixing time. Invoking 6100 GtC as a leak following a 2000 GtC pulse is problematic: 6100 GtC is larger than the entire modern terrestrial biosphere including soil carbon (~2,700 GtC, Wang et al. (2010)). Furthermore, the carbon isotopic composition of the larger leak would have to be significantly more ^{13}C-enriched than the initial release in order to reproduce the shape of the CIE, which features a rapid onset (a result of the carbon pulse) followed by ~70 kyr minimum. As such, methane could not be a component of this long-term slow carbon leak, and since the mass exceeds that of the terrestrial biosphere, no plausible mechanism for such a large leak is known.

At the other extreme, in the case of the high C release scenario (Figure 7, 7,000 GtC over 10,000 years), an additional 14,700 GtC are required over 60,000 years to sustain acidification. The main reason for this very large leak is that this simulation (and indeed, all simulations that can accommodate such a large initial release without violating CCD constrains) is run with double LOSCAR's default weathering feedback strength, which works to expedite pH recovery relative to scenarios run at default weathering strength. Hence, more carbon is needed to keep

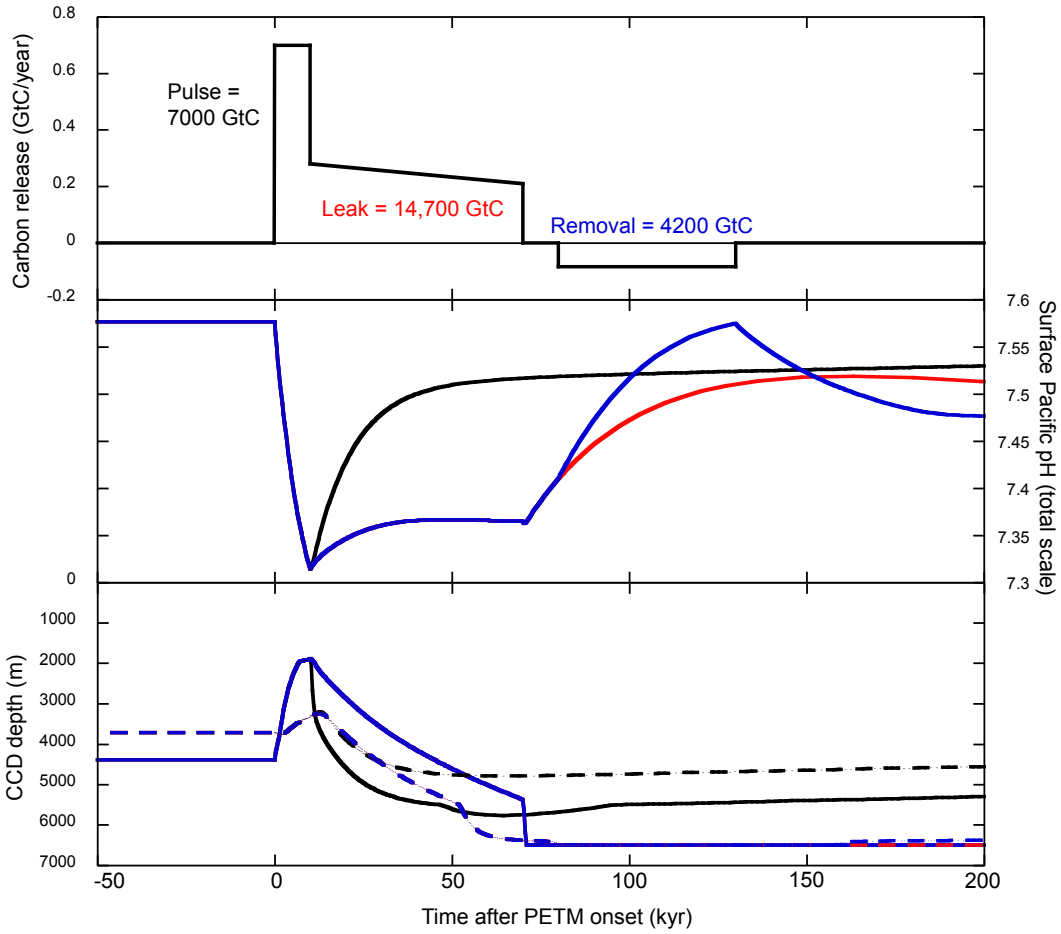

Figure 7: High C release scenario. Black lines = only the initial C pulse, red lines = Pulse leak C, blue lines = pulse, leak, and removal. Dashed CCD lines represent the Pacific, solid lines represent the Atlantic.

pH low despite the influence of greater weathering influx. A side effect of this massive carbon leak combined with rapid weathering is the complete decoupling of pH and carbonate saturation state, which recovers far more quickly and results in a CCD overshoot that occurs too soon (in contrast to the overshoot documented at Site 1403) and is too large, covering the entire seafloor to a depth of 6.5 km, the deepest sediment level in LOSCAR. This stands in conflict with records of the PETM from the deep sea, for example North Pacific Site 1211 which remains carbonate barren (hence below the CCD) throughout the event (Colosimo et al., 2005). Moreover, this large leak would have to be more ^{13}C-depleted than organic matter in order to match the shape of the CIE, for which a source or mechanism for release seems incompatible with modern understanding of the global carbon cycle.

In the intermediate C release scenario (Figure 8, 3300 GtC over 5000 years, which is longer than ocean turnover), a leak of an additional 3800 GtC over 65,000 years is required to sustain acidification. The resulting CCD curves fall within constraints throughout the event, and a CCD overshoot in the Atlantic occurs ~75,000 years after the CIE onset, in line with the record at Site 1403.

LOSCAR modeling of the CIE recovery

After the PETM body, all three of the pulse + leak scenarios feature a recovery in surface pH that is far more gradual and prolonged than indicated by the δ^{11}B -based pH record. In order to match the rapidity of the pH recovery, removal of organic carbon (δ^{13}C = -25 ‰) from the atmosphere over ~60 kyr was required. In the

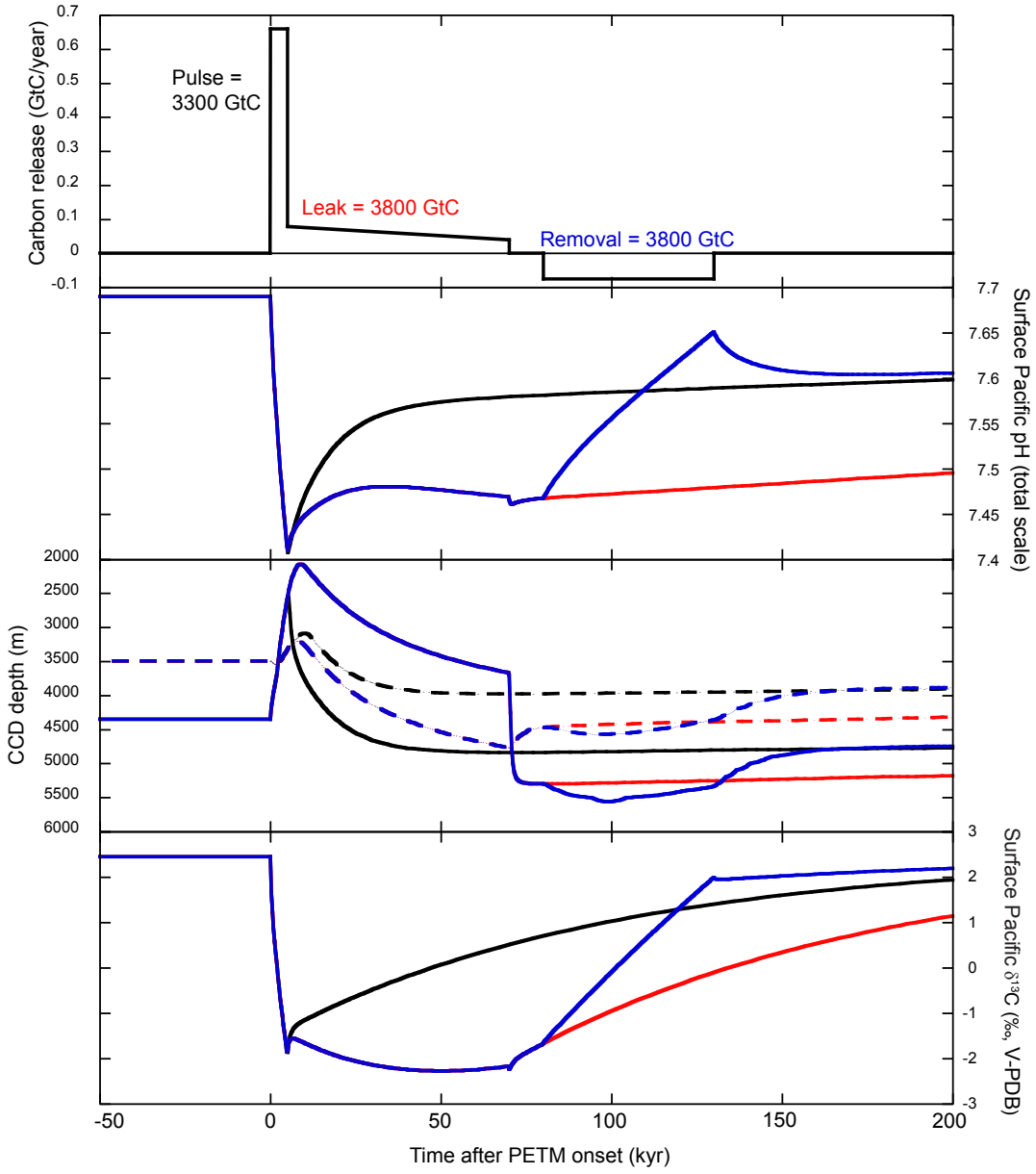

Figure 8: Intermediate C release scenario. Black lines = only the initial C pulse, red lines = Pulse leak C, blue lines = pulse, leak, and removal. Dashed CCD lines represent the Pacific, solid lines represent the Atlantic.

case of the low C release scenario (Figure 6), 4500 GtC were removed, while 3800 and 4200 GtC were removed in the intermediate (Figure 8) and high (Figure 7) release scenarios, respectively. In all cases, removal of carbon acts to temporarily deepen the CCD, aiding the CCD overshoot during the PETM recovery.

Consistent scenario

The intermediate carbon release scenario most closely conforms to all constraints on carbonate chemistry over the PETM without invoking an unreasonable carbon release scenario (as is the case of the low carbon input). In order to generate a CIE of -3.5 ‰, the intermediate carbon release scenario requires an input carbon of -38‰, which can be interpreted as a mixture of organic carbon and methane. Interestingly, in this scenario (and all conformable scenarios that feature sustained acidification) at least half of the total carbon release occurs after the initial onset, suggesting a significant slow positive feedback between warming and carbon release. Both methane (Dickens et al., 1995; Zeebe, 2013) and terrestrial organic carbon (Bowen, 2013) have been proposed as potential long-term feedbacks capable of releasing carbon at similar rates to the leak in the intermediate release scenario (~0.1 GtC/year) over tens of thousands of years. Given that much of the carbon released during the PETM was the result of a slow feedback, it is likely that the PETM resulted from positive feedback(s) to a modest initial warming, either the result of some small trigger (such has volcanism, Svensen et al. (2004)) or simply the crossing of a temperature threshold during the warming trend across the Late Paleocene – Early Eocene (Zachos et al., 2001). It is important to identify the exact source of these

feedbacks, as they may be important components of the Earth System on the thousand to tens of thousand year time-scale following current anthropogenic carbon release.

The inconsistencies of the low and high C release scenarios with the sustained acidification and rapid recovery of the PETM can be used to further constrain the range of realistic scenarios in the PETM onset experiment. We can exclude runs that have a carbon input duration less than an ocean mixing time on the basis of problematic mechanism of carbon leak, as in the low C release scenario, above. Furthermore, all runs that feature greater than default weathering strength can be excluded on the basis of the rapidity of CCD recovery/overshoot that conflicts with existing CCD records such as the timing of the CCD overshoot at Site 1403. Finally, we can likely exclude runs starting from an initial pCO_2 of 500ppm, which would stand in conflict with the lack of large Antarctic Ice sheets during the Paleogene (DeConto and Pollard, 2003). Once those runs are excluded, only 43 simulations of the PETM onset are considered successful, and span a much more narrow range of input and output parameters (Figure 9). Only runs starting from an initial pCO_2 of 750 or 1000 ppmv are consistent with the revised requirements, and require a carbon release of 3,000 or 4,000 GtC, although the C input duration still spans 2,000 to 10,000 years. All of the successful runs require the circulation switch of Zeebe et al., 2009, with variable deep Atlantic injection (from 0 to 100%). Minimum surface Pacific saturation state in the successful runs ranges from 1.6 to 1.9 for aragonite and from 3.5 to 4.1 for calcite, far less severe than predicted for future anthropogenic

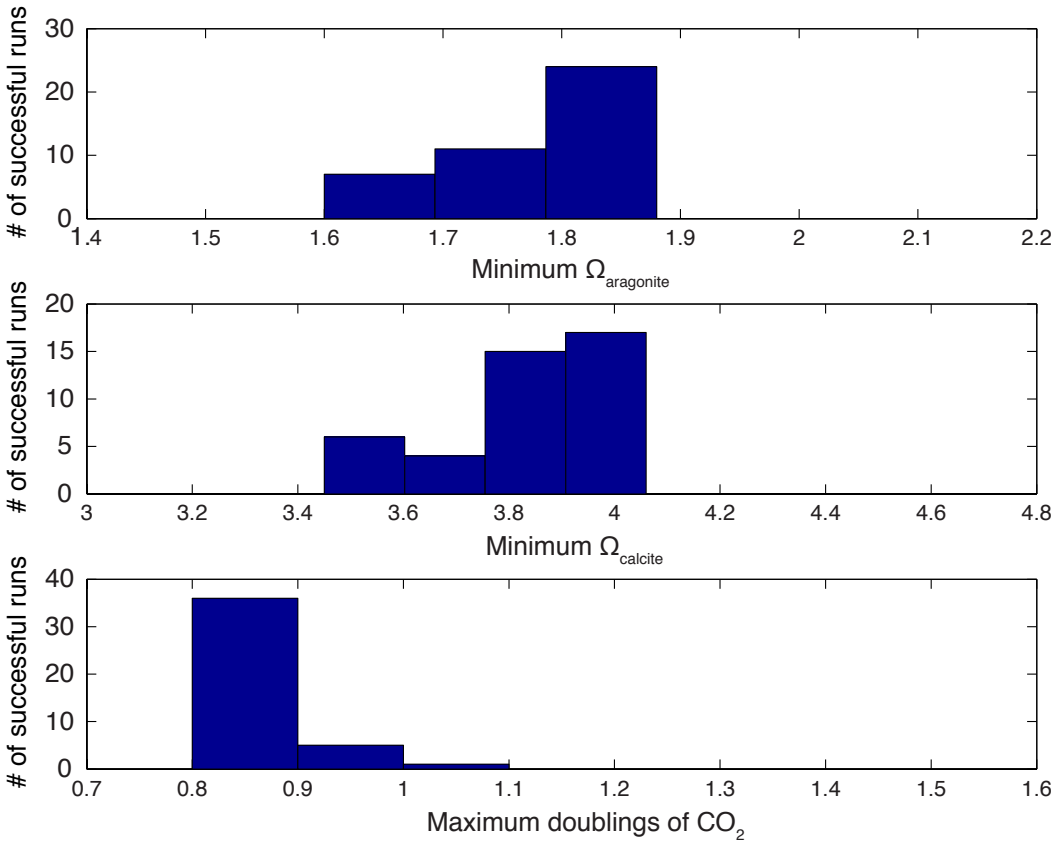

Figure 9: Histograms of output from successful LOSCAR runs from the PETM onset experiment featuring initial pCO_2 greater than or equal to 750ppm, initial carbon release duration greater than or equal to 2,000 years, weathering feedback strength less than or equal to default: minimum aragonite saturation state (Ω_{arag}) of the low-latitude surface Pacific, minimum calcite saturation state (Ω_{calc}) of the low-latitude surface Pacific, and maximum atmospheric pCO_2 expressed as doublings of pre-event (initial, equilibrium) pCO_2. Doublings = $\log_2$(maximum pCO_2 / initial pCO_2).

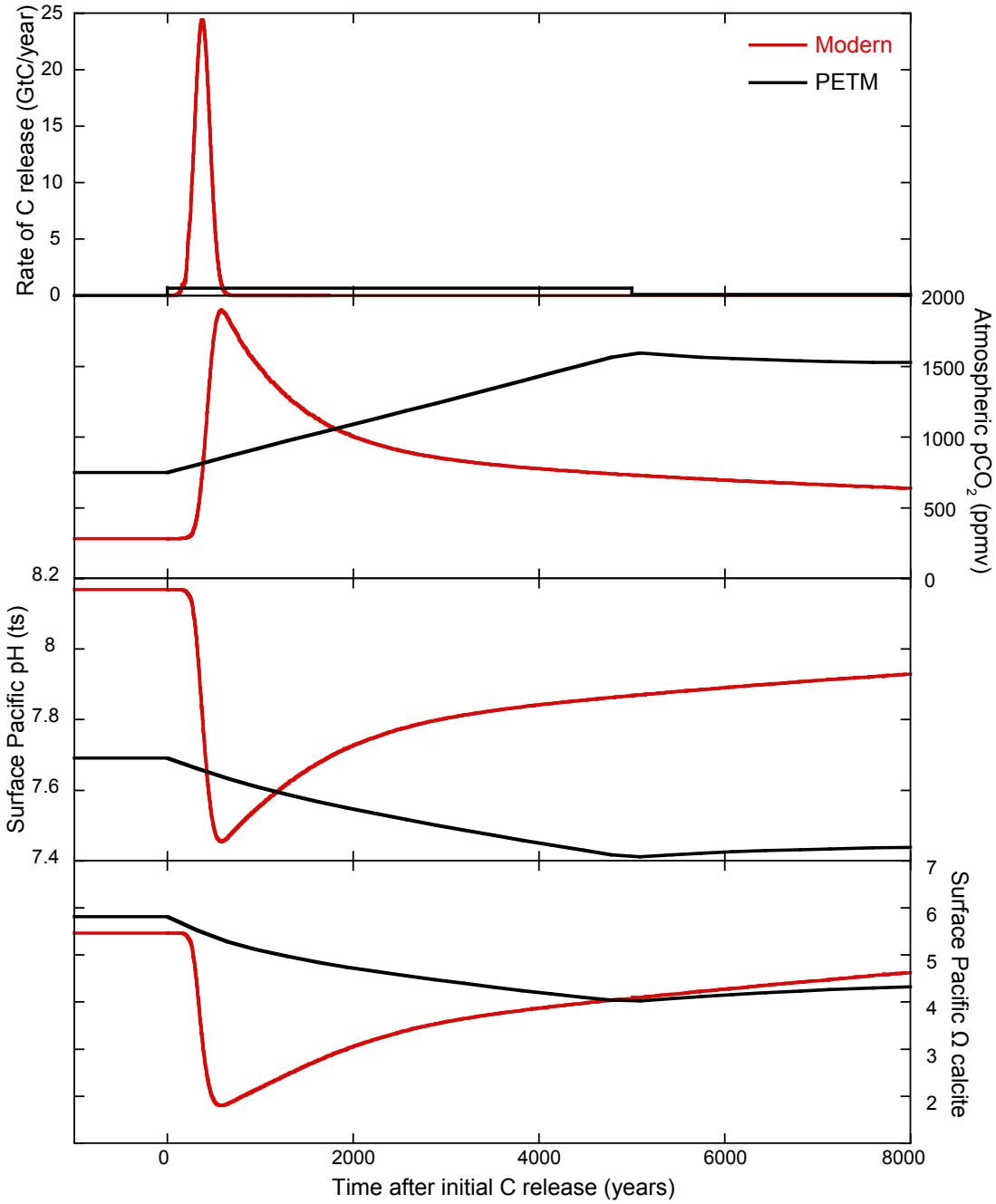
Modern
PETM
Rate of C release (GtC/year)
25
20
15
10
5
0
2000
1500
1000
500
0
Atmospheric pCO2 (ppmv)
8.2
8
7.8
7.6
7.4
Surface Pacific pH (ts)
7
6
5
4
3
2
Surface Pacific Ω calcite
0
2000
4000
6000
8000
Time after initial C release (years)

Figure 10: Comparison of consistent PETM simulation with future anthropogenic simulation of (Zeebe and Zachos, 2013) featuring the release of 5,000GtC over 500 years. After Zeebe and Zachos, 2013.

acidification (Figure 10) and occurring far more slowly. The pCO_2 increase in successful runs ranges from 0.8 to 1.1 doublings of pCO_2, which, when combined with warming estimates of 4-5 °C of global temperature increase during the PETM (Dunkley-Jones et al., 2013), is consistent with 10^3 year climate sensitivities of 3.6 to 6.2 °C per doubling of pCO_2 during the PETM onset, which overlaps only with the higher end of fast climate sensitivities considered by the IPCC (1.5 to 4.5 °C per doubling of pCO_2

Suggestions for future work

While the intermediate C release scenario is consistent with all available constraints on carbonate chemistry over the PETM, the assumptions made about pre-PETM boundary conditions in the intermediate release scenario represent a source of uncertainty. Further constraining several free parameters in the model would help to improve confidence in a consistent PETM scenario. Initial (Paleocene) pCO_2 is not precisely known (Beerling and Royer, 2011), and the wide range of possible values introduces considerable uncertainty on the magnitude of ocean acidification used to constrain PETM scenarios. Hence, better paleo-CO_2 proxy estimates of Late Paleocene pCO_2 would greatly improve our quantitative interpretation of $\delta^{11}B$ records of the event and improve confidence in our PETM simulations. The strength of the weathering feedback is also an area of uncertainty that greatly affects the range of possible PETM simulations. The simple parameterization of weathering in LOSCAR as a function of pCO_2 is unlikely to fully represent the complex interaction between pCO_2, continental temperatures, global hydrology, and soil chemistry that determine

the rates of silicate and carbonate weathering. Either a more complete mechanistic understanding of the global response of weathering rates to pCO_2/temperature increase (e.g. Maher and Chamberlain (2014)), or quantitative interpretation of geochemical records of silicate weathering change over the PETM (e.g. Ravizza et al. (2001); (Wieczorek et al., 2013)), when combined with records of CCD change, could be used to further constrain PETM scenarios. Furthermore, uncertainty in timing of the PETM onset (or carbon pulse duration) introduces a wide range of possible PETM scenarios: our PETM onset experiment resulted in successful runs ranging in input duration from 1,000 to 10,000 years. Further constraints on the timing of the onset (perhaps from expanded continental sections that are unaffected by dissolution at the PETM onset, such as Bowen et al (2015)) would refine the range of possible PETM scenarios.

Supplementary Table 1: LOSCAR parameters for 3 simulations (low, intermediate, and high carbon release) of the full PETM including body and recovery.

Supplementary Appendix A: LOSCAR parameters for all successful simulations of the PETM onset as constrained by $\delta^{11}B$-based ΔpH and CCD shoal records.

References

Agnini, C., Fornaciari, E., Rio, D., Tateo, F., Backman, J., and Giusberti, L., 2007, Responses of calcareous nannofossil assemblages, mineralogy and geochemistry to the environmental perturbations across the Paleocene/Eocene boundary in the Venetian Pre-Alps: Marine Micropaleontology, v. 63, no. 1-2, p. 19-38.

Beerling, D., and Royer, D. L., 2011, Convergent Cenozoic CO2 history: Nature Geoscience, v. 4, p. 418-420.

Bice, K. L., and Marotzke, J., 2002, Could changing ocean circulation have destabilized methane hydrate at the Paleocene/Eocene boundary? - art. no. 1018: Paleoceanography, v. 17, no. 2, p. 1018.

Bowen, G. J., 2013, Up in smoke: A role for organic carbon feedbacks in Paleogene hyperthermals: Global and Planetary Change, v. 109, p. 18-29.

Bowen, G. J., Clyde, W. C., Koch, P. L., Ting, S. Y., Alroy, J., Tsubamoto, T., Wang, Y. Q., and Wang, Y., 2002, Mammalian dispersal at the Paleocene/Eocene boundary: Science, v. 295, no. 5562, p. 2062-2065.

Bowen, G. J., and Zachos, J. C., 2010, Rapid carbon sequestration at the termination of the Palaeocene-Eocene Thermal Maximum: Nature Geoscience, v. 3, no. 12, p. 866-869.

Bralower, T. J., 2002, Evidence of surface water oligotrophy during the Paleocene-Eocene thermal maximum: Nannofossil assemblage data from Ocean Drilling Program Site 690, Maud Rise, Weddell Sea (vol 17, pg 1023, 2002) - art. no. 1060: Paleoceanography, v. 17, no. 4, p. 1060.

Colosimo, A. B., Bralower, T. J., and Zachos, J. C., 2005, Evidence for lysocline shoaling and methane hydrate dissociation at the Paleocene-Eocene thermal maximum on Shatsky Rise, ODP Leg 198, *in* Bralower, T. J., Premoli Silva, I., and Malone, M., eds., Proc. ODP, Sci. Results, Volume 198: College Station, TX, Ocean Drilling Program.

Cui, Y., Kump, L. R., Ridgwell, A. J., Charles, A. J., Junium, C. K., Diefendorf, A. F., Freeman, K. H., Urban, N. M., and Harding, I. C., 2011, Slow release of fossil carbon during the Palaeocene-Eocene Thermal Maximum: Nature Geoscience, v. 4, no. 7, p. 481-485.

DeConto, R. M., and Pollard, D., 2003, Rapid Cenozoic glaciation of Antarctica induced by declining atmospheric CO2: Nature, v. 421, no. 6920, p. 245-249.

Dickens, G. R., Castillo, M. M., and Walker, J. C. G., 1997, A blast of gas in the latest Paleocene: Simulating first-order effects of massive dissociation of oceanic methane hydrate: Geology, v. 25, no. 3, p. 259-262.

Dickens, G. R., Oneil, J. R., Rea, D. K., and Owen, R. M., 1995, Dissociation of Oceanic Methane Hydrate As a Cause of the Carbon Isotope Excursion At the End of the Paleocene: Paleoceanography, v. 10, no. 6, p. 965-971.

Dunkley-Jones, T., Lunt, D. J., Schmidt, D. N., Ridgwell, A., Sluijs, A., Valdes, P. J., and Maslin, M., 2013, Climate model and proxy data constraints on ocean warming across the Paleocene-Eocene Thermal Maximum: Earth-Science Reviews, v. 125, p. 123-145.

Farley, K. A., and Eltgroth, S. F., 2003, An alternative age model for the Paleocene-Eocene thermal maximum using extraterrestrial He-3: Earth and Planetary Science Letters, v. 208, no. 3-4, p. 135-148.

Hönisch, B., Ridgwell, A., Schmidt, D. N., Thomas, E., Gibbs, S., Sluijs, A., Zeebe, R., Kump, L., Martindale, R. C., Greene, S., Kiessling, W., Ries, J. B., Zachos, J., Royer, D. L., Barker, S., Marchitto, T., Moyer, R., Pelejero, C., Ziveri, P., Foster, G. L., and Williams, B., 2012, The Geological Record of Ocean Acidification: Science, v. 335, no. 6072, p. 1058-1063.

IPCC, 2007, Climate change 2007, http://www.ipcc.ch/ipccreports/assessments-reports.htm.

Kelly, D. C., Nielsen, T. M., and Schellenberg, S. A., 2012, Carbonate saturation dynamics during the Paleocene–Eocene thermal maximum: Bathyal constraints from ODP sites 689 and 690 in the Weddell Sea (South Atlantic): Marine Geology, v. 303, p. 75-86.

Kelly, D. C., Zachos, J. C., Bralower, T. J., and Schellenberg, S. A., 2005, Enhanced terrestrial weathering/runoff and surface ocean carbonate production during the recovery stages of the Paleocene-Eocene thermal maximum: Paleoceanography, v. 20, no. 4, p. -.

Kennett, J. P., and Stott, L. D., 1991, Abrupt Deep-Sea Warming, Palaeoceanographic Changes and Benthic Extinctions At the End of the Palaeocene: Nature, v. 353, no. 6341, p. 225-229.

Leon-Rodriguez, L., and Dickens, G. R., 2010, Constraints on ocean acidification associated with rapid and massive carbon injections: The early Paleogene record at ocean drilling program site 1215, equatorial Pacific Ocean: Palaeogeography, Palaeoclimatology, Palaeoecology, v. 298, no. 3, p. 409-420.

Maher, K., and Chamberlain, C., 2014, Hydrologic regulation of chemical weathering and the geologic carbon cycle: Science, v. 343, no. 6178, p. 1502-1504.

McCarren, H., Thomas, E., Hasegawa, T., Rohl, U., and Zachos, J. C., 2008, Depth dependency of the Paleocene-Eocene carbon isotope excursion: Paired benthic and terrestrial biomarker records (Ocean Drilling Program Leg 208, Walvis Ridge): Geochemistry Geophysics Geosystems, v. 9, p. -.

McInerney, F. A., and Wing, S., 2011, The Paleocene-Eocene Thermal Maximum: A Perturbation of Carbon Cycle, Climate, and Biosphere with Implications for the future: Annual Review of Earth & Planetary Sciences, v. 39, p. 489-516.

Murphy, B. H., Farley, K. A., and Zachos, J. C., 2010, An extraterrestrial He-3-based timescale for the Paleocene-Eocene thermal maximum (PETM) from Walvis Ridge, IODP Site 1266: Geochimica Et Cosmochimica Acta, v. 74, no. 17, p. 5098-5108.

Panchuk, K., Ridgwell, A., and Kump, L. R., 2008, Sedimentary response to Paleocene-Eocene Thermal Maximum carbon release: A model-data comparison: Geology, v. 36, no. 4, p. 315-318.

Penman, D. E., Hönisch, B., Zeebe, R. E., Thomas, E., and Zachos, J. C., 2014, Rapid and sustained surface ocean acidification during the Paleocene‐Eocene Thermal Maximum: Paleoceanography.

Pollard, D., and DeConto, R. M., 2005, Hysteresis in Cenozoic Antarctic ice-sheet variations: Global and Planetary Change, v. 45, no. 1, p. 9-21.

Ravizza, G., Norris, R. N., Blusztajn, J., and Aubry, M. P., 2001, An osmium isotope excursion associated with the late Paleocene thermal maximum: Evidence of intensified chemical weathering: Paleoceanography, v. 16, no. 2, p. 155-163.

Ridgwell, A., and Schmidt, D. N., 2010, Past Constraints on the vulnerability of marine calcifiers to massive carbon dioxide release: Nature Geoscience, v. 3, p. 196-200.

Röhl, U., Westerhold, T., Bralower, T. J., and Zachos, J. C., 2007, On the duration of the Paleocene-Eocene thermal maximum (PETM): Geochemistry Geophysics Geosystems, v. 8, p. -.

Sluijs, A., Bowen, G. J., Brinkhuis, H., Lourens, L., and Thomas, E., 2012a, The Palaeocene-Eocene Thermal Maximum super greenhouse: biotic and geochemical signatures, age models and mechanisms of global change, *in* Williams, M., Haywood, A. M., Gregory, F. J., and Schmidt, D. N., eds., Deep-Time Perspectives on Climate Change: Marrying the Signal from

Computer Models and Biological Proxies: London, The Geological Society, p. 267-293.

Sluijs, A., Zachos, J. C., and Zeebe, R. E., 2012b, Constraints on hyperthermals: Nature Geosci, v. 5, no. 4, p. 231-231.

Svensen, H., Planke, S., Malthe-Sorenssen, A., Jamtveit, B., Myklebust, R., Eidem, T. R., and Rey, S. S., 2004, Release of methane from a volcanic basin as a mechanism for initial Eocene global warming.: Nature, v. 429, p. 524-527.

Thomas, D. J., Zachos, J. C., Bralower, T. J., Thomas, E., and Bohaty, S., 2002, Warming the fuel for the fire: Evidence for the thermal dissociation of methane hydrate during the Paleocene-Eocene thermal maximum: Geology, v. 30, no. 12, p. 1067-1070.

Thomas, E., and Shackleton, N. J., 1996, The Paleocene-Eocene benthic foraminiferal extinction and stable isotope anomalies, *in* Knox, R. W. O. B., Corfield, R. M., and Dunay, R. E., eds., Correlation of the early Paleogene in Northwest Europe, Volume 101: London, p. 401-441.

Wang, Y., Law, R., and Pak, B., 2010, A global model of carbon, nitrogen and phosphorus cycles for the terrestrial biosphere: Biogeosciences, v. 7, no. 7, p. 2261-2282.

Wieczorek, R., Fantle, M. S., Kump, L. R., and Ravizza, G., 2013, Geochemical evidence for volcanic activity prior to and enhanced terrestrial weathering during the Paleocene Eocene Thermal Maximum: Geochimica et Cosmochimica Acta, v. 119, p. 391-410.

Wing, S. L., Harrington, G. J., Smith, F. A., Bloch, J. I., Boyer, D. M., and Freeman, K. H., 2005, Transient floral change and rapid global warming at the Paleocene-Eocene boundary: Science, v. 310, no. 5750, p. 993-996.

Zachos, J., Pagani, M., Sloan, L., Thomas, E., and Billups, K., 2001, Trends, rhythms, and aberrations in global climate 65 Ma to present: Science, v. 292, no. 5517, p. 686-693.

Zachos, J. C., Dickens, G. R., and Zeebe, R. E., 2008, An early Cenozoic perspective on greenhouse warming and carbon-cycle dynamics: Nature, v. 451, no. 7176, p. 279-283.

Zachos, J. C., Rohl, U., Schellenberg, S. A., Sluijs, A., Hodell, D. A., Kelly, D. C., Thomas, E., Nicolo, M., Raffi, I., Lourens, L. J., McCarren, H., and Kroon, D., 2005, Rapid Acidification of the Ocean During the Paleocene-Eocene Thermal Maximum: Science, v. 308, no. 5728, p. 1611-1615.

Zachos, J. C., Wara, M. W., Bohaty, S., Delaney, M. L., Petrizzo, M. R., Brill, A., Bralower, T. J., and Premoli-Silva, I., 2003, A Transient Rise in Tropical Sea Surface Temperature During the Paleocene-Eocene Thermal Maximum: Science, v. 302, no. 5650, p. 1551-1554.

Zeebe, R., 2012, LOSCAR: Long-term ocean-atmosphere-sediment carbon cycle reservoir model v2. 0.4: Geoscientific Model Development, v. 5, no. 1, p. 149-166.

Zeebe, R., and Zachos, J., 2012, Long-term legacy of massive carbon input to the Earth system: Anthropocene vs. Eocene: Philosophical Transactions of the Royal Society, p. 1-22.

Zeebe, R. E., 2013, What caused the long duration of the Paleocene‐Eocene Thermal Maximum?: Paleoceanography, v. 26, p. 1-13.

Zeebe, R. E., Dickens, G. R., Ridgwell, A., Sluijs, A., and Thomas, E., 2014, Onset of carbon isotope excursion at the Paleocene-Eocene thermal maximum took millennia, not 13 years: Proceedings of the National Academy of Sciences, v. 111, no. 12, p. E1062-E1063.

Zeebe, R. E., and Zachos, J. C., 2007, Reversed deep-sea carbonate ion basin gradient during Paleocene-Eocene thermal maximum: Paleoceanography, v. 22, no. 3, p. -.

Zeebe, R. E., and Zachos, J. C., 2013, Long-term legacy of massive carbon input to the Earth system: Anthropocene versus Eocene: Philosophical Transactions of the Royal Society of London A: Mathematical, Physical and Engineering Sciences, v. 371, no. 2001, p. 20120006.

Zeebe, R. E., Zachos, J. C., and Dickens, G. R., 2009, Carbon dioxide forcing alone insufficient to explain Palaeocene-Eocene Thermal Maximum warming: Nature Geoscience, v. 2, no. 8, p. 576-580.